

T.C.
DOKUZ EYLÜL UNIVERSITY
IZMIR INTERNATIONAL
BIOMEDICINE AND GENOME
INSTITUTE

**MODELLING hTERT CANCER-ASSOCIATED
MUTATIONS VIA CRISPR-Cas9 IN 3D LIVER
ORGANOIDS**

CANAN ÇELİKER

MOLECULAR BIOLOGY AND GENETICS MASTER'S
PROGRAM

MASTER OF SCIENCE THESIS

IZMIR-2019

THESIS CODE: DEU.IBG.MSc.2016850032

T.C.
DOKUZ EYLÜL UNIVERSITY
IZMIR INTERNATIONAL
BIOMEDICINE AND GENOME
INSTITUTE

**MODELLING hTERT CANCER-ASSOCIATED
MUTATIONS VIA CRISPR-Cas9 IN 3D LIVER
ORGANOIDS**

MOLECULAR BIOLOGY AND GENETICS MASTER'S
PROGRAM

MASTER OF SCIENCE THESIS

CANAN ÇELİKER

Supervising Faculty Member: Prof. Dr. Ş. Esra ERDAL
Co-Supervising Faculty Member: Assoc. Prof. Şerif ŞENTÜRK

This research was supported by the TUBITAK 1001 Scientific and Technological Research
Projects Support Program with a project number of 117Z858.

THESIS CODE: DEU.IBG.MSc.2016850032

MASTER THESIS DEFENSE EXAM REPORT

Dokuz Eylül University İzmir International Biomedicine and Genome Institute Department of Genomics and Molecular Biotechnology, Molecular Biology and Genetics Graduate Program Master of Science student Canan ÇELİKER has successfully completed her Master of Science thesis titled "Modelling hTERT Cancer-Associated Mutations via CRISPR-Cas9 in 3D Liver Organoids" on the date of December 25, 2019.



CHAIR

Prof. Dr. Ş. Esra ERDAL

Dokuz Eylül University
Faculty of Medicine Basic Medical Sciences
Department of Medical Biology



MEMBER

Assoc. Prof. Şerif ŞENTÜRK

İzmir International Biomedicine and Genome
Institute Department of Genomics and
Molecular Biotechnology



MEMBER

Asst. Prof. Yavuz OKTAY

Dokuz Eylül University Faculty of
Medicine Basic Medical Sciences
Department of Medical Biology



MEMBER

Prof. Dr. Nur ARSLAN

Dokuz Eylül University Faculty of
Medicine Internal Medicine
Department of Pediatrics



MEMBER

Assoc. Prof. Zeynep FIRTINA

KARAGONLAR

İzmir University of Economics
Faculty of Engineering Department
of Genetics and Bioengineering

SUBSTITUTE MEMBER

Asst. Prof. Hani ALOTAİBİ

İzmir International Biomedicine and
Genome Institute Department of Biomedicine
and Health Technologies

SUBSTITUTE MEMBER

Asst. Prof. Ayşe Banu DEMİR

İzmir University of Economics
Faculty of Medicine Department of
Basic Medical Sciences

YÜKSEK LİSANS TEZ SAVUNMA SINAVI TUTANAĞI

Dokuz Eylül Üniversitesi İzmir Uluslararası Biyotıp ve Genom Enstitüsü Genom Bilimleri ve Moleküler Biyoteknoloji Anabilim Dalı, Moleküler Biyoloji ve Genetik Yüksek Lisans programı öğrencisi Canan ÇELİKER “Kanser İlişkili hTERT Mutasyonların 3D Karaciğer Organoidlerinde CRISPR-Cas9 ile Modellenmesi” konulu yüksek lisans tezinde 25 Aralık, 2019 tarihinde yapılan savunma sınavı sonucunda başarılı olmuştur.



BAŞKAN

Prof. Dr. Ş. Esra ERDAL

Dokuz Eylül Üniversitesi Tıp Fakültesi
Temel Tıp Bilimleri
Tıbbi Biyoloji Anabilim Dalı



JÜRİ ÜYESİ

Doç. Dr. Şerif ŞENTÜRK

İzmir Uluslararası Biyotıp ve Genom
Enstitüsü Genom Bilimleri ve Moleküler
Biyoteknoloji Anabilim Dalı



JÜRİ ÜYESİ

Dr. Öğr. Üyesi Yavuz OKTAY

Dokuz Eylül Üniversitesi Tıp
Fakültesi Temel Tıp Bilimleri Tıbbi
Biyoloji Anabilim Dalı



JÜRİ ÜYESİ

Prof. Dr. Nur ARSLAN

Dokuz Eylül Üniversitesi Tıp Fakültesi
Dahili Tıp Bilimleri Çocuk Sağlığı ve
Hastalıkları Anabilim Dalı



JÜRİ ÜYESİ

Doç. Dr. Zeynep FIRTINA

KARAGONLAR
İzmir Ekonomi Üniversitesi
Mühendislik Fakültesi Genetik
ve Biyomühendislik

YEDEK JÜRİ ÜYESİ

Dr. Öğr. Üyesi Hani ALOTAİBİ

İzmir Uluslararası Biyotıp ve
Genom Enstitüsü Biyotıp ve Sağlık
Teknolojileri Anabilim Dalı

YEDEK JÜRİ ÜYESİ

Yrd. Doç. Dr. Ayşe Banu DEMİR

İzmir Ekonomi Üniversitesi
Tıp Fakültesi Temel Tıp
Bilimleri

TABLE OF CONTENTS

INDEX OF TABLES	iv
INDEX OF FIGURES	v
ABBREVIATIONS	vii
Acknowledgements	viii
ABSTRACT	1
ÖZET	2
1. INTRODUCTION AND PURPOSE.....	3
1.1. Statement and Importance of the Problem	3
1.2. Aim of the Study	3
1.3. The hypothesis of the Study	4
2. GENERAL INFORMATION	5
2.1. Hepatocellular Carcinoma.....	5
2.2. Dysregulated signaling pathways and mutated genes in HCC development	6
2.3. Human TERT Promoter Mutations in HCC.....	8
2.4. Genome Editing Technologies	11
2.4.1. CRISPR Cas9 System	11
2.5. Organoid Technology.....	13
2.5.1. Liver organoids.....	13
2.5.2. Disease Modelling in Organoids	15
3. MATERIALS AND METHODS	18
3.1. Type of Research.....	18
3.2. Time and Place of Research	18
3.3. Working Material	18
3.3.1. Primers.....	18
3.3.2. Vectors and Bacterial Strains	19
3.3.3. Enzyme and Kits	21
3.3.4. Commonly used Softwares and databases.....	22
3.3.5. Commonly used buffers, solutions, and media.....	22
3.3.6. Special Instruments	23
3.3.7. Mammalian cell lines	24
3.4. Research Variables	24
3.5. Data Collection Tools/Methods.....	24
3.5.1. Primer design.....	24
3.5.2. Polymerase Chain Reaction (PCR)	24
3.5.2.1. Two-Step PCR for Mutagenesis.....	24

3.5.2.2. PCR for HR determination	27
3.5.2.3. Colony PCR.....	27
3.5.3. Molecular Cloning.....	28
3.5.3.1. Cloning of sgRNAs	28
3.5.3.2. Cloning of Mutant PCR products after 2 Step PCR	28
3.5.3.3. Restriction Digest	29
3.5.3.4. Ligation	29
3.5.3.5. Transformation of chemically competent E. coli Stbl3	30
3.5.4. Agarose Gel Extraction and PCR clean up.....	30
3.5.5. Genomic DNA Purification.....	30
3.5.6. Miniprep and Midiprep of Plasmid DNA.....	30
3.5.7. Cell culture	31
3.5.8. Hepatic Organoid Culture.....	31
3.5.9. Transfection Methods.....	32
3.5.9.1. HEK293T Transfection	32
3.5.9.2. Organoid Transfection.....	32
3.5.10. FACS and Flow Cytometry	32
4. RESULTS.....	34
4.1. PCR amplification to introduce mutations into DT-Plasmids	36
4.2. Cloning of the Two-Step PCR Fragments into DT-Plasmids.....	38
4.3. Cloning of the gRNAs into the pX330 Plasmid	41
4.4. Transfection of Hek293T cells for single base-pair modification in the endogenous TERT promoter	43
4.5. Transfection of Hepatic Organoids for single base-pair modification in the endogenous TERT promoter	55
4.6. Transfection of Hepatic Organoids for the Knock-Out of TP53	65
5. DISCUSSION	72
6. CONCLUSION AND FUTURE ASPECTS	76
7. REFERENCES	77
8. CURRICULUM VITAE (CV)	82

INDEX OF TABLES

Table 2.1: Genes most frequently mutated in hepatocellular carcinoma, identified in large-scale studies	7
Table 3.1: Primers used in experiments.	18
Table 3.2: Vectors and their bacterial strains used in experiments.	19
Table 3.3: Enzyme and Kits	21
Table 3.4: Commonly used Softwares and databases	22
Table 3.5: Commonly used buffers, solutions, and media	22
Table 3.6: Special Instruments	23
Table 3.7: PCR conditions and cycles with NEB Phusion HF DNA Polymerase.....	26
Table 3.8: PCR conditions and cycles with Thermo Fisher Phusion HF DNA Polymerase	26
Table 3.9: PCR conditions and cycles for Colony PCR.....	27
Table 3.10: Restriction Digestion components	29
Table 3.11: Ligation components.....	29



INDEX OF FIGURES

Figure 2.1: Histology and Main Genetic Alterations in Hepatocellular Carcinoma.	6
Figure 2.2: hTERT transcription and promoter mutations.	10
Figure 2.3: CRISPR- Cas9 System and its working mechanism.....	12
Figure 2.4: Schematic presentation of hepatic organoid production and functional analysis of the organoids.	15
Figure 2.5: Disease modeling strategies in organoid culture.....	16
Figure 3.1: Scheme of the HR-TERT SV40 GFP Plasmid.	20
Figure 3.2: Scheme of the HR-TERT Promoter Plasmid.	20
Figure 3.3: Scheme of the px330 plasmid.	21
Figure 3.4: Workflow of the two-step PCR.....	25
Figure 4.1: Schematic workflow for the single base-pair modification in the endogenous TERT promoter in Hepatic Organoids.....	35
Figure 4.2: Pop in and pop out a strategy that modifies a single base pair at the endogenous TERT promoter.	35
Figure 4.3: Gel image of uncut and cut plasmids after isolation.	36
Figure 4.4: Schematized results of two Steps PCR for single base-pair modification for production of DT GFP 146C>T, DT Promotor 124C>T and DT Promotor 146C>T plasmids.....	37
Figure 4.5: Schematized results of two Steps PCR for single base-pair modification for production of DT Promotor 124 + 146C>T plasmid.	38
Figure 4.6: Gel image of cut plasmids.....	39
Figure 4.7: Gel image of cut plasmids after isolation.	39
Figure 4.8: Sanger sequencing chromatograms of plasmids to show single base pair alterations.	40
Figure 4.9: Agarose gel image of cut pX330 plasmid.....	41
Figure 4.10: Agarose gel image of PCR results after gRNA cloning.....	42
Figure 4.11: Sanger sequencing chromatograms of gRNA plasmids.....	43
Figure 4.12: Agarose gel image of all cloned plasmids.	43
Figure 4.13: Scheme of the HEK293T cell GFP+ cell enrichment after first step transfection.	44
Figure 4.14: Florescence microscopy images of Hek293 T single-cell clones after FACS on day 7 and 14.....	45
Figure 4.15: Florescence microscopy images of some Hek293 T single-cell clones after passage.	45
Figure 4.16: PCR result with HR primers in eight GFP+ single-cell clones.....	45
Figure 4.17: Flow analysis in clones C2 and C12, 7 days after the second transfection.....	46
Figure 4.18: GFP + cell sorting before the second transfection in five GFP + single-cell clones.	47
Figure 4.19: Flow analysis 10 days after GFP + cell enrichment.	48
Figure 4.20: GFP- single cell&bulk sorting on day 11 after the second transfection.	49
Figure 4.21: PCR results with HR primers of GFP-Bulk sorted cells.....	50
Figure 4.22: Agarose gel images of PCR results for sequencing of C12 GFP-Bulk groups.....	51
Figure 4.23: Sanger sequencing chromatograms of GFP- bulk groups.....	52
Figure 4.24 :GFP + / GFP- cell numbers obtained from 96 wp after the second transfection.	52
Figure 4.25: Agarose gel images of PCR results for selecting and sequencing of GFP-single cell clones.	54
Figure 4.26: Sanger sequencing chromatograms of C12 single-cell clones and BLAST results of these clones.....	54
Figure 4.27: Organoid culture bright-field (BF) images under EM culture condition.	55
Figure 4.28: Workflow of the organoid transfection.....	56
Figure 4.29: Transfection of Hepatic Organoids with x-tremeGENE and PEI.	57
Figure 4.30: Transfection method of hepatic organoids with Lipofectamine 2000 and its results.....	58
Figure 4.31: Transfection of Hepatic Organoids and HEK293T cells with Nucleofector System.....	59

Figure 4.32: Transfection of Hepatic Organoids with Nucleofector System. 61
Figure 4.33: Transfection of Hepatic Organoids with Nucleofector System for the first step of hTERT modification. 63
Figure 4.34: BF and fluorescence microscopy image after transfection. 64
Figure 4.35: Transfection of Hepatic Organoids with Nucleofector System for the TP53 knock-out.. 69
Figure 4.36: BF images of WT Hepatic Organoid and P53 Clone G5-2..... 70
Figure 4.37: Brightfield images of wild-type and TP53- mutant organoid after 7 days of Nutlin-3 selection..... 71



ABBREVIATIONS

3D	Three Dimensional
A1AT	Alpha 1 Antitrypsin Glycoprotein
aSC	Adult Stem Cell
BF	Bright-Field
Cas9	CRISPR-Associated Protein 9
CC	Cholangiocarcinoma
CHC	Combined HCC/CC
CRISPR	Clustered Regularly Interspaced Short Palindromic Repeats
crRNA	CRISPR RNA
DSBs	Double-Stranded Breaks
DT	Donor Template
ECM	Extracellular Matrix
eHEPO	Hepatic Organoid
EM	Expansion Medium
ESC	Embryonic Stem Cell
ETS/TCF	E-Twenty-Six/ Ternary Complex Factors
FDA	Food and Drug Administration
GAPs	GTPase-Activating Proteins
GEFs	Guanine Nucleotide Exchange Factors
GEMMs	Genetically Engineered Mouse Models
HBV	Hepatitis B Virus
HCC	Hepatocellular Carcinoma
HCV	Hepatitis C Virus
HDR	Homology Directed Repair
hTERT	Human TERT
IPSC	Induced Pluripotent Stem Cell
NAFLD	Nonalcoholic Fatty Liver Disease
NF1	Neurofibromin
NHEJ	Non-Homologues End Joining
PDXs	Patient-Derived Xenografts
sgRNA	Single guide RNA
TALENs	Transcription Activator-Like Effector Nucleases
TP53	Tumor Protein 53
WT	Wild Type
ZNFs	Zinc-Finger Nucleases

Acknowledgements

Foremost, I would like to express my sincere gratitude to my advisor Prof. Dr. Esra ERDAL for giving me the opportunity of joining her Lab, the continuous support of my M.Sc. study and research, her motivation, enthusiasm, and assistance. I could not have imagined having a better advisor and mentor for my M.Sc. study. I would like to express my deepest acknowledge to Assoc. Prof. Şerif ŞENTÜRK for his patience, and immense knowledge. His guidance helped me in all the time of research and carrying out my experiments.

I am particularly grateful for the assistance given by all lab mates during the experiments equally Mr. Mustafa KARABIÇİCİ for cell culture, and teamworking. Mr. Soheil AKBARI for his helping me in both theoretical and experimental sides. Both Mrs. Kadriye GÜVEN and Mrs. Bilge KARAÇİCEK Mrs. Gülsün BAĞCI, Mrs. Kübra Nur KAPLAN, Mrs. Burcu AKMAN, Mrs. Berru ŞAHİN, and Mr. Muhammed MEMON for the companionship and encouragement. Mrs. Aslı Kurden PEKMEZCİ, Mrs. Yağmur TOKTAY, and Mrs. Ece ÇAKIROĞLU for the assistance I received during the molecular cloning techniques.

My deep thanks go to the members Dr. Melek ÜÇÜNCÜ and Dr. Xiaozhou HU from “optical imaging core facility, flow cytometry, and cell sorting core facility of IBG-IZMIR” for making my work very easy.

Last but not least, my lovely thanks go to all the members of my family for continuous tenderness, confidence, and believing in me.

MODELLING hTERT CANCER-ASSOCIATED MUTATIONS VIA CRISPR-Cas9 IN 3D LIVER ORGANOIDS

Canan ÇELİKER

İzmir International Biomedicine and Genome Institute Dokuz Eylül University
Health Campus Balçova 35340 İzmir/ TURKEY

ABSTRACT

Human TERT (hTERT) promoter mutations, C-124T and C-146T are the most common genetic alterations in hepatocellular carcinoma, has an early stage in hepatocarcinogenesis, and associate with the progression. Mechanism of TERT promotor mutations which collaborates with carcinogenesis is not well explained yet. In this study, we generated a hepatic organoid (eHEPO) culture system using human induced pluripotent stem cell (iPSC)-derived EpCAM-positive endodermal cells as an intermediate. eHEPOs can be produced within 2 weeks and expanded long term without any loss of differentiation capacity to mature hepatocytes. In this study, we aimed to introduce hTERT promoter mutations in hepatic organoids using CRISPR-Cas9 based genome editing. For the editing of TERT promoter, a homology-directed repair (HDR) based CRISPR Cas9 system called “pop-in pop-out” strategy was used. This system was optimized in HEK293T cells. Genome modified clones which included C-146T mutation in the promoter were obtained with small deletion mutations. We tried to utilize this system in hepatic organoids. Transfection of the hepatic organoids with CRISPR-Cas9 via chemical and physical-based transfection agents displayed different efficiencies. Low transfection efficiency hampers to edit promoter of hTERT in hepatic organoids. Therefore, to obtain higher transfection efficiency in organoids further, optimization is critical. Also, we tried to knockout the TP53 gene in hepatic organoids with a similar approach. Transfection and editing of hepatic organoids exhibited that the CRISPR-Cas9 system works in hepatic organoids and isogenic organoid clones can be obtained.

Keywords: Hepatic Organoid, Hepatocellular Carcinoma Modelling, hTERT promoter mutations, CRISPR-Cas9

KANSER İLİŞKİLİ hTERT MUTASYONLARININ 3D KARACİĞER ORGANOİDLERİNDE CRISPR-Cas9 İLE MODELLENMESİ

Canan ÇELİKER

**İzmir Uluslararası Biyotıp ve Genom Enstitüsü, Dokuz Eylül Üniversitesi
Sağlık Yerleşkesi Balçova 35340 İzmir/TÜRKİYE**

ÖZET

İnsan TERT (hTERT) promotör mutasyonları C-124T ve C-146T, hepatoselüler karsinomda en sık görülen genetik değişikliklerdir. Bu mutasyonlar hepatokarsinogenezde erken olaylardan biri olarak kabul edilir ve hastalık progresyonu ile anlamlı şekilde ilişkilidir, ancak TERT'in tümörögeneze yol açan mekanizması net bir şekilde keşfedilememiştir. Son yıllarda gelişen üç boyutlu (3D) organoid teknolojileri ile, laboratuvar koşullarında, karaciğerde dahil çeşitli organların, küçültülmüş ve/veya basitleştirilmiş bir yapısal ve işlevsel versiyonunu üretmek mümkün hale gelmiştir. Buna göre, biz EpCAM pozitif endodermal hücrelerin ara basamak olduğu, insan kaynaklı pluripotent kök hücre (iPSC) kaynaklı hepatik organoid (eHEPO) kültür sistemi ürettik. eHEPO'lar 2 hafta içinde üretilebilir ve olgun hepatositlere farklılaşma kapasitesi kaybı olmadan uzun süre büyütülebilmektedir. Bu çalışmada, CRISPR-Cas9 bazlı genom düzenlemesini kullanarak hepatik organoidlerde hTERT promotör mutasyonlarını oluşturmayı amaçladık. TERT promotörünün düzenlenmesi için "pop-in pop-out" stratejisi adı verilen homoloji yönlendirmeli tamir (HDR) temeline dayanan CRISPR-Cas9 sistemi kullanıldı. Öncelikle bu sistem HEK293T hücrelerinde optimize edildi. Bu şekilde, promotörde C-146T mutasyonu içeren genomu modifiye edilmiş klonlar küçük delesyon mutasyonlarıyla beraber elde edildi. İkinci olarak, bu sistem hepatik organoidlerde denendi. Hepatik organoidlerin CRISPR-Cas9 ile kimyasal ve fiziksel bazlı transfeksiyon ajanları yoluyla transfeksiyonu farklı verimlilikler göstermiştir. Düşük transfeksiyon verimi, hepatik organoidlerde hTERT promoterini düzenlemek için engel oluşturmaktadır. Bu nedenle, organoidlerde daha yüksek transfeksiyon etkinliği elde etmek için daha fazla optimizasyon yapılması önemlidir. Bunlara ek olarak, TP53 genini hepatik organoidlerde benzer bir yaklaşımla nakavt edilmeye çalışılmıştır. Hepatik organoidlerin transfeksiyonu ve düzenlenmesi, CRISPR-Cas9 sisteminin hepatik organoidlerde çalıştığını ve izojenik organoid klonlarının elde edilebileceğini göstermiştir.

Anahtar Kelimeler: Hepatik Organoid, Hepatoselüler Karsinoma Modellemesi, hTERT promoter mutasyonları, CRISPR-Cas9

1. INTRODUCTION AND PURPOSE

1.1. Statement and Importance of the Problem

Telomerase reverse transcriptase (TERT) expression that allows cells to overcome replicative senescence and escape apoptosis, is reactivated in human solid tumors with more than 95%. The mechanism behind the activation of TERT in cancers mostly remains unknown. However, recently, recurrent somatic mutations in the TERT promoter have been discovered in most cancers. Especially, TERT promoters have been found to be mutated in more than 50% of HCC. Therefore, TERT promoter mutations are mainly common genetic alterations in HCC and C-124T and C-146T are two major types of alterations in the TERT promoter region. While TERT promoter mutations are considered to be an early event in hepatocarcinogenesis, the mechanism of TERT in the early stage of HCC could not be discovered clearly. Although diverse mouse models have been developed and studied to prove the physiological roles of telomerase as a telomere-elongating enzyme, there has not been established a realistic model for hTERT promoter mutations in human context (Sung, Ali, and Lee 2014). There is no experimental model to understand the role of hTERT promoter mutations having a role in telomerase activation in the process of uncontrolled proliferation of human hepatocyte during liver cancer development.

1.2. Aim of the Study

More recently, our group has established a model for iPSC derived hepatic organoid. In this study, we aimed to further improve this model to understand stepwise alterations on the driver mutations including hTERT during the transformation of normal hepatocytes to the cancer cells. For this aim, we first introduce hTERT mutations into healthy hepatic organoids using CRISPR-Cas9 system. This model provides a platform to investigate the effect of hTERT mutations in the early stage of liver carcinogenesis, especially regarding proliferation.

1.3. The hypothesis of the Study

We hypothesize that human TERT promoter mutations can be modeled *in vitro* by 3D hepatic organoids using the CRISPR-Cas9 system. Subsequently, this model can be used to investigate the role of TERT promoter mutations via mimicking the early stages of hepatocarcinogenesis.



2. GENERAL INFORMATION

2.1. Hepatocellular Carcinoma

Primary liver cancer is the sixth most common cancer and the fourth most common cause of cancer-related death worldwide, 90% of which are hepatocellular carcinoma (HCC) (Desai et al. 2019). While incidence rates of liver cancer vary widely between geographic regions, the World Health Organization predicts that more than 1 million patients will die from liver cancer in 2030 (Villanueva 2019).

Diagnosis of HCC at an early stage and its curative therapies has considerably improved the 5-year survival. So, it became important to screening and surveillance of target populations at particularly high risk for developing HCC to facilitate early-stage detection (Tang et al. 2018). For a long time, Sorafenib, known as the only Food and Drug Administration (FDA) approved drug in the treatment of HCC, has been shown to extend patient life by 3 months. The majority of patients have been reported to develop drug-based or time-dependent resistance. Regorafenib, also known as fluoro-sorafenib and structurally different from Sorafenib only one fluoride supplement, received FDA approval in April 2017 for use only in patients resistant to Sorafenib (Mody and Abou-Alfa 2019).

There are several well-defined risk factors for HCC including cirrhosis, hepatitis B virus (HBV) infection, hepatitis C virus (HCV) infection, excess alcohol consumption, non-alcoholic fatty liver disease, type 2 diabetes mellitus, and smoking (Tang et al. 2018). HCC generally arises with the development of liver inflammation and fibrosis, which eventually results in the disordered liver architecture characteristic of liver cirrhosis but, approximately 20% of HCC's have been known to develop in a non-cirrhotic liver (Dhanasekaran, Bandoh, and Roberts 2016);(Desai et al. 2019). In the histopathological progression of HCC, Cirrhosis in liver cancer may develop with the effect of the mentioned risk factors. These factors promote the increase of necrosis and proliferation in the liver, and over time triggers a destructive regeneration of the liver, promoting the formation of chronic disease, cirrhosis. Cirrhosis is characterized by abnormal liver nodules surrounded by collagen. These nodules eventually form hyperplastic nodules and dysplasia nodules in them, followed by the development of HCC, which is becoming progressively malignant in the form of well-differentiated, moderately differentiated and weakly differentiated by genomic instability and loss of p53. Telomere shortening during

cirrhosis and telomere reactivation and p53 loss during HCC formation is a characteristic feature of liver cancer (Figure 2.1),(Villanueva 2019). However, the stage of reactivation of telomeres and loss of p53 can also be seen in earlier stages (Farazi and DePinho 2006).

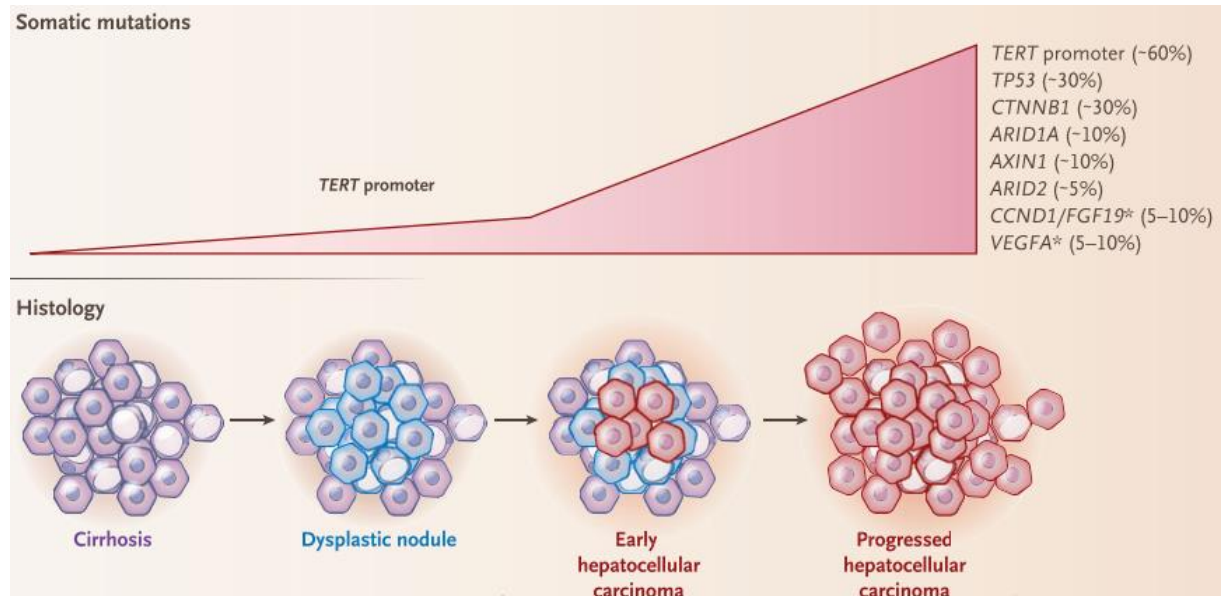


Figure 2.1: Histology and Main Genetic Alterations in Hepatocellular Carcinoma.

The main molecular and histologic changes occurring during human hepatocarcinogenesis are summarized (Villanueva 2019).

2.2. Dysregulated signaling pathways and mutated genes in HCC development

Recently in next-generation sequencing has provided significant information about the genomic landscape of HCC. Several studies have researched multiple aspects of HCC by using whole-genome sequencing, whole-exome sequencing, RNA sequencing, and genome-wide methylation analysis. According to these results of studies, genetic and epigenetic changes described which exhibit the complex and heterogeneous malignancy of HCC (Dhanasekaran, Bandoh, and Roberts 2016). Several pathways are altered in HCC development and HCC cells accumulate somatic DNA alterations, including mutations and chromosomal aberrations. Some major pathways are mostly effected in HCC, bearing WNT/ β -catenin, telomere maintenance, TP53/cell cycle, chromatin remodeling, PI3K/RAS/mTOR pathway, oxidative stress pathways and angiogenesis (Ding et al. 2017). HCCs generally have typically 20–100 number of mutations per genome similar to other solid tumors (Dhanasekaran, Bandoh, and Roberts 2016). While most of all genetic alterations occurred in passenger genes that have not predicted

functional carcinogenic consequences, some of the mutations occurred in cancer driver genes that have key signaling pathways involved in liver carcinogenesis (Table 2.1) (Zucman-Rossi et al. 2015).

Table 2.1: Genes most frequently mutated in hepatocellular carcinoma, identified in large-scale studies (Lee 2015).

Gene*	Mutation frequency (%)	Function	References
TERT	47.1	Maintaining telomere length	27, 30
TP53	29.2	Tumor suppressor	25-30
CTNNB1	27.4	Transcriptional regulator	25-30
ARID1A	10.0	Chromatin remodeling	29, 30
ARID2	9.5	Chromatin remodeling	29, 30
JAK1	7.7	Kinase	27, 28
ALB	7.6	Serum protein	25, 29, 30
AXIN1	7.5	Signal transducer	25, 27-30
NFE2L2	5.1	Transcriptional regulator	29, 30
RPS6KA3	4.6	Kinase	25, 29, 30
CDKN2A	4.1	Cell cycle regulator	29, 30
COL11A1	4.1	Cytoskeletal protein	28, 30
RB1	4.0	Tumor suppressor	25, 29, 30
ACVR2A	3.9	Kinase receptor	29, 30
KEAP1	3.2	Proteinase adaptor	26, 29, 30
AR	3.2	Growth hormone receptor	26, 30
BRINP3	2.9	Unknown	28, 30

*Frequently mutated genes were selected from 6 published papers, and mutation frequency represents the average mutation rate in pooled data from the studies indicated in the far right column.

Telomerase promoter mutations are one of the key mutations in the HCC progression. These mutations that lead telomerase reactivation found in 59% of HCC cases (Dhanasekaran, Bandoh, and Roberts 2016). The WNT/b-catenin pathway that is crucial in embryogenesis and metabolic control of the liver, is the most affected oncogenic pathway in HCC. In this pathway, there are activating mutations of CTNNB1 (11%-37%), and inactivating mutations of AXIN1 (5%-15%), or APC (1%-2%),(Zucman-Rossi et al. 2015). Abnormal activation of β -catenin has been observed in 20-30% of HCC patients. Tumor protein 53 (TP53) which function as a tumor suppressor gene by initiating cell-cycle arrest, apoptosis, and senescence, is the second most frequently mutated gene in HCC cases (30%). Most mutations of TP53 in HCC are missense mutations located in the DNA-binding domain of TP53. These mutations cause a lower affinity to bind the sequence-specific response elements of TP53 target genes. While most mutations in TP53 result in loss of function, some mutations produce novel oncogenic activities that are independent of wild-type TP53 (gain-of-function mutations), such as angiogenesis, metastasis, and resistance to standard therapies. ARID1A and ARID2 which are epigenetic modifiers in

chromosome remodeling are also frequently mutated in HCC (in up to 20% of cases). Most cancer-associated mutations are loss-of-function mutations in ARID1A. These nonsense or frameshift rather than missense mutations in ARID1A are the dominant forms in HCC, showing that ARID1A is a tumor suppressor. ARID2 mutations that are less common than those in ARID1A, are also loss-of-function mutations in HCC (Lee 2015). The oxidative stress pathway is altered by activating mutations of NRF2 (coded by NFE2L2) or inactivating KEAP1 in 5%-15% of the HCC cases (Zucman-Rossi et al. 2015). Ras proteins are the switches of a large number of signaling pathways that control cell biology. Ras proteins have 2 main forms that are GDP-bound inactive and GTP-bound active. Proteins that determine the transition between these two forms are Ras guanine nucleotide exchange factors (GEFs) and Ras GTPase-activating proteins (GAPs). Although Ras, Raf activating mutations are not frequently observed in HCC (<2%), inhibition of Neurofibromin (NF1), a Ras GAPs, has been found to play a major role in keeping the Ras / MAPK signaling pathway active (Calvisi et al. 2011). In the CRISPR-Cas9 library scans at the genome level, NF1 is an important tumor suppressor gene in liver cancer and has an important role in the regulation of liver bipotent cell population during the carcinogenesis process (Song et al. 2017; Zender et al. 2010).

2.3. Human TERT Promoter Mutations in HCC

Telomeres that protect chromosomes from degradation, end-to-end fusion, and recombination, are short repeated DNA sequences (TTAGGG) located at the end of each chromosome. Because of the replication end problem, telomere shortened at each cell division. The telomerase complex composed of the core catalytic enzyme named telomerase reverse transcriptase (TERT) and of the RNA template named TERC, is to maintain the length of each chromosome to avoid DNA damage. Here, the TERT gene in humans that is positioned at chromosome 5p15.33 encodes for the catalytic subunit of the telomerase reverse transcriptase and it is an RNA-dependent DNA polymerase especially expressed in germ cells, stem cells, and cancer cells. While the activity of TERT is blocked in normal tissues, it is reactivated in tumors (Pezzuto et al. 2017; Ding et al. 2017; Nault and Zucman-Rossi 2016).

Senescent hepatocytes with short telomere and absence of telomerase activity are characterized by Cirrhosis. Studies showed that telomere deficient mice have a high rate of

cirrhosis when there is a chronic liver injury in the liver. However, for the malignant transformation on a cirrhotic background, telomerase reactivation is needed. TERT promoter mutation is identified as the first recurrent genetic alteration in cirrhotic preneoplastic macro nodules. Besides, TERT is shown as the earliest genomic happening currently identified in the multistep process of liver carcinogenesis on cirrhosis (Nault and Zucman-Rossi 2016). The upregulation of telomerase or its reactivation is a crucial property in over 90 % of cancers. Especially, TERT promoters have been found to be mutated in more than 50% of HCC tissue samples analyzed, this is the evidence of that TERT promoter mutation is the most frequently occurring single-nucleotide mutations observed in HCC (Jafri et al. 2016; Lee 2015). HCV positive HCC generally have higher TERT promoter mutations rates than HBV positive tumors, in which TERT overexpression is frequently caused by HBV integration. Besides, the remarkably high frequency of TERT promoter mutations in HCC caused by non-viral factors, such as alcohol consumption, metabolic syndrome or nonalcoholic fatty liver disease (NAFLD) is showed in studies. Because of these different factors, there is significant heterogeneity in the mutation frequency in HCC between geographic regions. The high ratio of the HCC mutated cases in different regions, and being one of the earliest events in the process of tumorigenesis show that TERT promoter mutation is a driver mutation and can be a reliable biomarker for early HCC diagnosis. (Pezzuto et al. 2017).

The TERT promoter region includes binding motifs for some factors that regulate the gene transcription and lacks a TATA box or a similar sequence. The region consists of 260 base pairs that designated as the hTERT promoter core is responsible for transcriptional activity. It contains at least five GC boxes (GGGCGG,) and two E-boxes (5'-CACGTG-3') that are transcription-factor binding sites. Zinc finger transcription factor SP1 binds to GC boxes and are essential for hTERT promoter activity. Also, p53 is shown to downregulate TERT transcription in an Sp1-dependent. MYC/MAX/ MXD1 family and USF1/2 enhancer-binding proteins are known as binding to E-boxes. While c-MYC required for promoter activation, MAD1 and USF1 to mediate hTERT repression so E-boxes are important for regulation. Besides, E-twenty-six (ETS) family members that comprise over 30 members, NF-kB, AP-2, and HIF-1 are the transcription factors for telomerase activation. Oncogenes EGF, Her2/Nez, Ras and Raf are shown to stimulate ETS transcription factors. For cellular immortalization through induction of TERT transcription during tumorigenesis, the activation of oncogenes and

inactivation of tumor suppressors are known to be considered (Jafri et al. 2016; Heidenreich et al. 2014).

Similar to other types of tumors, in HCC, promoter mutations create a potential binding site for E-twenty-six/ternary complex factors (ETS/TCF) to increase promoter activity and expression of TERT. Recently, a specific transcription factor called GABP that is a member of the ETS family, needed in the mutated form of the TERT promoter for the activation of the TERT expression has been found. These promoter mutations that create a new consensus binding sequence (CCGGAA or CCGGAT), are located in two hot spots found at 124 and 146 base-paired before the ATG start. One of them consists of C to T (-124C>T), substitutions with 93 percent of HCC in all cases. The second hot spot was situated at -146 bp from the ATG and characterized by C to T substitutions (-146C>T), with 6 percent of all HCC cases (Figure 2.2) (Jafri et al. 2016; Stern et al. 2015; Nault et al. 2013).

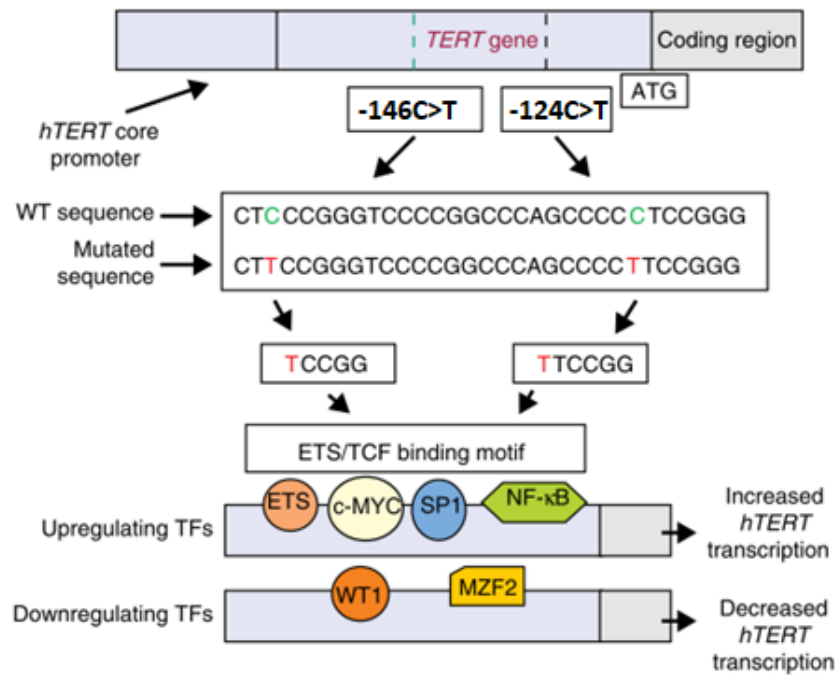


Figure 2.2: hTERT transcription and promoter mutations.

The hTERT gene is tightly repressed in almost all normal cells. However, hTERT promoter mutations are part of cancer progress leading to increased transcription of hTERT. There are some transcription factors (TFs) that regulate the hTERT transcription. While hTERT promoter mutations create ETS/TCF binding motifs, TFs such as ETS, c-MYC, SP1 and NF-κB bind to their binding sites and can promote hTERT transcription (Jafri et al. 2016).

2.4. Genome Editing Technologies

Recently, the rise of highly versatile genome-editing technologies has provided to introduce specific modifications to the genomes of many types of cells and organisms. These systems are transcription activator-like effector nucleases (TALENs), zinc-finger nucleases (ZFNs) and clustered regularly interspaced short palindromic repeats (CRISPR)-CRISPR-associated protein 9 (Cas9) (Gaj et al. 2016). TALENs and ZFNs are meganucleases which are artificial fusion proteins include an engineered DNA binding domain fused to a non-specific nuclease domain from the FokI restriction enzyme (Sander and Joung 2014). ZFN dimers make targeted DNA double-strand breaks (DSBs) that induce a DNA damage response. TALEs include multiple 33–35 amino acid repeat domains which each recognizes a single base pair. to enable custom alterations TALEs to induce targeted DSBs like ZNFs (Gaj, Gersbach, and Barbas 2013). While these platforms supply important advances, each has its own advantages and challenges. But recently, a novel platform CRISPR-Cas9 system has shown the highest specificity and efficiency and has become the most popular and powerful tool for genome engineering. In contrast to ZFN and TALEN platforms that use protein–DNA interactions, CRISPR-Cas9 system uses simple base pairing rules between an engineered RNA and the target DNA site (Sander and Joung 2014).

2.4.1. CRISPR Cas9 System

The CRISPR system is an adaptive immune mechanism of many bacteria and Archaea to fight invading nucleic acids, such as plasmids or bacteriophages. Cellular memory of the bacteria is created by the addition of short ‘protospacer’ sequences of foreign DNA into the CRISPR locus of the bacterial genome. Thus, under the same infection, inserted sequences can be transcribed into CRISPR RNA (crRNA), which recognizes complementary sequences on foreign DNA. Then crRNA can hybridize with trans-activating crRNA (tracrRNA) to be functional, to guide Cas nuclease for the cleavage of foreign DNA (Wang, La Russa, and Qi 2016). A combination of crRNAs with tracrRNAs into a single guide RNA (sgRNA) further simplified usage of the system and showed higher efficiency. There are identified three different types of CRISPR systems, and type II is the most commonly used system for genome editing because it needs only one Cas protein, Cas9 (Thurtle-Schmidt and Lo 2018).

Cas9 is a large DNA endonuclease from *Streptococcus pyogenes* which induces DSBs in a genomic target sequence directed by RNA guide. Before cleavage of the target DNA, the Cas9 nuclease is conformationally changed by sgRNA binding and is directed to the target genomic site (Zhan et al. 2018). After the CRISPR system components, Cas9 protein, and sgRNA have entered a cell, sgRNA designed as 20 nucleotide binds to its complementary DNA site. Then Cas9 cuts 3 base pairs (bp) upstream of a protospacer adjacent motif (PAM, consisting of an NGG or NAG sequence) site which serves as a binding signal for Cas9. For Cas9, the PAM sequence NGG has higher efficiency than NAG (Figure 2.3) (Ventura and Dow 2018).

In the host cell, there are two different repair mechanism response to DSB induced by Cas9. One of them is non-homologous end joining (NHEJ) which rapidly piece together the ends of DNA. This generally leads to insertions or deletions (indel) in the genome near the cut site of the Cas9-sgRNA complex. Formed indels can cause frameshift mutations and early stop codons in the target gene, which result in loss-of-function (Zhan et al. 2018). Another system is homology-directed repair (HDR) which is based on assisted DNA recombination to rebuild cleaved DNA. Thus, there is a need for a homologous template to fix the damage. Thanks to a single-stranded or double-stranded DNA template, a defined change at a specific locus of a cell's genome can be performed (Figure 2.3) (Adli 2018).

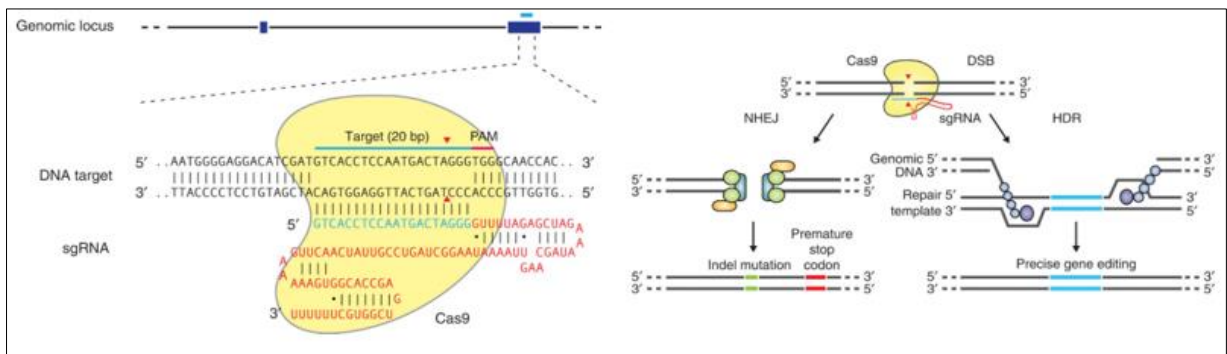


Figure 2.3: CRISPR- Cas9 System and its working mechanism.

The Cas9 nuclease (in yellow) is targeted to genomic DNA by a sgRNA (blue) and a scaffold (red). The guide sequence pairs with the DNA target (blue bar on the top strand), directly upstream of a requisite 5'-NGG adjacent motif (PAM; pink). Cas9 mediates a DSB ~3 bp upstream of the PAM (red triangle). DSB repair promotes gene editing. DSBs induced by Cas9 (yellow) can be repaired in two ways that are NHEJ pathway or the HDR pathway (Ran et al. 2013).

2.5. Organoid Technology

Organoids are 3D cell structures that mimic some of the functional and structural characteristics of an organ. These characteristics of an organ mimicked by organoids are that the organoids contain more than one cell type of the organ, exhibit some function specific to the organ, and have the cell organization similarity as the organ itself. Besides, there should be a similarity to the behavior in which the organ set up its typical organization during development. (Kratochvil et al. 2019; Lancaster and Knoblich 2014). Specific stem cell signaling pathways are important for development, and they manage organoid formation. So, there is a need for growth factors and small molecules in the organoid culture environment to sustain self-renewal, differentiation, and proliferation often in a tissue-specific manner. There is a different source of starting material for organoid formation. These are pluripotent embryonic stem cells (ESC), induced pluripotent stem cell (iPSC) and adult stem cells (aSCs). Modeling of organoids such as the brain, retina, intestine, pancreas, liver, and kidney from these materials has been established in different studies (Clevers 2016).

2.5.1. Liver organoids

After the discovery of self-renewing stem cells and the discovery of Lgr5 protein expressed from all stem cells in the intestinal epithelium, Lgr5 becomes a marker of stem cells in the tissues for example liver (Barker et al. 2007). One of the early liver organoid studies is established from aSCs by Huch et al in 2013. In this work, extracted Lgr5+ cells after post damage induction from mouse livers cultured in Matrigel was used to form mature liver organoids. Cells showed self-organization in long-term expansion as adult ductal progenitor cells while retaining the ability to differentiate into functional hepatocyte-like cells *in vitro* (Huch et al. 2013). In 2015, the same group uses EPCAM+ human bile duct-derived bipotent progenitor cells. Cultured cells *in vitro* for a long period have proliferation and differentiation capacity into functional liver organoids, like Lgr5+ cells. These organoids differentiate into functional liver tissue after implanted into immunodeficient mice (Huch et al. 2015). In another study was done by Vyas et al in 2017, human fetal liver progenitor cells were cultured inside a cellular liver extracellular matrix (ECM) scaffolds to form 3D liver organoids. 3D organoid

structures exhibited some of the physiological functions and the liver-biliary anatomy of mature liver tissue (Vyas et al. 2018).

Besides, there are works for the liver organoid establishment by using iPSCs. One of the studies differentiate iPSC cells into hepatic endodermal cells and mixed them with mesenchymal and endothelial cells for vascularization. 3D mixed structure showed vascularization, and iPSC derived tissue showed hepatic functions such as protein production and human-specific drug metabolism (Takebe et al. 2013). iPSCs derived organoid study were worked by Guan et al in 2017. They established hepatic organoids from iPSCs, which include both cholangiocytes and hepatocyte. Cholangiocyte markers show that the lumina of ductal structures and hepatocytes surrounded by cholangiocytes (Guan et al. 2017). In 2018, Zhang et al established liver bud tissue differentiated from human iPSCs. They differentiate iPSCs into posterior gut endoderm cells, then liver bud tissue was differentiated from progenitor cells of the posterior intestine. In immunodeficient mice, there were shown mature functional liver cells and biliary epithelial cells formed from liver bud tissue (Zhang et al. 2018). Recently, our team who work on an iPSC derived hepatic organoids, published their data which includes modeling of Citrullinemia Type 1. There are shown that hepatic organoids display long-term expansion, *in vitro* maturation. When transferred from expansion median to differentiation median, liver organoids showed functional hepatocyte characteristics of albumin production and cytochrome activity. According to the *in vitro* functional assays they are able to uptake LDL, accumulate lipid and store glycogen. They express CK18 (specific marker for hepatocyte), E cadherin (epithelial marker), Ck19 (hepatoblasts&cholangiocyte marker), ZO1 (for tight junctions between cells), A1AT (Alpha-1 antitrypsin-glycoprotein) and ALB which are specific proteins synthesized in the liver. There are tight junctions between cells and secretory villus on the apical side of hepatocytes. In immunohistochemical analysis, cells in organoids display pseudostratified structure and epithelioid structure specific to epithelial tissue, and biliary ductal shapes specific to the liver. Besides, gene enrichment analysis shows liver-specific signatures (Figure 2.4) (Akbari, Sevinc, et al. 2019)

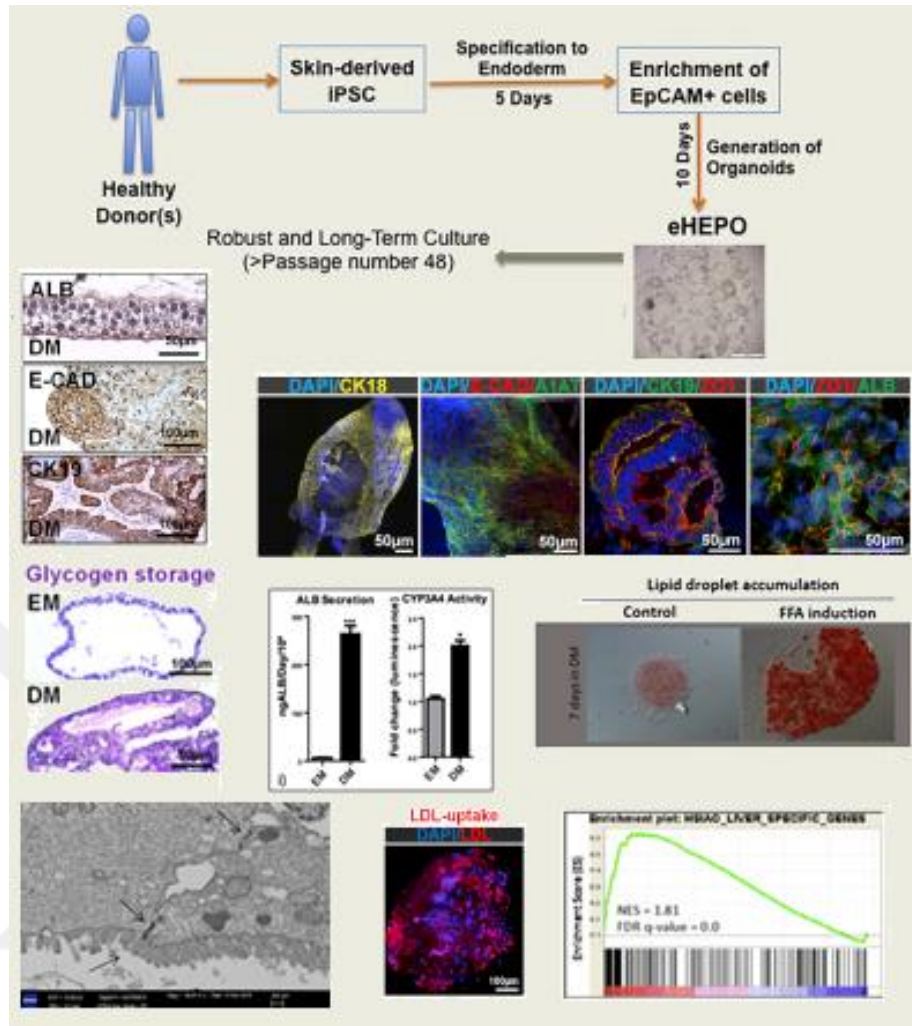


Figure 2.4: Schematic presentation of hepatic organoid production and functional analysis of the organoids.

Mature hepatic organoids (DM organoids) express CK18, E cadherin, Ck19, ZO1, A1AT, and ALB. There are tight junctions between cells and secretory villus on the apical side of hepatocytes. In immunohistochemical analysis, cells in organoids display pseudostratified structure and epithelioid structure specific to epithelial tissue, and biliary ductal shapes specific to the liver. Gene enrichment analysis shows liver-specific signatures (Akbari, Sevinc, et al. 2019).

2.5.2. Disease Modelling in Organoids

Organoids are a powerful new system to work a wide range of studies especially on disease modeling such as infectious disease, hereditary disease, and cancer. The main aim of modeled human disease organoids is establishing a source for drug screening, genotype-phenotype testing, biobanking for specific diseases and future personalized treatments.

Organoids can be used to model inborn conditions from stem cells of patients carrying the genetic mutation. Besides, they can be used to model acquired diseases such as those in the case of cancer (Lancaster and Huch 2019). Thus, they are a new system comparable to genetically engineered mouse models (GEMMs), cell lines, and patient-derived xenografts (PDXs) to study tumorigenesis (Tuveson and Clevers 2019).

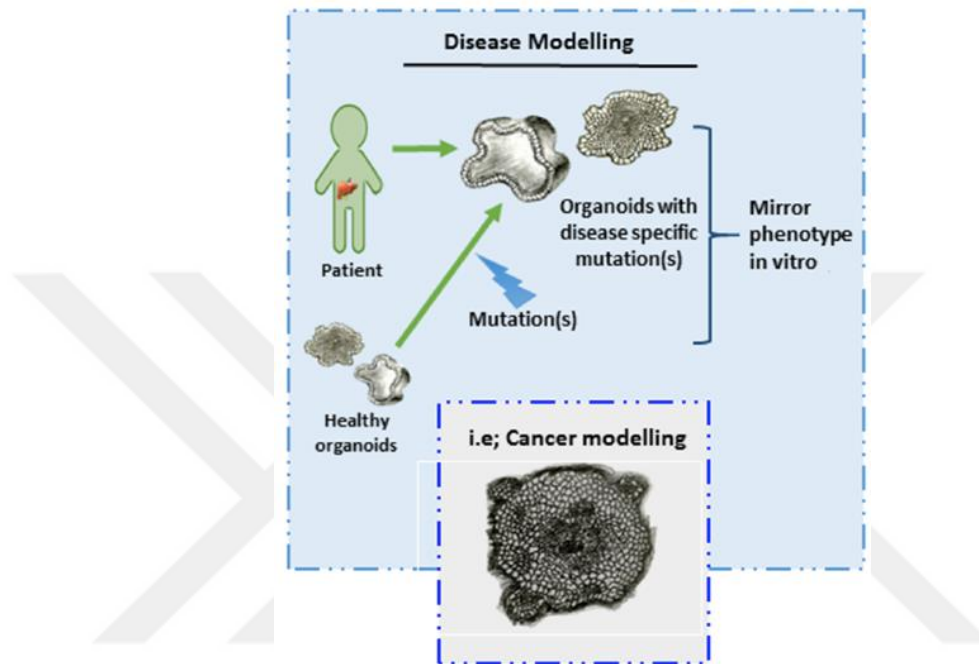


Figure 2.5: Disease modeling strategies in organoid culture.

For the disease/cancer modeling in organoids, one of the sources can be directly tissue of the patient. Also, healthy organoids derived from the aSC or ESC can be used by introducing mutations with gene-editing systems such as CRISPR/Cas9 system (Akbari, Arslan, et al. 2019).

The human cancer organoids not only can be generated directly from neoplastic tissues as patient-derived organoids but, they can be developed from normal tissue by genetic modification of organoids. (Figure 2.5). There are organoids derived from primary carcinoma samples that have been generated under ASC-organoid conditions to study such as prostate cancer, breast cancer and pancreatic ductal adenocarcinoma (Tiriatic et al. 2018; Buzzelli et al. 2018; Gao et al. 2014). However, there are also iPSC/ASC-based organoids generated by introducing of cancer-causing mutations via CRISPR-Cas9 technology. One of the studied modeled colorectal cancer by introducing a combination of genes commonly mutated (APC, KRAS, SMAD4, TP53) in normal intestinal organoids through CRISPR/Cas9 genome editing

(Matano et al. 2015). Recently, organoids and CRISPR/Cas9 systems have also been used together to study the mechanism of pancreatic cancer progression (Huang et al. 2015; Seino et al. 2018). There is another study that modeled glioblastoma by CRISPR/Cas9 introducing RAS and TP53 mutations in ES cell-derived cerebral organoids (Ogawa et al. 2018). Recently, the organoid model for cholangiocarcinoma has been established from human liver organoids by combining four common cholangiocarcinoma mutations TP53, PTEN, SMAD4, and NF1 (Artegiani et al. 2019). All of these studies show that organoid technology combined with CRISPR/Cas9 provides an experimental platform for mechanistic studies of cancer gene function in a human context. Despite cholangiocarcinoma organoids were established via CRISPR-Cas9, HCC organoids through CRISPR/Cas9 genome editing in normal liver organoids have not been reported yet (Wu et al. 2019).

3. MATERIALS AND METHODS

3.1. Type of Research

The type of research carried out in this study is experimental.

3.2. Time and Place of Research

Experimental procedures were carried out at Erdal Lab at Izmir Biomedicine and Genome Center between July 2018 and December 2019.

3.3. Working Material

3.3.1. Primers

Mutation primers (Table 3.1) were designed by using tmcalculator.neb.com and bugaco.com. Sequencing and HR primers and gRNAs were designed according to the reference paper (Xi et al. 2015).

Table 3.1: Primers used in experiments.

Red-colored sequences are restriction sites; blue-colored sequences represent the extra bases required by the restriction enzymes. The yellow highlight shows C >T mutation region. Green colored sequences are cloning sites for gRNA.

PRIMER NAME	SEQUENCE (5'-3')
Mutation Primers	
hTERT-prom-F	CCAGTGAATTC ^{CCCTTCACGTCCGGCATT}
hTERT-prom-R	GAGCCAAGCTT ^{TCGGGCCACCAGCTCCTT}
hTERT-C124T-F	CCCAGCCCC ^T TCGGGGCCCTCCCA
hTERT-C124T-R	TGGGAGGGCCCGGA ^A GGGGCTGGG
hTERT-C146T-F	TCCCGACCCCT ^T CCGGGTCCCCGG
hTERT-C146T-R	CCGGGGACCCGGA ^A AGGGGTTCGGGA
SV40 hTERT-prom-F	ATTAAGTGAATTC ^{CCCGGAGCCCGACGC}

SV40 hTERT-prom-R	AATACCAAGCTTCGCATGTCGCTGGTTC
SV40 hTERT-C146T-F	GTCCCGACCCCTCCGGGTGGTCGA
SV40 hTERT-C146T-R	TCGACCACCCGGAAGGGGTCTGGGAC
Sequencing Primers	
M13/pUC Forward	CCCAGTCACGACGTTGTAAAACG
M13/pUC Reverse	AGCGGATAACAATTTACACAGG
EGFP-N (Reverse)	CGTCGCCGTCCAGCTCGACCAG
hU6-F	GAGGGCCTATTTCCCATGATT
Guide RNAs	
G1 (G148/147)-F	CACCGCGCCCCGTCCCGACCCCTCC
G1 (G148/147)-R	AAACGGAGGGGTCTGGGACGGGGCGC
G2 (GupGFP)-F	CACCGATTCCACAGGGTCTGACCACC
G2 (GupGFP)-R	AAACGGTGGTCTGACCCTGTGGAATC
G3 (GdownGFP)-F	CACCGTCTTCGGACCTCGCGGCC
G3 (GdownGFP)-R	AAACGGGCCGCGAGGTCCGAAGAC
HR Primers	
a'	CGTCCAGGGAGCAATGCGT
e'	ACGCTGGTGGTGAAGGCCTC

3.3.2. Vectors and Bacterial Strains

All the vectors are listed in table 3.2. Their maps are shown in Figure 3.1,3.2 and 3.3.

All cloning experiments are achieved with DH5a or Stab13 *E. coli* cells, which were used for cloning a desired gene/plasmid.

Table 3.2: Vectors and their bacterial strains used in experiments.

Vector Name	Addgene Number	Backbone	Size (bp)	Bacterial Strain	Antibiotic
pX330-U6-Chimeric_BB-CBh-hSpCas9	#42230	pUC	8494	DH5a	Kanamycin
HR-TERT-SV40-GFP	#72397	pUC57	4596	Stab13	Ampicillin
HR-TERT-Promoter	#71398	pUC57	3538	Stab13	Ampicillin

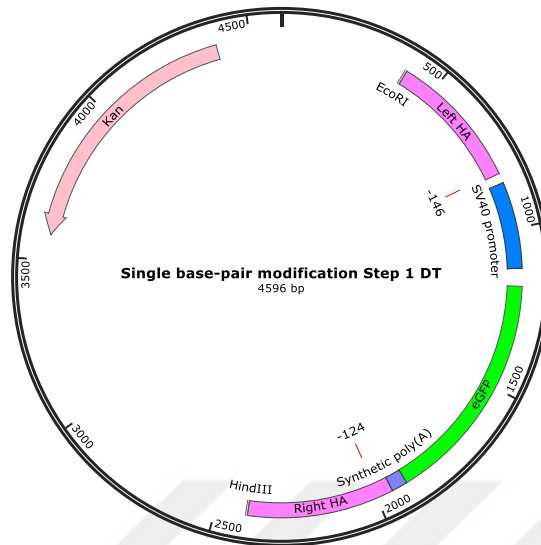


Figure 3.1: Scheme of the HR-TERT SV40 GFP Plasmid.

Homologs recombination donor plasmid for the TERT promoter region introducing an SV-40 (blue) driven GFP marker (green) in the TERT promoter (pink). Includes 1kb of the TERT coding region in the right homologs arm. It has a kanamycin resistance cassette (orange), which enables the selection of positive bacterial clones used for plasmid expansion. The plasmid map was generated using SnapGene Viewer, version 4.2.6.

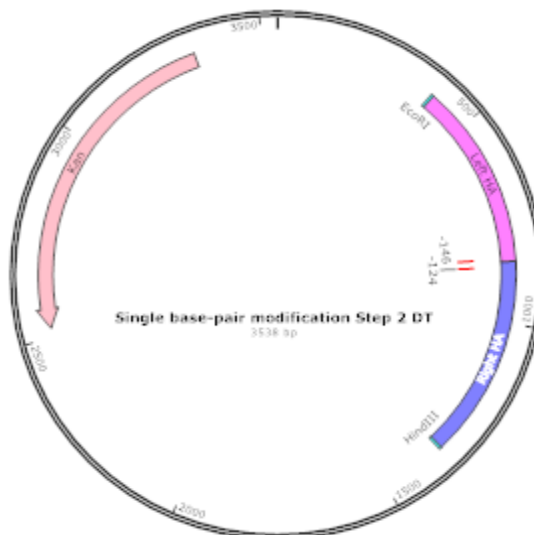


Figure 3.2: Scheme of the HR-TERT Promoter Plasmid.

Homologs recombination donor plasmid of the wild type TERT promoter region (pink-blue). Includes 1kb of TERT coding region in the right homologs arm. It has a kanamycin resistance cassette (orange), which enables the selection of positive bacterial clones used for plasmid expansion. The plasmid map was generated using SnapGene Viewer.

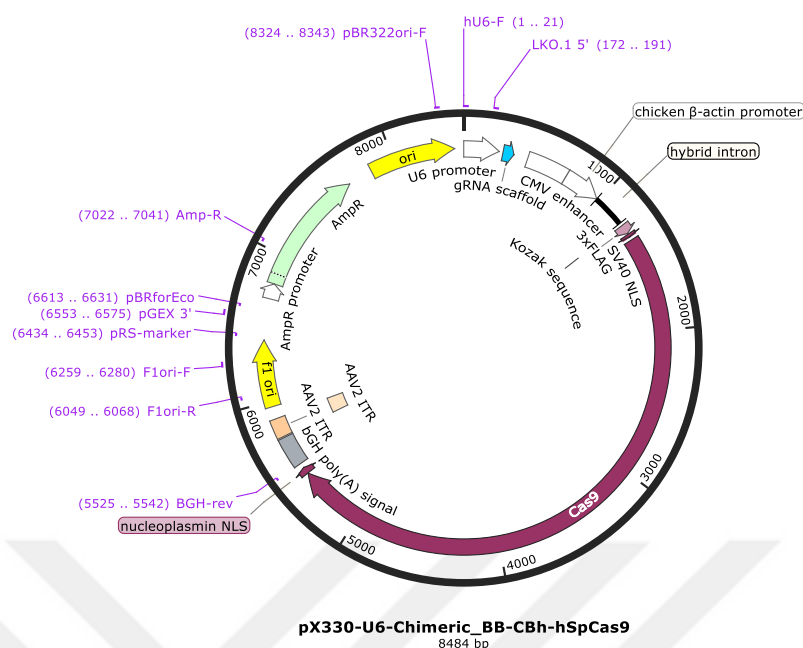


Figure 3.3: Scheme of the px330 plasmid.

The plasmid encodes Cas9 nuclease (purple). It harbors a BbsI restriction site for sgRNA insertion (blue) under U6 promoter (white), and an ampicillin resistance cassette (light green), which enables the selection of positive bacterial clones used for plasmid expansion. The plasmid map was generated using SnapGene Viewer.

3.3.3. Enzyme and Kits

Table 3.3: Enzyme and Kits

<i>Enzyme/Kit</i>	<i>Vendor</i>	<i>Catalogue#</i>
FastAP Thermosensitive Alkaline Phosphatase	Thermo Scientific	EF0651
Phusion High-Fidelity Polymerase	NEB	M0530S
Phusion High-Fidelity Polymerase	Thermo Scientific	F-530S
Dream Taq DNA Polymerase	Fermentas	EP0709
Hot Start Taq DNA	Fermentas	EP0602
FastDigest Restriction Enzymes 1. EcoRI 2. HindIII 3. Bpil	1-2.NEB 3.Thermo Scientific	1.R3101S 2.R3104S 3.FD1014

T4 DNA Ligase	NEB	M0202L
6X Loading Dye	Fermentas	R0611
Generuler 100bp DNA Ladder	Fermentas	SM0241
Generuler 1kb DNA Ladder	Fermentas	SM0318
1kb DNA Ladder	NEB	N3232S
T4 Polynucleotide Kinase	NEB	M0201S
Purelink Genomic DNA Minikit	Invitrogen	K1820-02
NucleoBond Xtra Midi Plus	MN	740412.10
QIAquick Gel Extraction Kit	QIAGEN	28704
PureLink Genomic DNA Mini Kit	Invitrogen	K1820-02

3.3.4. Commonly used Softwares and databases

Table 3.4: Commonly used Softwares and databases

Software	Purpose of Use	Company/Web page
National Center for Biotechnology Information web site	To obtain DNA sequences and to make a literature search	www.ncbi.nlm.nih.gov
Image Lab 5.2.1	To analyze gel images	Bio-Rad
ImageJ	To edit microscopy images	
Flow Jo	To analyze the flow and cell sorting results	
SnapGene Viewer	To create, browse, and share annotated DNA and plasmid sequence files	https://www.snapgene.com/

3.3.5. Commonly used buffers, solutions, and media

Table 3.5: Commonly used buffers, solutions, and media

Buffer/Media	Components
LB medium, 1lt	10g tryptone, 5g yeast extract, 10gNaCl, pH:7.4 (autoclaved)
LB plates, 400ml	4g tryptone, 2g yeast extract, 5g NaCl, 6g agar (autoclave in a flask, cool down to 40-45°C, add antibiotics and pour into petri dishes)
1X TAE electrophoresis buffer, 1lt	20 ml 50X TAE electrophoresis buffer, 980ml distilled water
1X PBS	50ml 10C PBS (Gibco) + 450 ml autoclaved ddH ₂ O

%10 High Glucose DMEM	500 ml High Glucose DMEM, (1% Pen/Strep, 1 % Nonessential amino acid, 1% Glutamax, 10% FBS (Gibco))
EM (Expansion) Media	Advance DMEM/F12 (Invitrogen) supplemented with 1% B27 (Gibco), 1.25 mM N-acetylcysteine (Sigma), 10 nM gastrin (Sigma), and the growth factors: 50 ng/mL epidermal growth factor (EGF) (Peprotech), 10% R-spo1 conditioned medium (home-made), 100 ng/mL fibroblast growth factor 10 (FGF10) (Peprotech), 25 ng/mL hepatocyte growth factor (HGF) (Peprotech), 10mMnicotinamide (Sigma), 5 mMA83.01 (Tocris), and 10 mM forskolin (Tocris).

3.3.6. Special Instruments

Table 3.6: Special Instruments

Instrument Name	Purpose of Use	Vendor
MicroCL_17R centrifuge	Tabletop high-speed centrifuge for purifying by centrifugation	Thermo Fisher Scientific
SimpliAmp Thermal Cycler	PCR, amplifying DNA	Applied Biosystems
Miniprotean Tetra System	SDS PAGE	Bio-Rad
OWL EasyCast B1A	Electrophoresis	Thermo Fisher Scientific
MaxQ4000	Orbital shaker for bacteria incubation	Thermo Fisher Scientific
Centrifuge 5810R	To obtain bacterial pellet	Eppendorf
NanoDrop2000 Spectrophotometer	Measure purified DNA concentration	Thermo Fisher Scientific
Gel Doc™ XR+ System	Agarose and SDS PAGE Imaging	Bio-Rad
Nucleofector 4d	Transfection with electroporation	Lonza
FACSaria™ III	Cell Sorting based on GFP signal	BD
LSRFortessa	Cell Analysis based on GFP signal	BD

3.3.7. Mammalian cell lines

HEK293T (Human embryonic kidney) cell line was used for optimizing the experiments.

3.4. Research Variables

Hepatic organoid and HEK293T cell culture are independent variables. Transfection of Hepatic organoid and HEK293T cells is the independent variable. GFP expression of the cells and insertion of hTERT promoter mutations are dependent variables.

3.5. Data Collection Tools/Methods

3.5.1. Primer design

In order to make mutations on HR-TERT-SV40-GFP and HR-TERT-Promoter WT plasmids, the HindIII and EcoRI restriction site region and mutation region on the hTERT promoter were used for primer design which includes HR-TERT-SV40-GFP 146C>T, HR-TERT-Promoter 146C>T, 124C>T mutations. Sequencing primers, HR primers, and gRNAs were synthesized according to the referenced article. (Xi et al. 2015) (Table:1). gRNAs were synthesized as two oligos of the form on the below;

5' – CACCGNNNNNNNNNNNNNNNNNNNN – 3'

3' – CNNNNNNNNNNNNNNNNNNNNCAAA – 5'

3.5.2. Polymerase Chain Reaction (PCR)

3.5.2.1. Two-Step PCR for Mutagenesis

This PCR procedure includes two stages. In step one, two different extension reactions are performed in separate tubes; one contains the forward primer (include C>T mutation) and

the other contains the reverse primer (Restriction Enzyme cut site). Subsequently, the two reactions are mixed, and the overlap extension was performed (Figure 3.4).

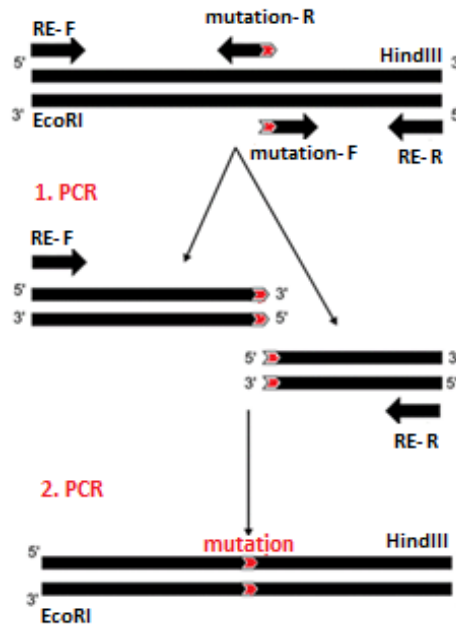


Figure 3.4: Workflow of the two-step PCR.

Two PCR was set up for the first step. The second PCR was performed for overlap extension with RE-F and RE-R primers (Castorena-Torres, Peñuelas-Urquides, and de León 2016).

High fidelity PCR was used to introduce mutations of hTERT Promoter on the HR-TERT-SV40-GFP/HR-TERT-Promoter WT plasmid. High Fidelity Phusion DNA Polymerase (NEB) was used (Table 3.7). All primers were purchased from BM Labosis and their size is approximately 30 nucleotides. For the first step, 10 ng of each plasmid, 3% DMSO concentration and mutation primers in Table 1 were used. For overlap extension primers include RE sites were used. After these reactions, 124C>T, 146C>T on HR-TERT-Promoter Plasmid were obtained. To obtain the 124 + 146C> T change on the TERT-Promoter plasmid, the 124C> T PCR product was used as the template, and the 146C> T change was added. Overlap extension for HR-TERT-SV40-GFP 146C> T change was performed with the Thermo Fisher Phusion High-Fidelity DNA Polymerase protocol, using 68°C for annealing temperature, after the reaction 146C>T transition on HR-TERT-SV40-GFP plasmid was obtained (Table 3.8)

Table 3.7: PCR conditions and cycles with NEB Phusion HF DNA Polymerase

NEB Phusion HF DNA Polymerase Components	20 μl Reaction	Final Concentration
Nuclease-free water	to 20 μ l	
5X Phusion GC Buffer	4 μ l	1X
10 mM dNTPs	0.4 μ l	200 μ M
10 μ M Forward Primer	1 μ l	0.5 μ M
10 μ M Reverse Primer	1 μ l	0.5 μ M
Template DNA	variable	< 250 ng
DMSO	10.6 μ l	3%
Phusion DNA Polymerase	0.2 μ l	0.02 uM each

Step	Tm	Time
Initial Denaturation	98°C	2 minutes
25-35 Cycles	98°C	15 seconds
	68°C	30 seconds
	72°C	45 seconds
Final Extension	72°C	10 minutes
Hold	4°C	

Table 3.8: PCR conditions and cycles with Thermo Fisher Phusion HF DNA Polymerase

Thermo Phusion HF DNA Polymerase Components	50 μl Reaction	Final Concentration
Nuclease-free water	to 50 μ l	
5X Phusion GC Buffer	10 μ l	1X
10 mM dNTPs	1 μ l	200 μ M
10 μ M Forward Primer	2.5 μ l	0.5 μ M
10 μ M Reverse Primer	2.5 μ l	0.5 μ M
Template DNA	variable	< 250 ng
DMSO	1.5 μ l	3%
Phusion DNA Polymerase	0.5 μ l	1 units/50 μ l PCR

Step	Tm	Time
Initial Denaturation	98°C	30 seconds
25-35 Cycles	98°C	10 seconds
	60°C	20 seconds
	72°C	30 seconds
Final Extension	72°C	10 minutes
Hold	4°C	

3.5.2.2. PCR for HR determination

After the first and second transfection of the plasmids into HEK293T, GFP+ /GFP- single cell/or bulk clones screened by PCR with the primer pair a'-e' (Table 1). For these reactions, Phusion DNA Polymerase was used after optimization (Table 3.8).

3.5.2.3. Colony PCR

In order to control the cloning of gRNAs, colony PCR was used as control before midprep. hU6 promoter primer, reverse gRNA primer and Tag DNA Polymerase were used. A single colony is used as template DNA, the colony is removed by the pipette tip and the pipette tip is inverted several times into the PCR tube (Table 3.9).

Table 3.9: PCR conditions and cycles for Colony PCR

Components	Reaction Volume (ul)
10X Taq Buffer	2,5
MgSO ₄	1
10mM dNTPs	0,5
Forward primer (U6 promoter primer) (10μM)	0,8
Reverse primer (Reverse oligo) (10μM)	0,8
Taq Polymerase (5U/μl)	0,25
dH ₂ O	19,75
Total	25

Step	Tm	Time
Initial Denaturation	95°C	5 minutes
25-35 Cycles	95°C	30 seconds
	60°C	30 seconds
	68°C	30 seconds
Final Extension	68°C	5 minutes
Hold	4°C	

3.5.3. Molecular Cloning

3.5.3.1. Cloning of sgRNAs

pX330-U6-Chimeric_BB-CBh-hSpCas9 plasmid was used for the simultaneous expression of the Cas9 enzyme with the gRNA. Feng Zhang Lab's gRNA cloning protocol was used. According to protocol the plasmid was cut using BbsI restriction enzyme according to the manufacturer's instructions and to prevent self-ligation alkaline phosphatase (FastAP, Thermo Scientific) was used in the reaction. The digested plasmid was extracted from a 1% agarose gel. Oligonucleotides were designed as forward and the reverse was phosphorylated and annealed in a thermocycler using T4 Polynucleotide Kinase (T4 PNK, NEB) and the following protocol: 37°C for 30 minutes, 95°C for 5 minutes, with cooling to 25°C at a rate of 5°C/min. Then, 50 ng of the digested pX330-U6-Chimeric_BB-CBh-hSpCas9 plasmid was set up for ligation with 1/20 diluted of the annealed oligonucleotides at 22°C for 2 hours using T4 DNA ligase according to manufacturer's protocol.

3.5.3.2. Cloning of Mutant PCR products after 2 Step PCR

After 2 step PCR, the mutant products have EcoRI and HindIII restriction enzyme sites on the ends of the DNA pieces cloned into the HR-TERT-SV40-GFP/HR-TERT-Promoter WT plasmid. The PCR products were loaded on the 1% agarose gel were extracted from gel. Then all extracted DNA was cut with both EcoRI and HindIII enzymes according to the manufacturer's protocol. 1 µg of HR-TERT-SV40-GFP/HR-TERT-Promoter WT plasmid was cut with both EcoRI and HindIII enzymes according to the same protocol and loaded on 1% agarose gel, the backbone part of the plasmid was purified from the gel. For the ligation reaction the calculation was used on the below;

$$\text{Insert Mass in ng} = 3 \times \left[\frac{\text{Insert Length in bp}}{\text{Vector Length in bp}} \right] \times \text{Vector Mass in ng}$$

50 ng of the digested HR-TERT-SV40-GFP/HR-TERT-Promoter WT plasmid was used for ligation with insert oligonucleotides at 22°C for 2 hours using T4 DNA ligase according to manufacturer's protocol.

3.5.3.3. Restriction Digest

Restriction digestions were carried out either for control of the plasmid's size or for the cloning of DNA. Restriction enzymes HF-HindIII, HF- EcoRI and their reaction buffers were purchased from NEB. Reaction mixtures were incubated at 37°C 5-15 minutes then 80°C for 20 min for heat inactivation. Restriction enzyme Fast Digest BbsI and their reaction buffers were purchased from Thermo Scientific. Reaction mixtures were incubated at 37°C for 30 minutes (Table 3.10).

Table 3.10: Restriction Digestion components

Restriction Digest for HF-HindIII and EcoRI	
Template DNA	1 µg
10 X NEBuffer	2µl
REnzyme	1µl
ddH2O	X
Total	50 µl

Restriction Digest for Fast Digest BbsI	
Plasmid	1 µg
10 X Fast Digest Buffer	2µl
Fast Digest BbsI	1µl
FastAP	1 µl
ddH2O	X
Total	20 µl

3.5.3.4. Ligation

All ligation reaction was performed by T4 DNA ligase purchased from NEB, and at room temperature for 2 hours (Table 3.11).

Table 3.11: Ligation components

Ligation reaction	
Vector DNA (4kb)	50ng
Insert DNA (1kb)	37.5ng
T4 DNA ligase (NEB)	1 µl
10X Ligation Buffer (NEB)	2µl
ddH2O	up to 20µl

3.5.3.5. Transformation of chemically competent E. coli Stbl3

Heat shock transformation was applied, for this 100µl aliquots of competent cells were thawed on ice and mixed with a 10µl completed ligation reaction. After incubation on ice for 30 min, heat shock was applied by incubating the cells at 42°C water bath for 90 seconds. Cells were immediately placed on ice for 2 minutes. 900 µl of LB medium added on the tubes and shake at 200rpm, 37°C for 1 hour. After the incubation, cells were centrifuged at 2500rpm for 3 minutes, the supernatant was removed. Pellet was resuspended in 100 ul of LB medium than spread on an ampicillin/kanamycin (according to plasmid was used) containing LB plate. LB plates were incubated at 37°C overnight, 16-18 hours, until colonies appeared. For miniprep, colonies of bacteria were grown in 5 ml of LB medium containing antibiotics. After miniprep, all plasmids were checked by Sanger sequencing (BM laborious).

3.5.4. Agarose Gel Extraction and PCR clean up

QIAquick Gel Extraction Kit was used according to the manufacturer's protocol to obtain DNA from agarose gel. QIAquick PCR Purification Kit was used according to manufacturer's protocol to PCR clean up and their concentration was measured using nanodrop.

3.5.5. Genomic DNA Purification

PureLink Genomic DNA Mini Kit was used according to manufacturer's protocol to obtain genomic DNA and their concentration was measured using nanodrop.

3.5.6. Miniprep and Midiprep of Plasmid DNA

For miniprep, the protocol in Current Protocols in molecular biology is used. NucleoBond Xtra Midi Plus Kit was used according to manufacturer's protocol to obtain vector DNA and their concentration was measured using nanodrop.

3.5.7. Cell culture

HEK293T cell line was provided from Izmir Biomedicine and Genome Center. These cells were grown in high glucose Dulbecco's modified Eagle medium (DMEM) supplemented with 10% FBS, 1% Penicillin/Streptomycin, 1% L-Glutamine and 1% Nonessential amino acids components. The whole process took place under the laminar flow cabinet and the cells were incubated at 37 C°, 5% CO₂, 95% humidified incubator. Usually, when the cell confluency was 70%-80%, they were washed with 1x PBS then they were treated with 0.25 % Trypsin/EDTA. Depending on the growth rate of cells, the cells were split into cell culture plates or flasks.

3.5.8. Hepatic Organoid Culture

In a previously completed Tubitak 1003 project, which was conducted jointly by Koç University and İzmir Biomedicine and Genome Institute, we already produced Hepatic Organoids from iPSCs. In this study previously produced EM hepatic organoids were used. We removed cryovials containing the frozen EM hepatic organoids from liquid nitrogen storage. We thawed the organoids in the medium. After organoids were centrifuged, the supernatant was removed. Then organoid pellet was mixed with Matrigel with a ratio of Matrigel to cell suspension of 7:3 and seeded in 6-well cell culture plates. These organoids were cultured in Expansion Medium (EM) which consisted of Advanced DMEM /F12 with 1% B27 without vitamin A and 1.25 mM N-acetylcysteine, 10nM gastrin, 50ng/ml EGF, 10% RSPO1 conditioned medium (CM) (home-made), 100ng/ml FGF-10, 25ng/ml HGF, 10mM Nicotinamide, 5uM A83.01, 10uM Forskolin. After 7-10 days, the organoids were removed from the Matrigel, mechanically dissected and transferred into the fresh matrix. When Matrigel was solidified, the EM culture medium was added. The passage was performed at a rate of 1:2 to 1:4 every 7-10 days.

3.5.9. Transfection Methods

3.5.9.1. HEK293T Transfection

X-tremeGENE HP DNA Transfection Reagent was used according to the manufacturer's instructions. Before the transfection cells were seeded in 6wp as 1×10^6 /well. For the first transfection of HEK293T 2 ug HR-TERT-SV40-GFP-146 and 2 ug pX330-G1 vectors were used with the 1:2 plasmid/reagent ratio, the control group was the cells that transfected with 2 ug HR-TERT-SV40-GFP-146 plasmid. For the second transfection of the GFP+ single-cell clones, pX330-G2 and pX330-G3 was used with the combination of HR-TERT-Promoter-124/HR-TERT-Promoter-146/HR-TERT-Promoter 124+146 plasmid.

3.5.9.2. Organoid Transfection

Initially, three different reagents were tested for the transfection of the hepatic organoids. These reagents were X-tremeGENE HP DNA Transfection Reagent, Polyethylenimine (PEI) and Lipofectamine 2000 Reagent. Different ratios of plasmid and reagent (1:5/ 1:7 /1:10) were used for optimization in 12/96 ultralow attachment well plates. Two different organoid transfection protocol with Lipofectamine 2000 were applied (Drost, Artegiani, and Clevers 2016; Broutier et al. 2016). After these trials, Amaxa 4D-Nucleofector System was used to introduce pX330 Cas9-gRNA G1 plasmid and HR-TERT-SV40-GFP DT plasmid into hepatic organoids. Amaxa P3 Primary Cell 4D-Nucleofector™ X Kit (S & L) was used to optimize the transfection conditions. For these optimization applications, 1×10^5 cells and 1ug HR-TERT-SV40-GFP DT plasmid were introduced with different pulse conditions (for S kit). These pulses were EX-147, FF-147, DC-100, EQ-133, EP-138, EY-147, CA-137.

3.5.10. FACS and Flow Cytometry

Trypsinized cells were spun down at 200 g for 5 min after resuspension in FACS buffer (1XPBS, 1mM EDTA, 25mM HEPES pH 7.0, 1% FBS) passed through 100 μ m and 40 μ m mesh. After centrifugation, the pellet was dissolved with FACS buffer and the cells were sorted based on the GFP signal on a BD FACSAria™ III cell sorter. DAPI is used to separate the alive

cell population. Single-cell sorting is performed on 96wp. For flow analysis, trypsinized cells were spun down at 200 g for 5 min, after resuspension in FACS buffer cells were analyzed based on the GFP signal.



4. RESULTS

The workflow for this study has been summarized below (Figure 4.1). The plasmids in the experiments supplied from addgene, one of them has eGFP expression cassette between -140 and -139 (DT-GFP Plasmid) with homology arms and another one has human TERT promoter region from -589 to +353 (DT-Promoter Plasmid). Human TERT promoter mutations were introduced into plasmids purchased as WT. We designed primers for amplifying the regions between homology arms to introduce mutations. These mutations were -124C>T and -146C>T for DT-Promoter plasmid and -146C>T for DT-GFP plasmid. Briefly, after amplification of the regions on the plasmids, PCR products were cloned back into plasmids. At the same time, 3 different gRNAs were cloned into the pX330 plasmid. After cloning and transformation, the presence of the correct insert was verified by Sanger sequencing. After identifying the right colony, plasmids were isolated using midiprep. Then “pop in and pop out” strategy (Figure 4.2) was used and optimized on the HEK293T cell line. According to this strategy, firstly, a double-strand break is generated at the endogenous TERT promoter with a gRNA that targets the -147 location on the promoter and SV40-driven eGFP expression cassette is introduced into cells. After that cell is sorted based on GFP signal three times using FACS and screened by PCR with primers a' and e' for confirmation of homologous recombination. Then the eGFP expression cassette is removed with two gRNA that generates two double-strand breaks and targets the ends of the eGFP cassette. At the same time, DT that contains the modified TERT promoter sequence is introduced into cells for Homologous Recombination (HR). Thus, cells can be screened based on the loss of the GFP signal and can be sequenced with the PCR products generated with primers a' and e' (Xi et al. 2015).

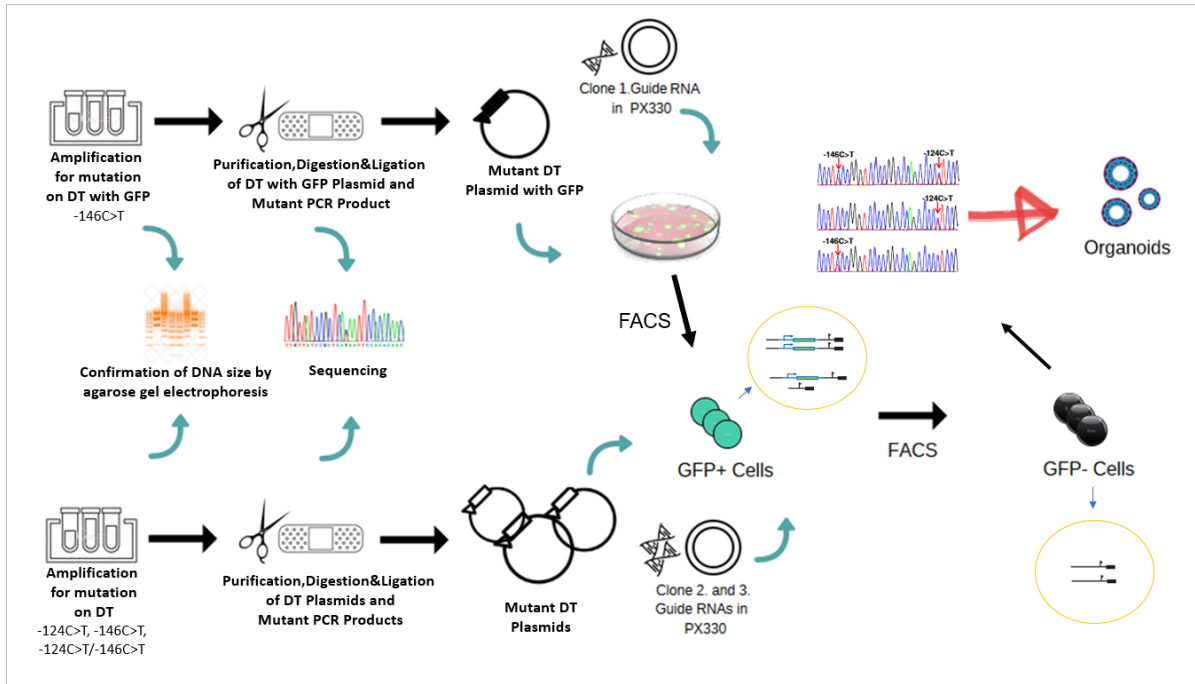


Figure 4.1: Schematic workflow for the single base-pair modification in the endogenous TERT promoter in Hepatic Organoids

Firstly, plasmids that contain desired mutations were obtained via amplification and cloning of the PCR products into WT donor template plasmids. Then cloning of the gRNAs was performed into pX330 plasmid. Two steps editing of TERT promoter via CRISPR Cas9 was optimized into HEK293T. Then, it was applied in hepatic organoids as a trial.

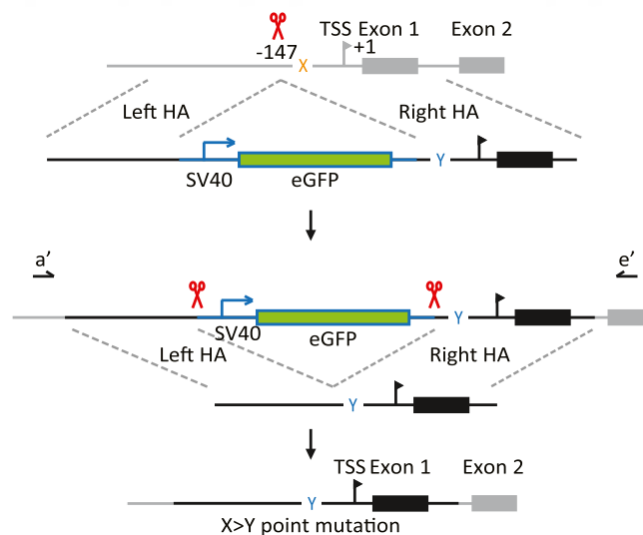


Figure 4.2: Pop in and pop out a strategy that modifies a single base pair at the endogenous TERT promoter.

According to "pop in pop out" system, a double-strand break was generated with the CRISPR-Cas9 system (red scissors) at the endogenous TERT promoter. In the first editing, SV40-driven eGFP expression cassette was inserted into the promoter. In the next step, the eGFP expression cassette was removed by two double-strand breaks generated with the CRISPR-Cas9 system. Donor Template containing the modified TERT promoter sequence was introduced for Homologous Recombination (Xi et al. 2015).

4.1. PCR amplification to introduce mutations into DT-Plasmids

In order to introduce mutations into DT plasmids, firstly plasmids were isolated from the purchased bacterial stock and confirmed by the restriction enzyme digestion with HF-EcoRI and HF-HindIII enzymes. The linear form of all plasmids was in the correct size after isolation from bacteria (Figure 4.3).

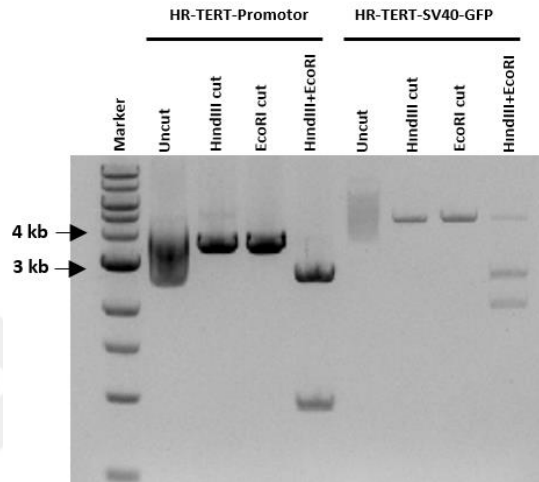


Figure 4.3: Gel image of uncut and cut plasmids after isolation.

Control of HR-TERT-Promoter and HR-TERT-SV40-GFP plasmids by RE digestion after midiprep.

A single base-pair substitution (-146C>T) was first introduced into the TERT promoter on the DT-GFP plasmid. In the first step transfection, this nucleotide change provided higher efficiency, because C-146T mutation disrupted the gRNA recognition site. Because of the single nucleotide change on the recognition site, gRNA cannot target the edited genome. For the second step transfection single base-pair substitutions (-146C>T, -124C>T) were introduced into the TERT promoter on the DT-Promoter plasmid. The introduction of the single base-pair substitutions was performed by two-step PCR. According to this protocol, primers were designed from the restriction enzyme sites on the end of the TERT promoter regions and from the region of the mutation needed. Then, for the first round PCR amplification, plasmids were used as a template and mutation primers were used as shown in Table 3.1. In the second-round PCR, first-round PCR products were used as a template, and overlap extension was performed with hTERT-prom-F/hTERT-prom-R and SV40 hTERT-prom-F/SV40 hTERT-prom-R primers. Also, C-146T and C-124T substitutions were prepared on the same template. For this purpose -124C>T second PCR product was used as a template and -146C>T was

introduced with hTERT-prom-F/ hTERT-C146T-R and hTERT-C146T-F/ hTERT-prom-R primers. All of the results of two-step PCR for the introduction of the mutations are summarized in Figures 4.4 and 4.5, and results show that the size of the PCR amplicons is in the correct size indicated in the colored squares.

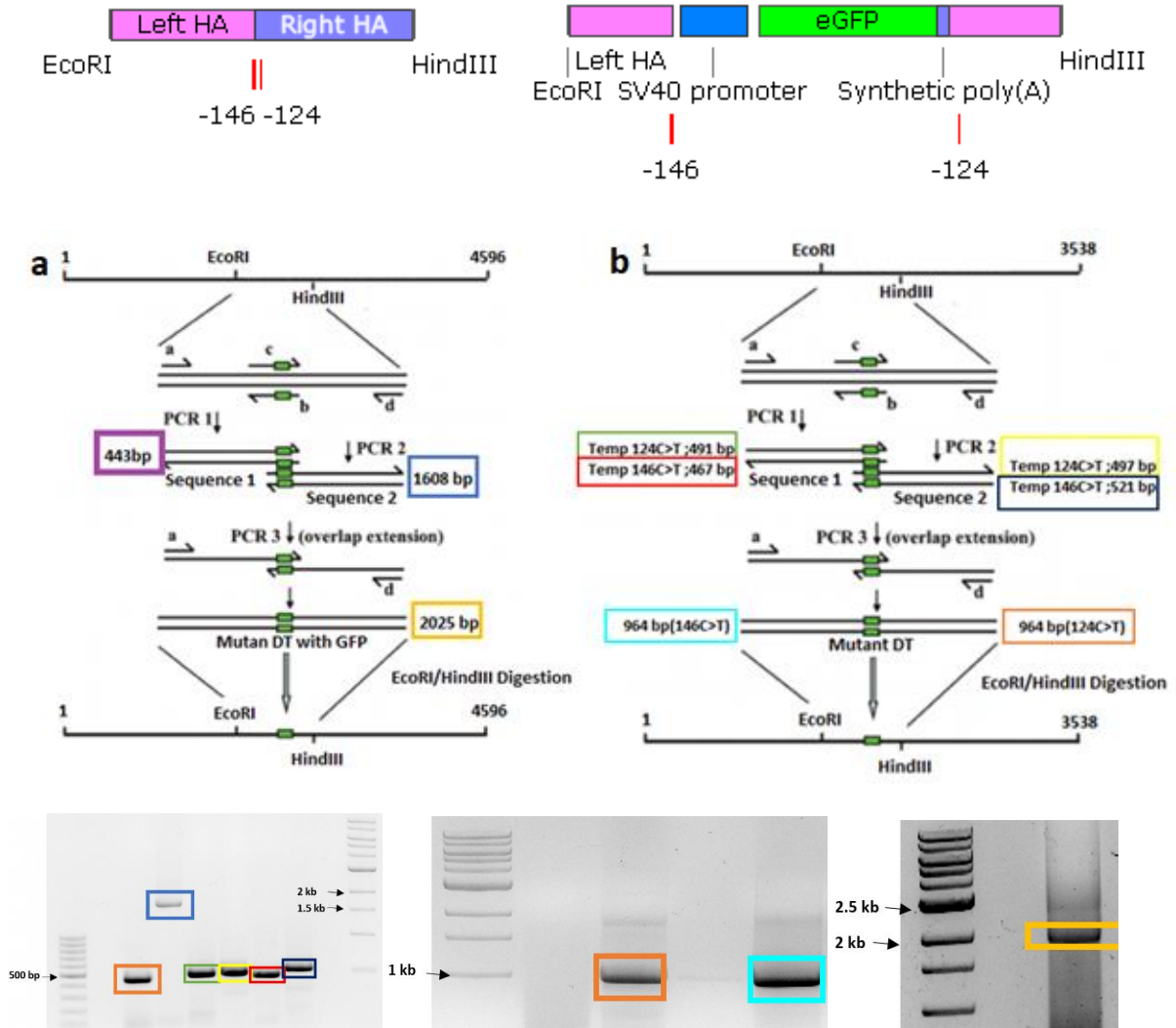


Figure 4.4: Schematized results of two Steps PCR for single base-pair modification for production of DT GFP 146C>T, DT Promotor 124C>T and DT Promotor 146C>T plasmids.

a. 146C>T on DT-GFP Plasmid, b. 124C>T and 146C>T on DT-Promoter Plasmid. Based on the gel images PCR amplicons in the correct size that marked as different colors on the representative scheme.

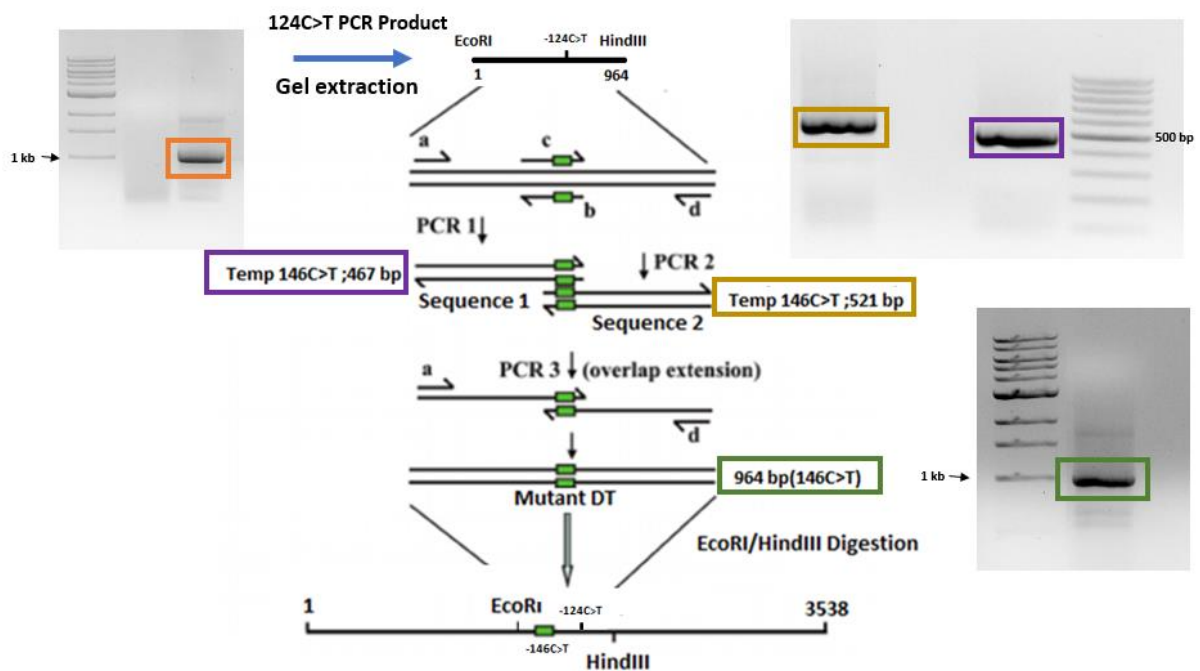


Figure 4.5: Schematized results of two Step PCR for single base-pair modification for production of DT Promotor 124 + 146C>T plasmid.

After extraction of the -124C>T fragment, PCR product was used as a template for the addition of the -146C>T substitution. Based on the gel images PCR amplicons in the correct size that marked as different colors on the representative scheme.

4.2. Cloning of the Two-Step PCR Fragments into DT-Plasmids

After amplification of mutated fragments, PCR bands of the correct size were extracted from the agarose gel. These fragments were cut with the HF-HindIII and HF-EcoRI restriction enzymes for cloning. PCR cleanup was used to obtain pure fragments. At the same time, DT-Plasmids were cut with the same enzymes and loaded on an agarose gel. The backbone of the plasmids was extracted from the agarose gel and their sizes were in the correct place in the agarose gel. (Figure 4.6). The ligation reaction was set up and the transformation was done into Stab13. Five colonies were chosen from each plasmid group for miniprep. Isolated plasmids with miniprep were cut with both RE EcoRI and HindIII to control the sizes of plasmids after cloning. After RE cut, both sizes of insert and sizes of the backbone were in the correct site in the agarose gel. (Figure 4.7). Glycerol stock was prepared from these colonies. Two colonies were sent for Sanger sequencing after confirming by restriction digestion. After analyzing the

sequencing results, C>T substitutions in the desired regions were shown (Figure 4.8) A midprep was prepared with the confirmed positive colony for each plasmid. (hTERT-124-C5, hTERT-146-C2, hTERT 124+146-C1 and SV40-146-C4). The linear size of all plasmids incorrect site was shown as a result of RE digestion (EcoRI) (Figure 4.12).

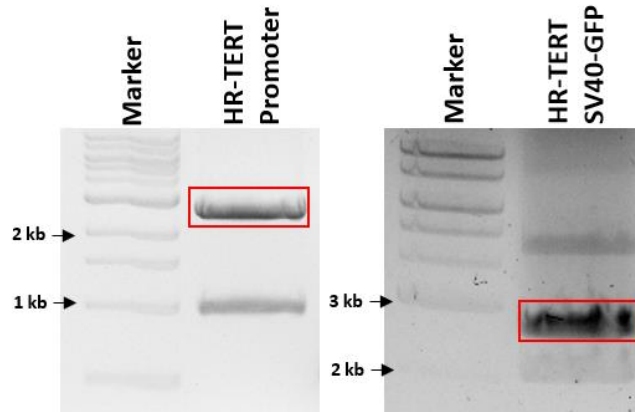


Figure 4.6: Gel image of cut plasmids.

Cutting of HR-TERT-SV40-GFP and HR-TERT-Promotor plasmids with EcoRI and HindIII enzymes. The red marked bands are in the correct size and isolated from the gel.

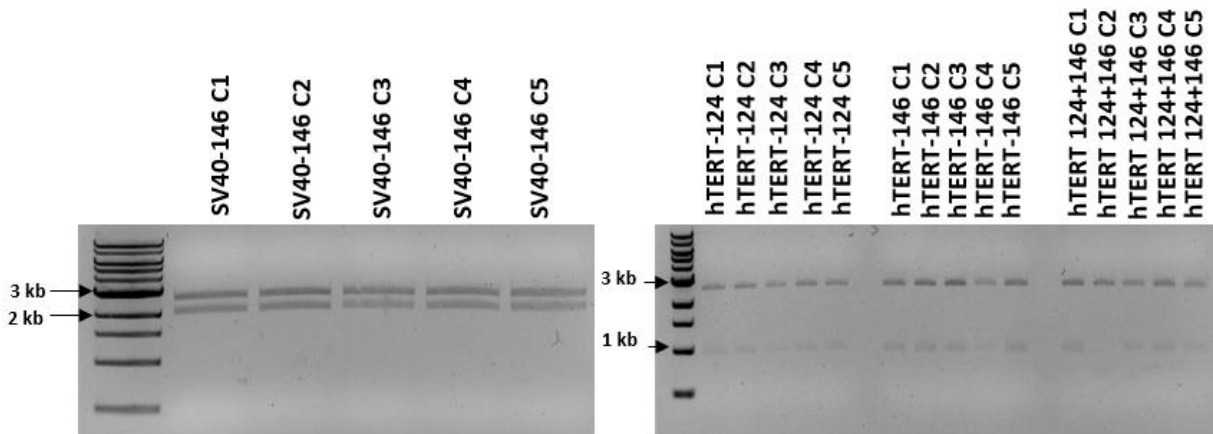


Figure 4.7: Gel image of cut plasmids after isolation.

Control of five colonies from each mutated group by RE digestion with EcoRI and HindIII enzymes after miniprep. Based on the gel images insert and the backbone of the plasmids in the correct size.

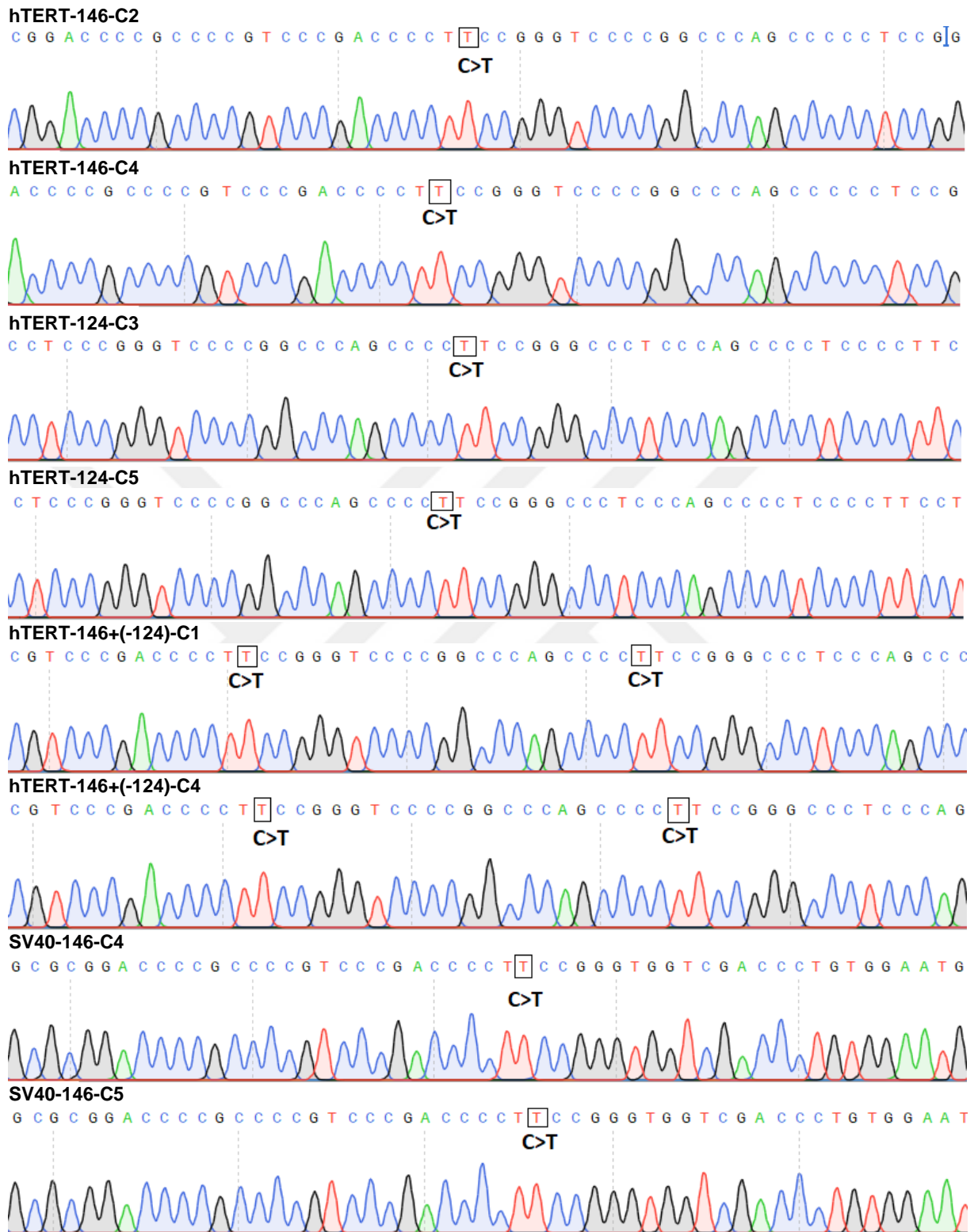


Figure 4.8: Sanger sequencing chromatograms of plasmids to show single base pair alterations.

Sequence results of plasmids of hTERT 124, hTERT 146, hTERT 124 + 146 and SV40-146. Each plasmid was C>T substitution in the correct site.

4.3. Cloning of the gRNAs into the pX330 Plasmid

In the CRISPR-mediated editing called “pop in pop out”, there was a gRNA to introduce eGFP cassette in the first round and there were two gRNAs that remove the eGFP cassette in the second round of the editing. gRNA sequences (Table 3.1) were cloned individually into the pX330 plasmid vector. Firstly, pX330 plasmid was cut with BbSI enzyme and loaded in agarose gel, then gel extraction of the backbone which is shown in the correct size was performed (Figure 4.9). After the cloning process, the transformation of the plasmids into *Stab13* was performed. Colony PCR was used to determine the presence of insert DNA. According to colony PCR results, we showed that the G2-1, G2-2, G3-6 and G3-8 clones had insert DNA (gRNA) (Figure 4.10.a). Colony PCR given results were fit with a few samples, so we used PCR, after miniprep for selecting the correct clones of G1. It was shown that all G1 clones had insert DNA according to PCR results (Figure 4.10.b). Positive two colonies were sent to Sanger sequencing for showing correct gRNA insertion. Results showed that out of six colonies five of them were sequenced and each of them had an impeccable gRNA sequence (Figure 4.11). Midiprep was used to replicate the plasmids (G1-C6, G2-C1, and G3-C6), and the size of the plasmids was checked by cutting with *EcoRI* after midiprep. Each linear plasmid was in the correct size in the agarose gel (Figure 4.12).

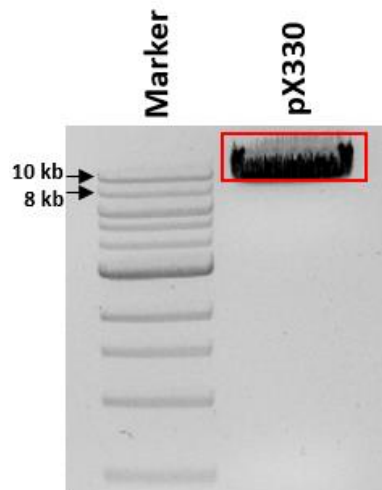


Figure 4.9: Agarose gel image of cut pX330 plasmid.

BbSI digestion of pX330 vector. Red marked band was isolated from gel.

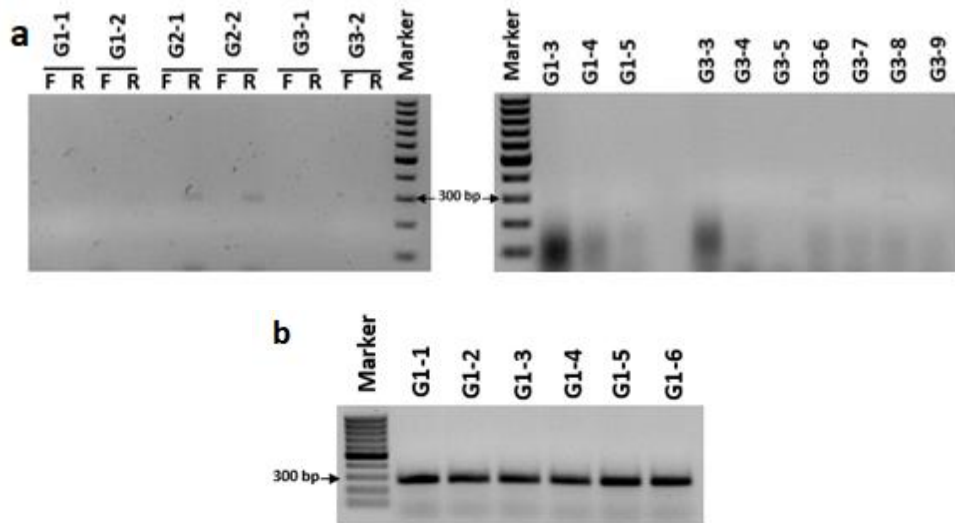
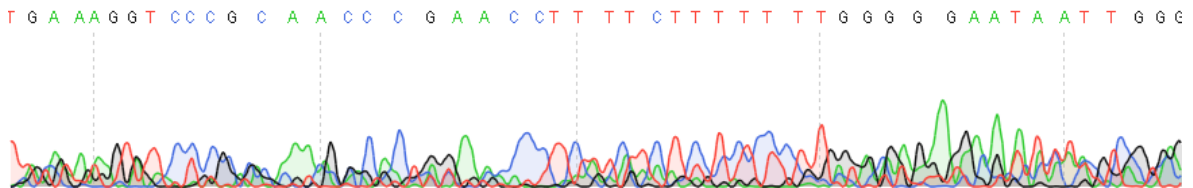


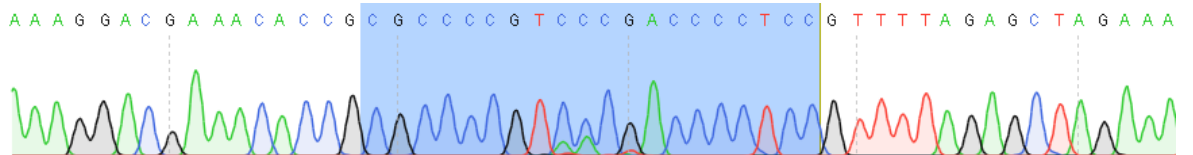
Figure 4.10: Agarose gel image of PCR results after gRNA cloning.

a. gRNA colony PCR results. b. gRNA PCR result after miniprep. Each PCR amplicon was in the correct size in the agarose gel.

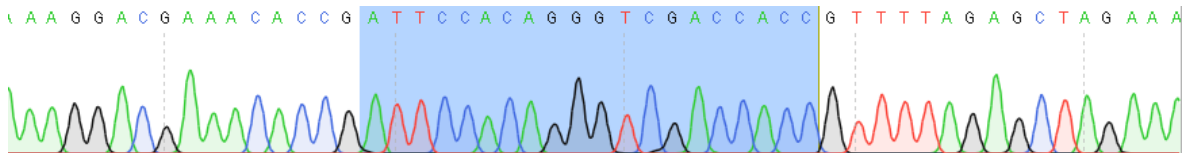
G1-C4



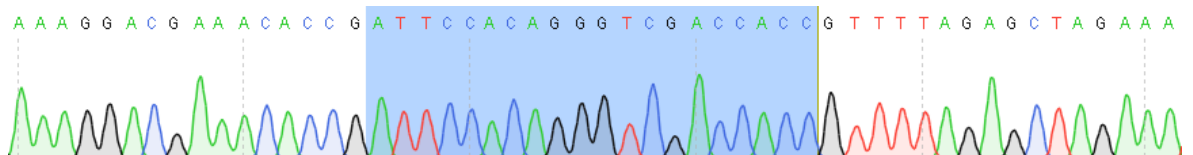
G1-C6



G2-C1



G2-C2



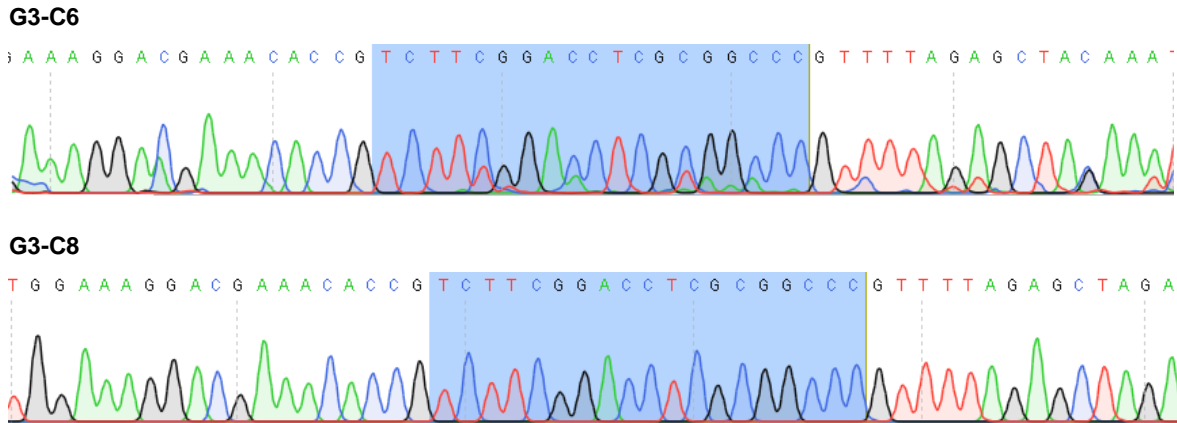


Figure 4.11: Sanger sequencing chromatograms of gRNA plasmids.

Sequence results of G1, G2, and G3 -pX330 Blue regions indicate the gRNA sequence.

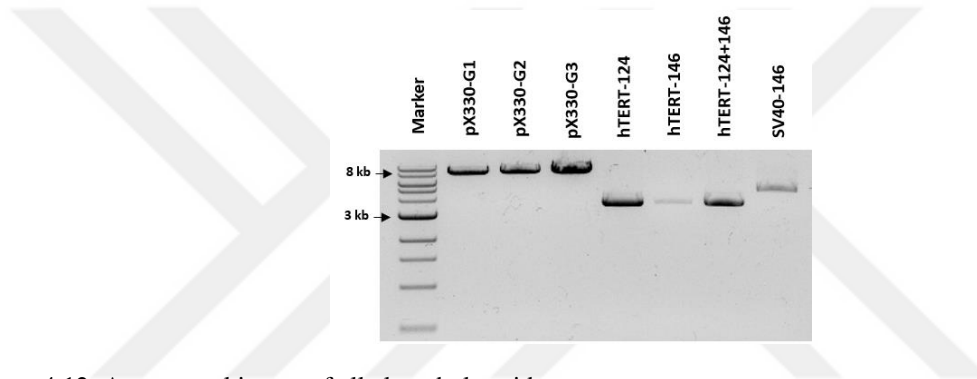


Figure 4.12: Agarose gel image of all cloned plasmids.

Based on the image linear plasmids were in the correct size after RE (EcoRI) digestion of plasmids.

4.4. Transfection of Hek293T cells for single base-pair modification in the endogenous TERT promoter

A single base-pair substitution was first introduced into the TERT promoter alongside an eGFP expression cassette, which was then removed by the second round of CRISPR-mediated editing, resulting in a TERT promoter with only a single base-pair alteration. The protocol was first tested using HEK293T cells, which contain WT TERT promoter sequences. After the preparation of the plasmids, HEK293T cells were transfected with DT for the first step contained the C-146T mutation and an eGFP cassette inserted. On days 7, 14 and 21 post-transfection, three rounds of FACS were carried out to enrich for the GFP positive cells, from which single-cell clones were generated. These enrichment steps provided higher targeting efficiency thanks to GFP tracking. When we used FACS on day 7 after transfection, 10% of

GFP+ population are shown and sorted. When we came on day 14, 7.8% GFP+ population was sorted. After transfection, on day 21, the GFP+ population increased to approximately 60%, the possible reason for this was the growth of the genome-edited cell population after day 14. So, we used a highly GFP+ population (6.9%) for the single-cell sorting to obtain GFP+ isogenic clones (Figure 4.13). After GFP+ single-cell sorting on 96 wp, 28 GFP+ clones were obtained. (Figure 4.14 and 4.15). PCR with the primer pair a'-e' (Table 3.1) was used to identify clones that had undergone HR. The endogenous TERT sequence PCR product was 1110 bp. The insertion of the eGFP expression cassette increases the size of the PCR product 2262 bp. Eight GFP+ clones were chosen from twenty-eight clones, PCR was performed with HR primers. PCR optimization was performed, but still, the results were not clear to figure out which clone is homozygous or heterozygous. Because of the hTERT promoter is high GC rich region, eGFP cassette inserted bands (2262 bp) were not shown clearly in PCR results for each sample. But it is shown that C12 clone was homozygous for GFP insertion (Figure 4.16) According to results five clones (C2, C5, C12, C17, and C20) were selected for the second step of the CRISPR-cas9 protocol.

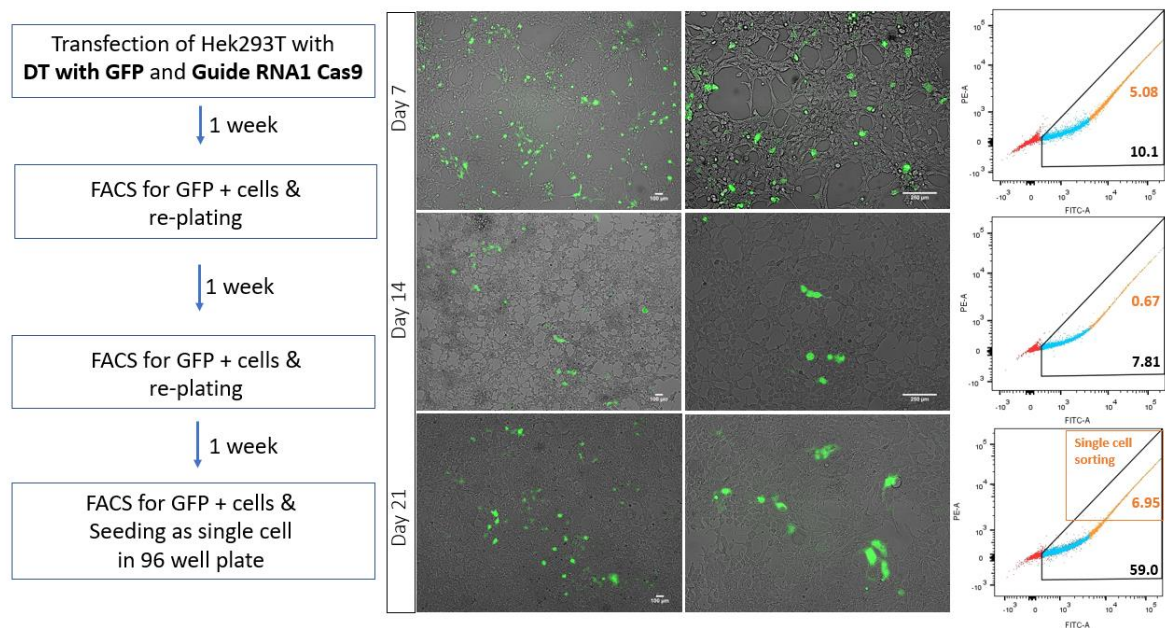


Figure 4.13: Scheme of the HEK293T cell GFP+ cell enrichment after first step transfection.

FACS and fluorescence microscopy of GFP+ Hek293T cells on the day 7, 14 and 21 after first step transfection. In the flow results, red indicates GFP- population, black gates indicate GFP+ population and orange indicate a highly GFP+ population in the sample. On day 7 and 14 black gates were sorted as bulk, and day 21 orange gate was sorted as a single cell on 2x96 wp.

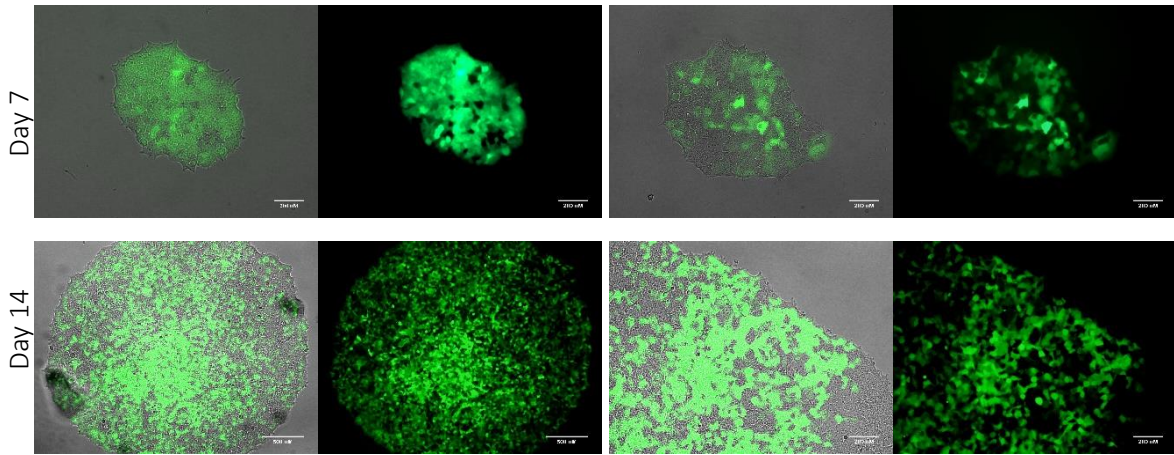


Figure 4.14: Fluorescence microscopy images of Hek293 T single-cell clones after FACS on day 7 and 14.

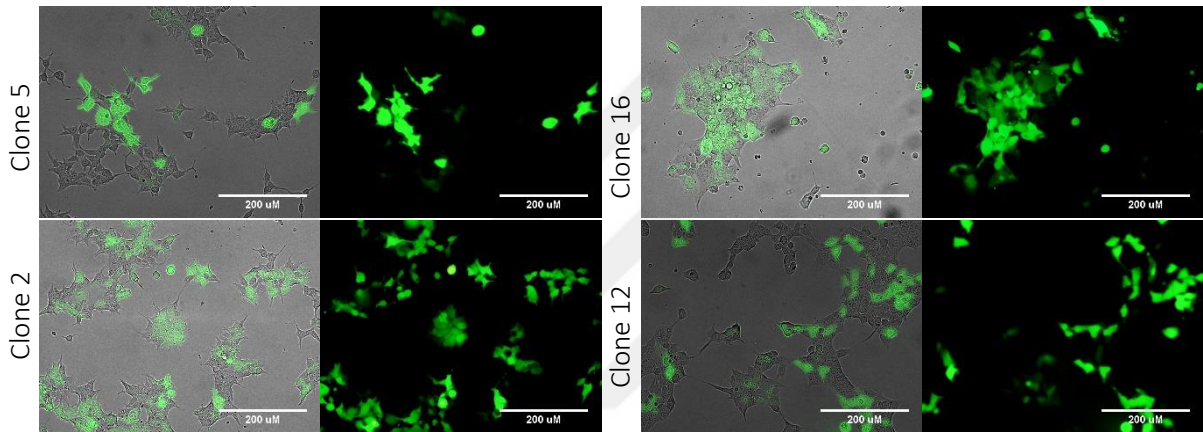


Figure 4.15: Fluorescence microscopy images of some Hek293 T single-cell clones after passage.

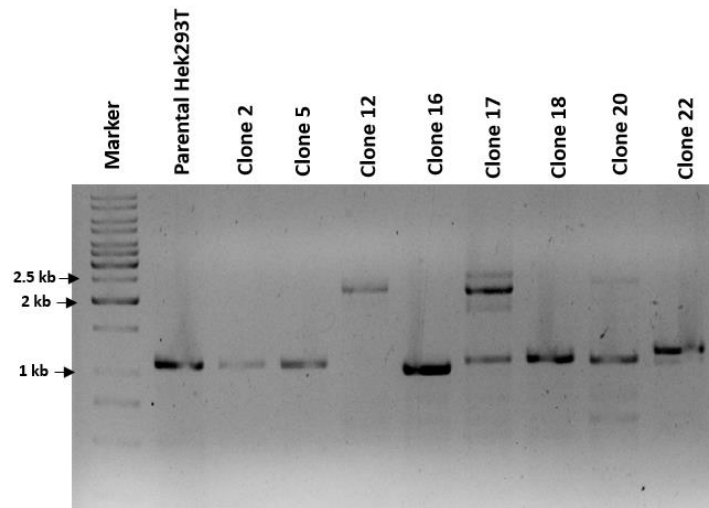


Figure 4.16: PCR result with HR primers in eight GFP+ single-cell clones.

Clone 12 is homozygous other clones are heterozygous for SV40-GFP-146 insertion.

Then, we used two clones (C2 and C12) to carry out the second step of the protocol, removing the eGFP cassette. Two Cas9-gRNA plasmids (px330 G2 and G3) targeting the edges of the eGFP cassette were co-transfected with the DT plasmids (DT-Promoter 146C>T, 124C>T and 146+124C>T), included the mutations. Seven days post-transfection, the cell population was analyzed by flow analysis. The Cas9 negative group (transfected with only the DT) contained ~30.9 % GFP-negative cells in Clone 2 and ~3.4 % in Clone 12. The Cas9+ groups contained a higher percentage of GFP-negative cells that range 1-5 % in C2 and approximately 3% in C12 (Figure 4.17). This result also was shown by Xi et al., and the possible reason was explained as epigenetic silencing of the eGFP expression cassette.

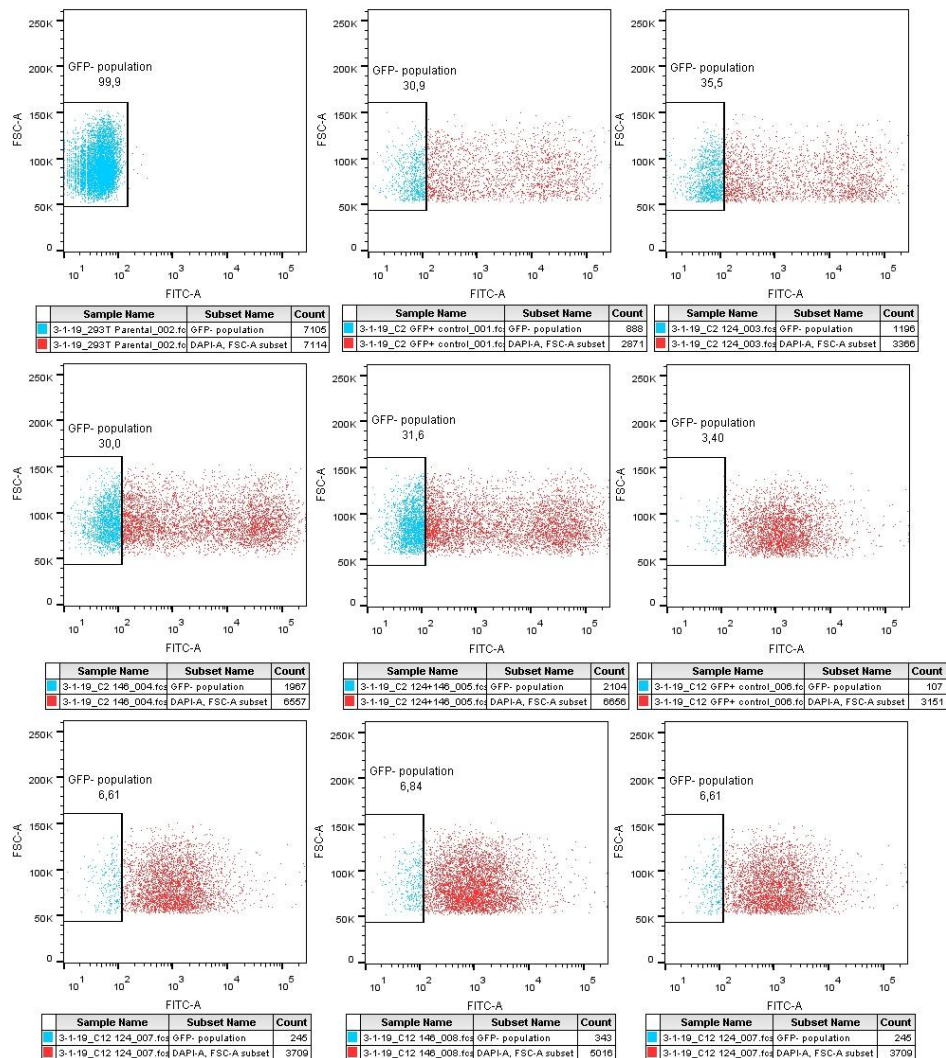


Figure 4.17: Flow analysis in clones C2 and C12, 7 days after the second transfection.

There were GFP- population (blue dots) in the control groups (Cas9 negative) while Cas9 + groups had a higher percentage of the GFP – population.

Because of the epigenetic silencing of the eGFP expression cassette, GFP+ cell enrichment was done in GFP+ clones (C2, C5, C12, C17, and C20) before the second transfection. Because we wanted to obtain higher efficiency in the second step editing that resulted in producing GFP- clones. As a result of the GFP + cell enrichment, highly GFP expressed cells were sorted by FACS using different gates according to the distribution of the population. In each population, GFP negative cells range between 2.44-39,9 % (Figure 4.18). In order to control the return of the GFP negative population in time, flow analysis was done 10 days after the sorting, and GFP-population with a more different percentage, from the previous analysis (between 6.93% and 33%) was detected in each clone (Figure 4.19).

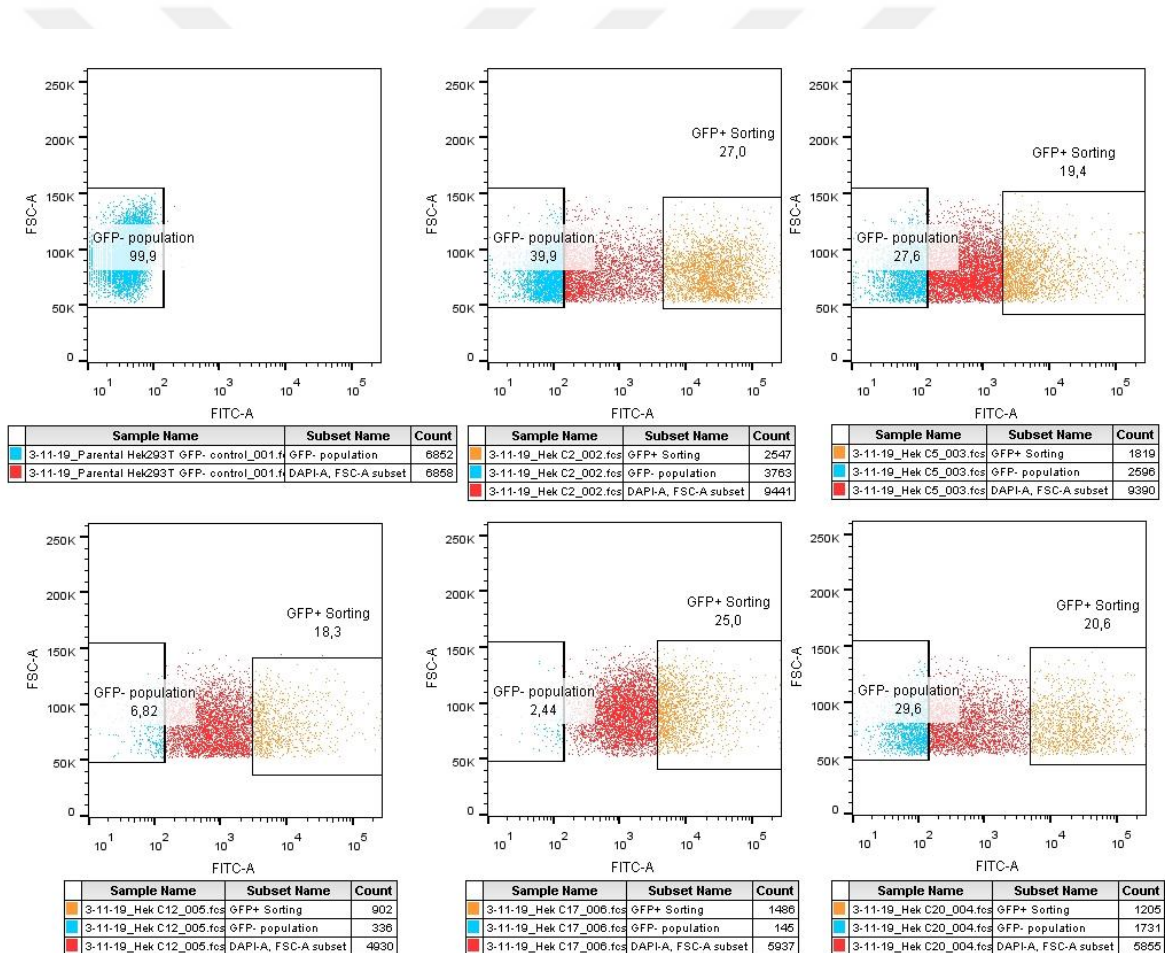


Figure 4.18: GFP + cell sorting before the second transfection in five GFP + single-cell clones.

Each clone includes GFP- (blue) population. For sorting, each gate has taken according to high GFP expression (orange).

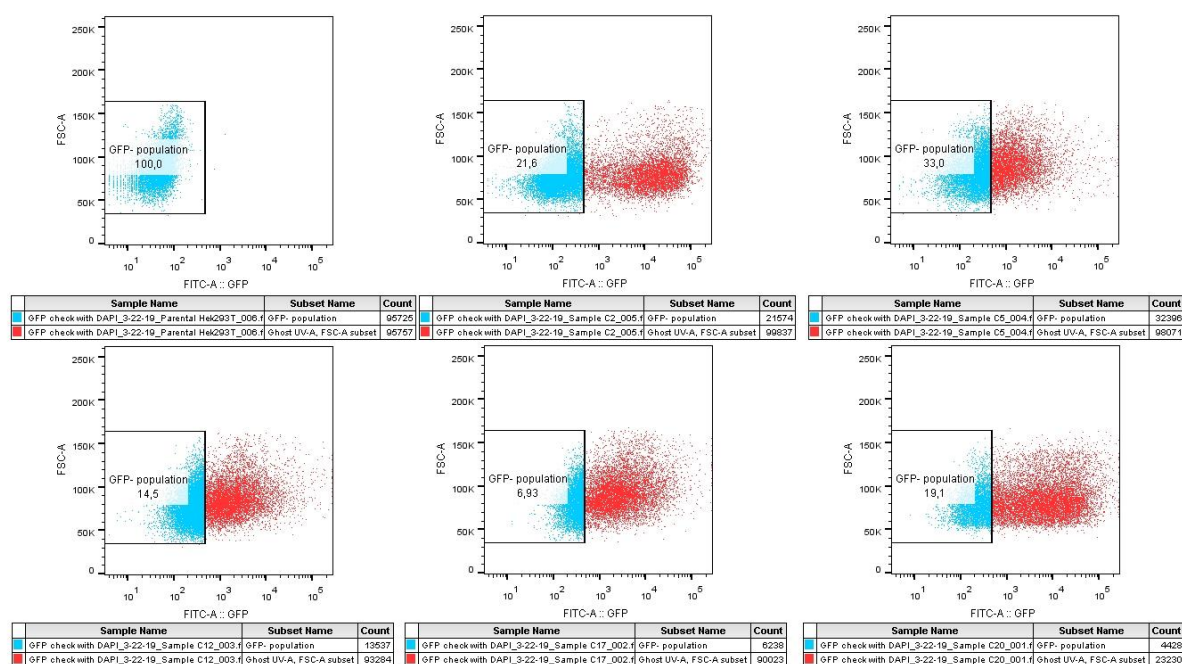


Figure 4.19: Flow analysis 10 days after GFP + cell enrichment.

There is a different amount of GFP- population (blue dots) in the GFP+ clones after 10 days of the GFP enrichment.

The second transfection was repeated in 5 selected clones. Eleven days after transfection, C5 and C12 clones were selected for their GFP expressions under the microscope and used for GFP negative single-cell sorting (C5 heterozygous / C12 homozygous). As a result of the analysis, GFP negative population in the Cas9 + groups increased by 2-6 % compared to the Cas9 - control group. In these clones, the GFP-population was sorted as a single cell and each experimental group was seeded into a 96 wp, while the remaining GFP-population was sorted as bulk (Figure 4.20).

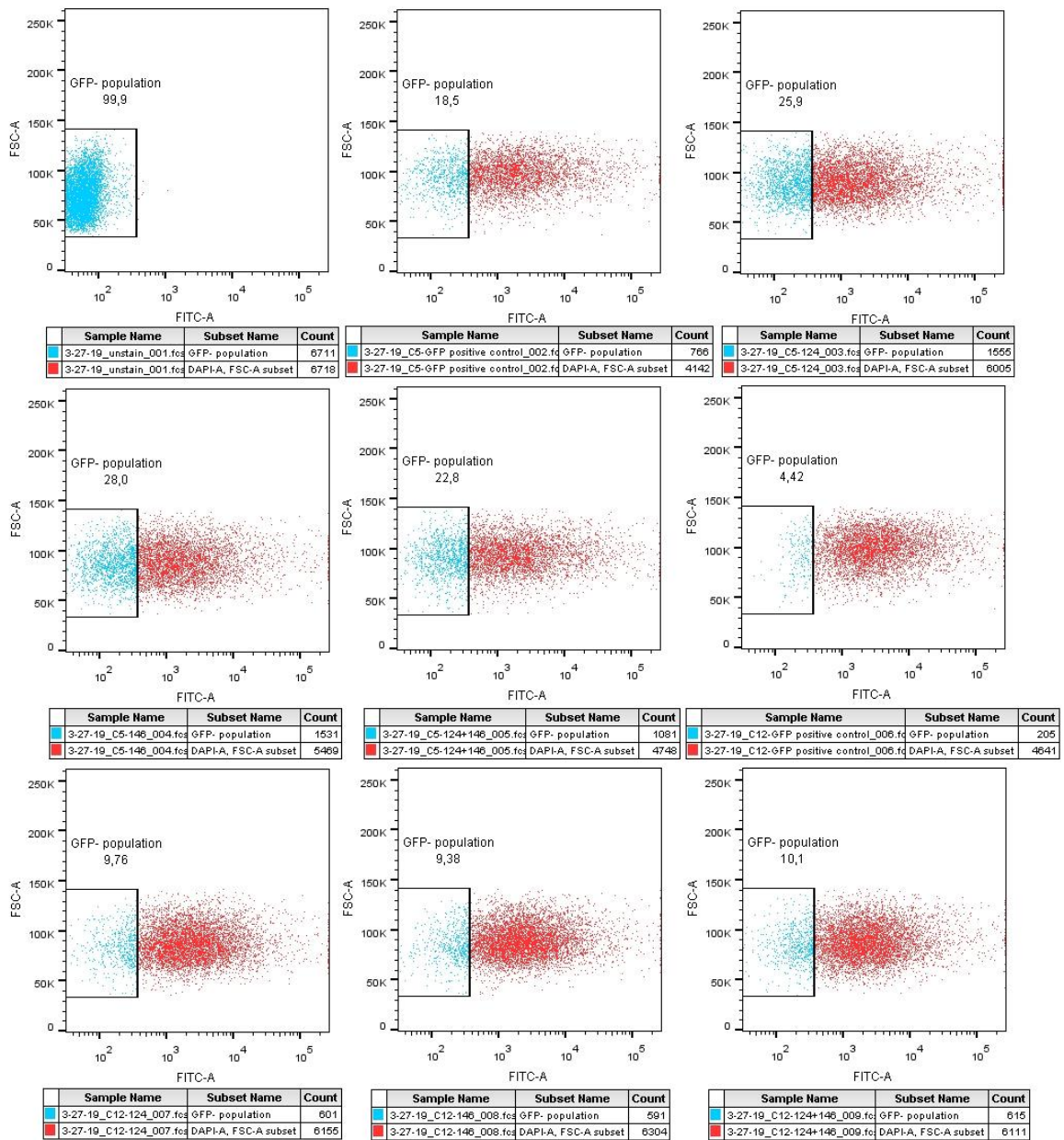


Figure 4.20: GFP- single cell&bulk sorting on day 11 after the second transfection.

There are higher GFP- population (blue dots) in the Cas9+ groups.

After GFP negative bulk sorting of two clones, cells were seeded and GFP + cells were observed in the culture. The reason of the GFP+ cells in the sorted population could be the gate taken in sorting or could be the efficiency of the sorting machine. The DNA of each group was isolated, and then PCR was performed with HR primers to identify that the clones underwent HR to remove the eGFP expression cassette and had incorporated the mutations. The C12 clone containing SV40-GFP-146 as homozygous was shown to contain the parental hTERT band which was predicted that have a mutation in the Cas9+ groups. There were increased in the parental hTERT band in the GFP – C5 124+146 bulk group while the eGFP cassette band was decreasing. So, second editing also was successful in the C5 group that is heterozygous (Figure 4.21).

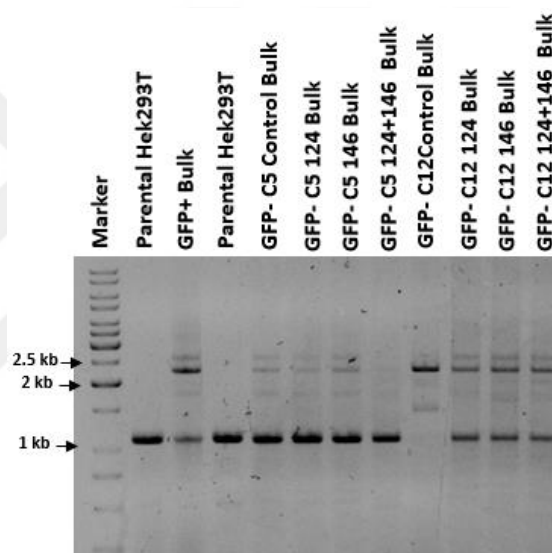


Figure 4.21: PCR results with HR primers of GFP-Bulk sorted cells.

Parental HEK293T and GFP+ bulk were used as control. In clone 12 experiment groups, there are bands that size in the parental HEK293T promoter, while in the control group does not exist. In clone 5-124+146, there is an increase in the band that size in the parental HEK293T promoter.

C12 GFP negative bulk groups were sequenced with HR primers to detect mutations. For this purpose, parental HEK293T (WT hTERT band), C12-control (SV40-GFP-146 band), C12-124, C12-146 and C12-146+124 (Mutant hTERT band) groups were used. In order to obtain a high amount of DNA for sequencing, the second PCR was set up from the first PCR bands which are correct size isolated from the agarose gel (Figure 4.22). Sequence results showed that only 146C>T mutations were observed in all groups and there are reading failures between the mutation regions. Introducing 124C>T mutation was not successful according to these results.

In the first step editing, eGFP cassette was successfully inserted into the targeted region (Figure 4.23).

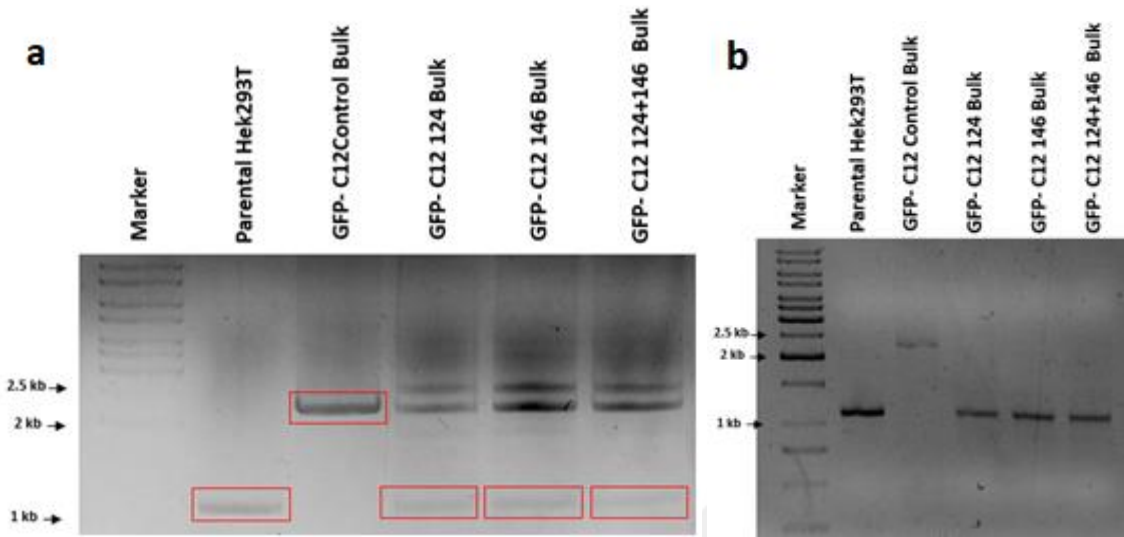
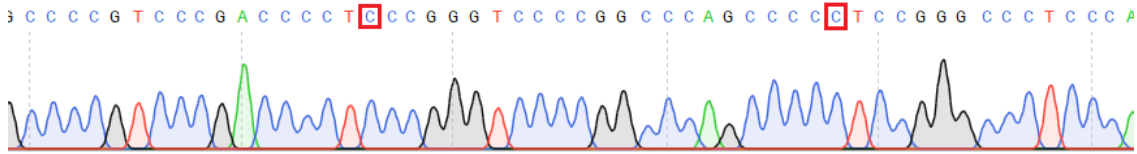


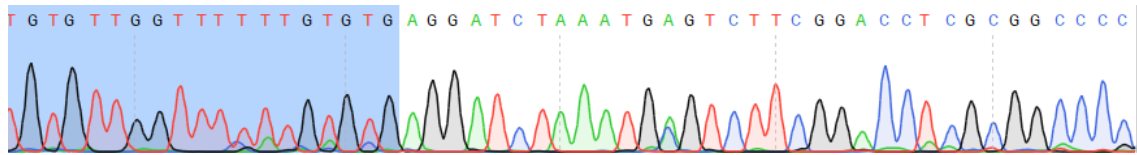
Figure 4.22: Agarose gel images of PCR results for sequencing of C12 GFP-Bulk groups

a. PCR with HR primers. Red bands were isolated for second PCR, b. Second PCR results

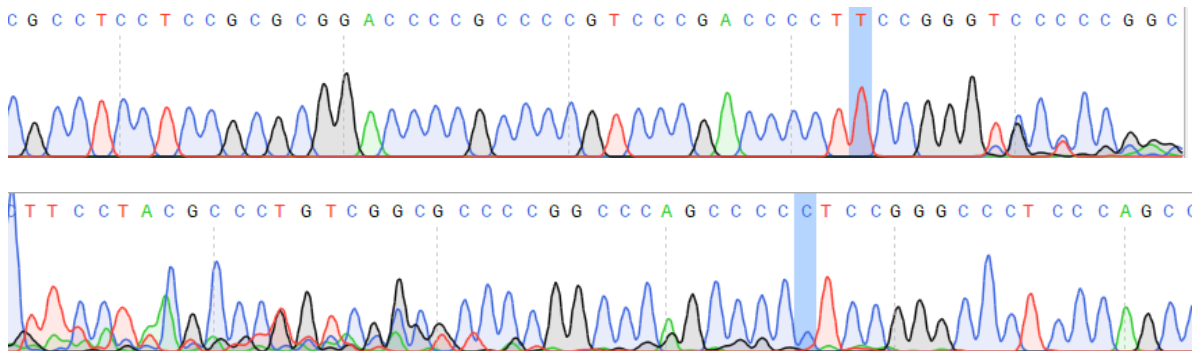
Parental HEK293T (WT hTERT Promoter)



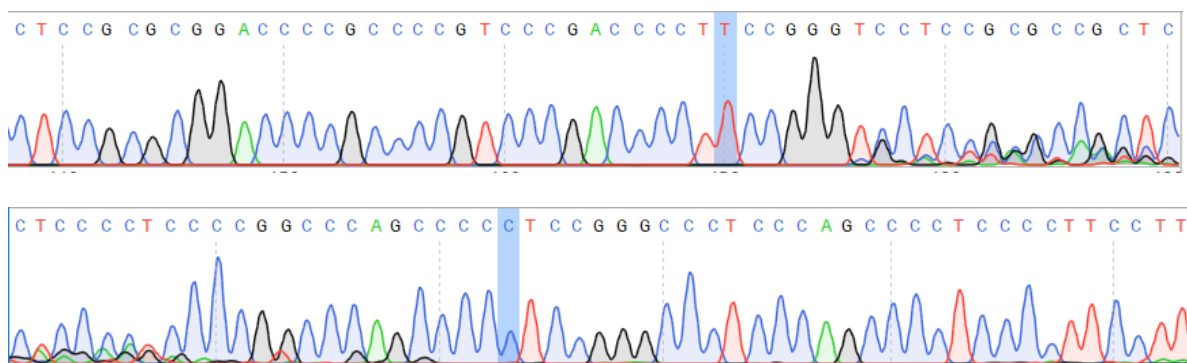
SV40-GFP (Synthetic Poly(A) + Right Homology Arm)



C12-124 (WT 124C>C + Mutant 146C>T)



C12-146 (WT 124C>C + Mutant 146C>T)



C12-124+146 (WT 124C>C + Mutant 146C>T)

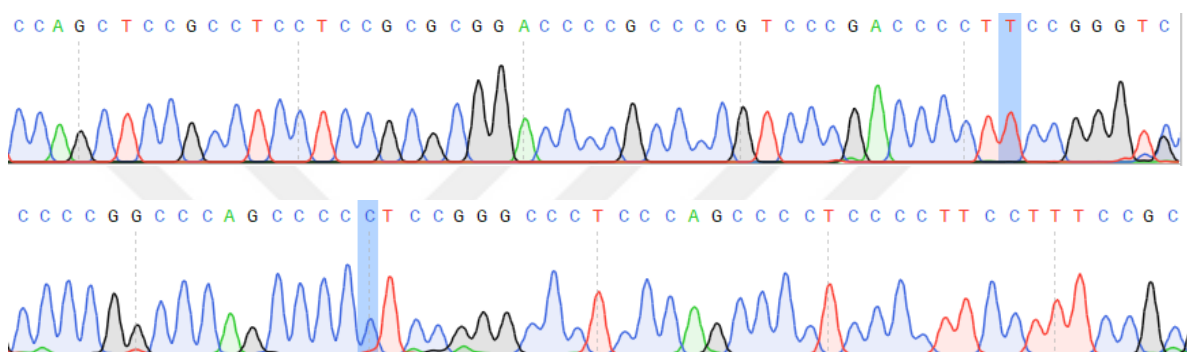


Figure 4.23: Sanger sequencing chromatograms of GFP- bulk groups

The blue regions indicate the region that is expected the change.

In addition, GFP + cells were observed in the C5 and C12 Cas9 + groups, which were separated as single cells in a 96-well plated GFP-population. The reason for the GFP + cells was the same as in the bulk groups. Totally, we obtained 39 GFP – clones in the second step of editing (Figure 4.24).

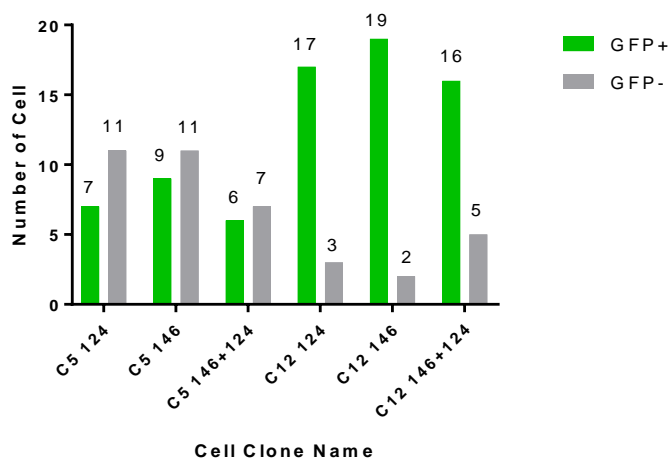
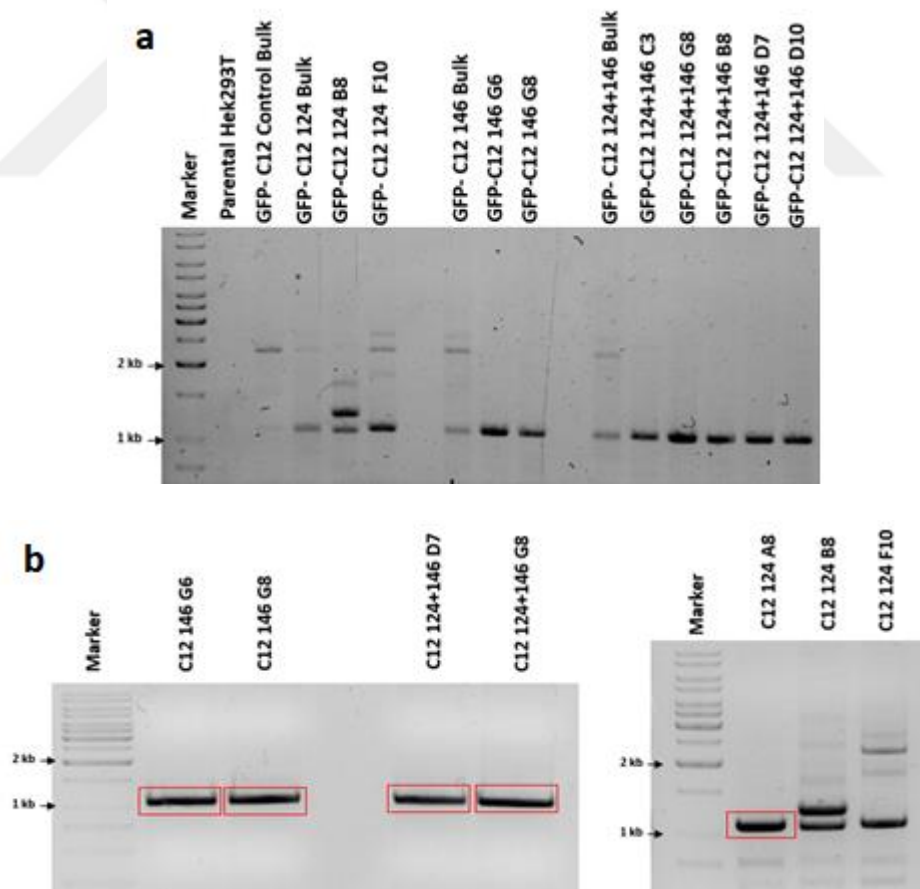


Figure 4.24 : GFP + / GFP- cell numbers obtained from 96 wp after the second transfection.

C12 groups were chosen for Sanger sequencing because this group was homozygous, they had a higher possibility for containing the desired mutation in the GFP- clones. Ten C12 GFP-single-cell clones in Figure 4.24 were sequenced. PCR was performed by using HR primers. After isolation of the bands from the gel, 2.PCR was established, 5 clones were selected according to PCR result (C12-124 A8, C12-146 G6 and G8, C12-146+124 D7 and G8) and were sent for sequencing. Selected clones clearly included the parental hTERT band (Figure 4.25). Sequence results of clones C12-124 + 146 D7 and C12-124 A8 were read, while sequencing was not successful in the other 3 clones, blast analysis was performed on the two clones obtained. According to sequence results, 124C> T mutation cannot be detected in the regions read, whereas there is 146C> T mutation in the group given 124C> T donor sequence. In addition, different deletions are observed in the region where two mutations are found and where the homology arms meet (Figure 4.26).



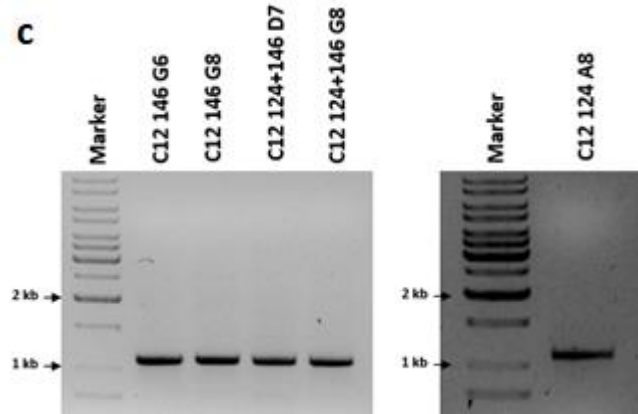


Figure 4.25: Agarose gel images of PCR results for selecting and sequencing of GFP-single cell clones.

a. PCR results with HR primers, b. PCR in the selected clones. Red bands were isolated from the gel for the second PCR. c. Second PCR results.

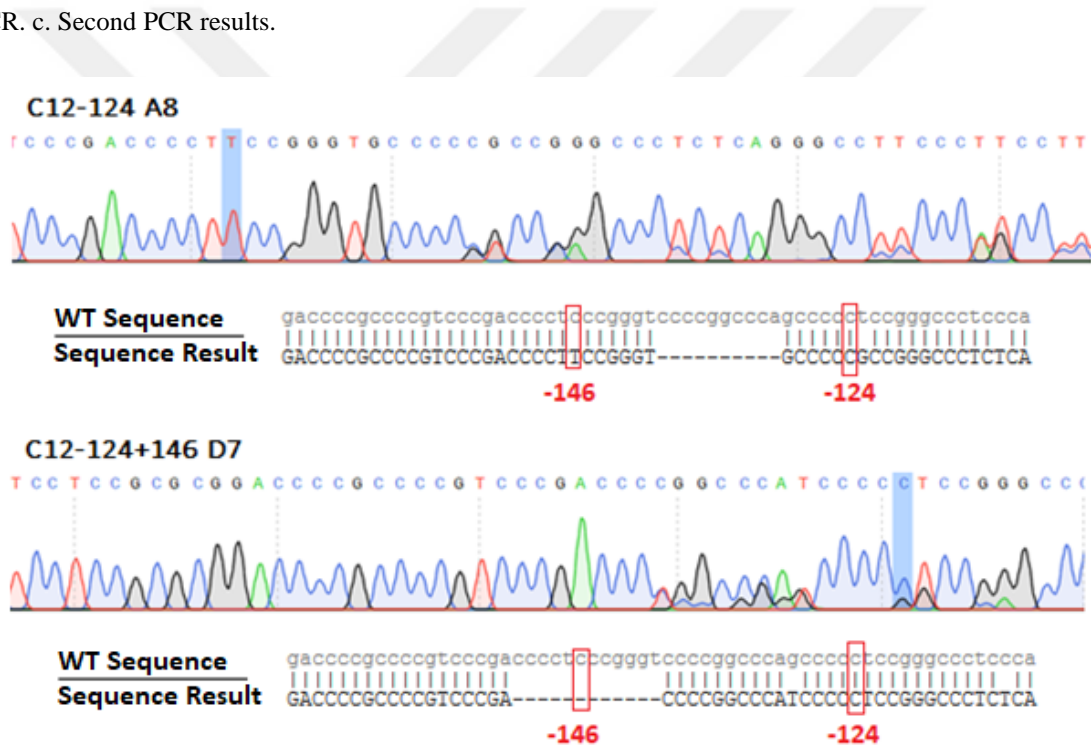


Figure 4.26: Sanger sequencing chromatograms of C12 single-cell clones and BLAST results of these clones.

Sequencing results of two isogenic clones showed that there is only C-146T mutation in the group which is used C-124T DT. There are not C-124T mutations in the group which is used C-124T & C-146T DT. Deletions between the region of the two mutations are shown.

4.5. Transfection of Hepatic Organoids for single base-pair modification in the endogenous TERT promoter

Hepatic organoids have generated iPSCs from a healthy donor via episomal reprogramming in our previous work (Akbari S.) These previously produced and characterized organoids were used for the single base-pair modification in the endogenous TERT promoter. These organoids were taken from liquid nitrogen storage and were cultured in EM (expansion medium) that mostly maintains a stable status of progenitor cells in organoid culture over the long term. After approximately 7-10 days of cell culture in EM medium, the organoids were formed and they were expanded to get the desired number of organoids which is necessary for further transfection experiments (Figure 4.27).

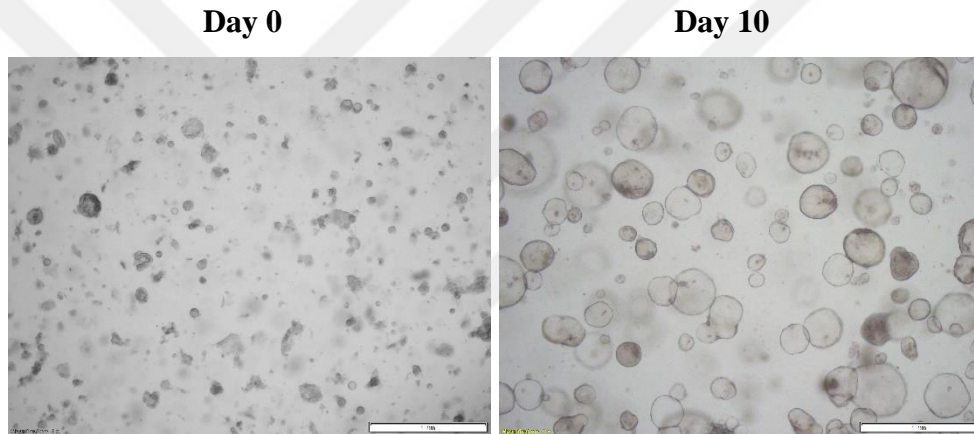


Figure 4.27: Organoid culture bright-field (BF) images under EM culture condition.

Transfection of the hepatic organoids was tried to optimize in two different techniques. These processes were summarized in Figure 4.28. Initially, to get the most efficient transfection, we used different transfection reagents. One of the tested reagents was X-tremeGENE used for a broad range of eukaryotic cells, and hard-to-transfect cell lines. Another one was Polyethylenimine (PEI), a cationic polymer with a high positive charge density that is among the most efficient polymeric gene delivery systems. After determination of reagent: plasmid ratio as 5:1 for PEI and 3:1 for X-tremeGENE, 1.5×10^4 cells were transfected with 30 ng plasmid in ultra-low attachment 96 well plate. After 24h incubation cells were seeded in Matrigel. For this experiment, SV40-GFP-146 and pX330-G1 plasmids were used. Three round GFP+ cell enrichment was not performed because of the low cell number. After transfection,

on days 7 and 21, GFP expression was controlled by fluorescence microscopy, and at day 21 FACS was performed for GFP+ single-cell sorting. Although GFP+ organoids were observed under a fluorescence microscope on day 21 after transfection, the number of GFP+ cells was extremely low for the sorting of the cells. GFP+ population was ranging between 1-2% when we compare with the control group (Figure 4.29). In addition, the published protocols by using Lipofectamine 2000 kit were used for the transfection of organoids (Drost, Artegiani, and Clevers 2016; Broutier et al. 2016). We could not observe any GFP signal after 72 h post-transfection (Figure 4.30).

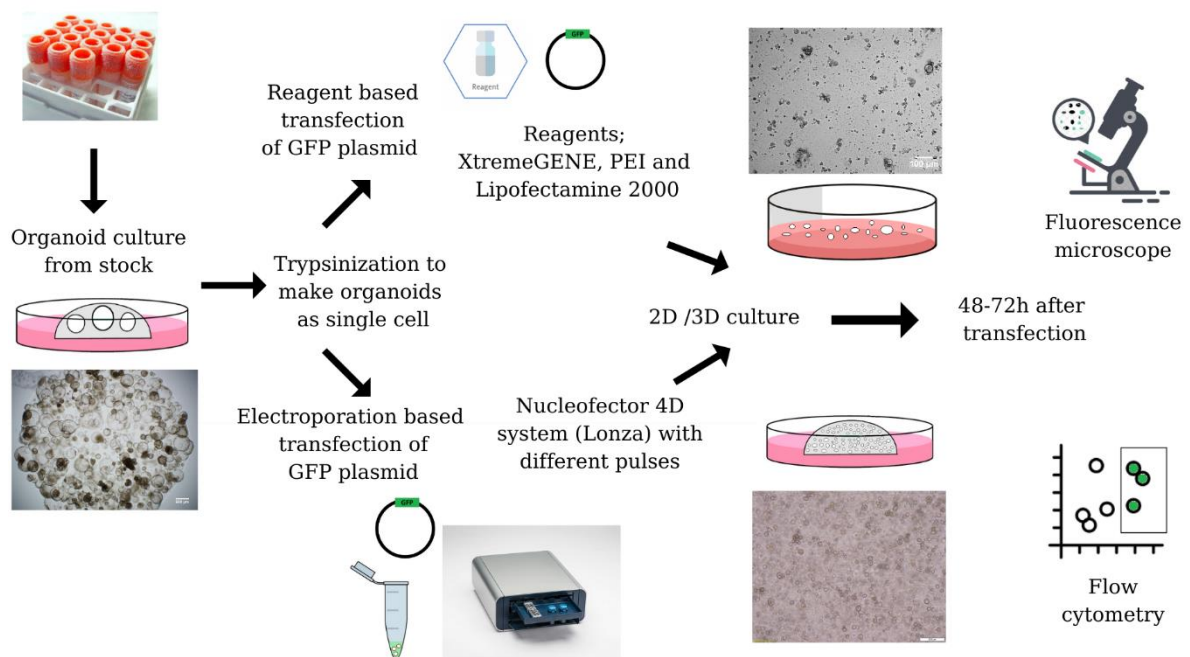


Figure 4.28: Workflow of the organoid transfection

EM organoid from stock was used for the transfection when they reach the optimum size. They were dissociated into single-cell with TrypLE. We used two main methods based on chemical and physical transfection. Firstly, x-tremeGENE, PEI and lipofectamine 2000 were used with various rates. Then the nucleofection system was used with different conditions. After post-transfection, cells were cultured into 2D/3D. GFP signal was followed under the fluorescent microscope and measured by flow analysis.

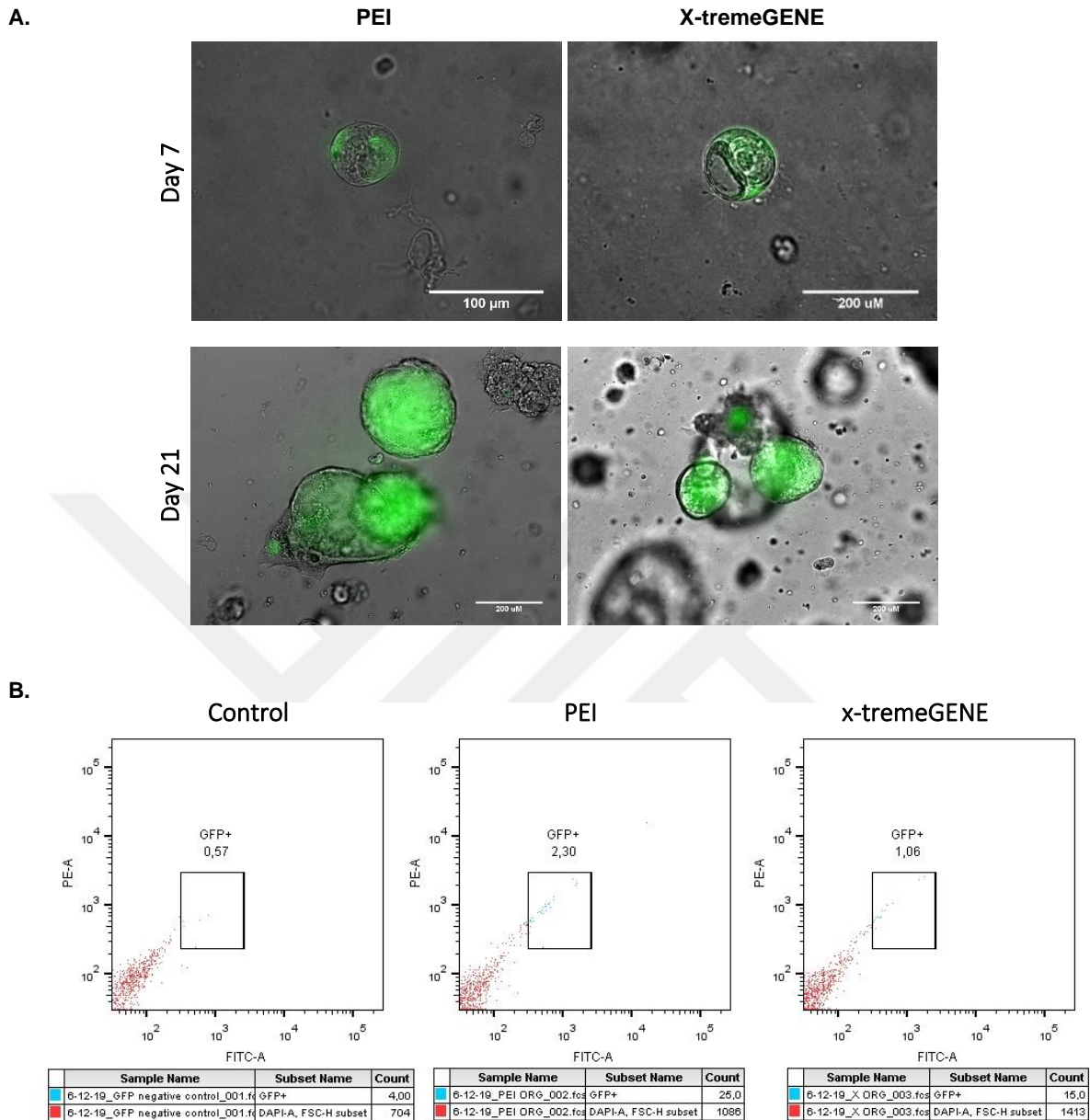


Figure 4.29: Transfection of Hepatic Organoids with x-tremeGENE and PEI.

A. Fluorescence microscopy images in 3D on days 7 and 21 after organoid transfection with SV40-GFP-146 and G1. B. Flow Cytometry analysis on day 21 after organoid transfection.

After unsuccessful trials with PEI, x-tremeGENE and Lipofectamine 2000 for transfection of hepatic organoids, we tried the nucleofector system based on electroporation and enables the transfer of a molecule directly into both the cells' cytoplasm and nucleus. Firstly, three different pulses that were FF-147, DC-100 and EQ-133 used to transfect hepatic organoids after trypsinization of the organoids (S kit, 1×10^5 organoids/pulse). Besides,

HEK293T cells were used as control of the transfection. Recovery and growth of organoids were not successful after transfection, because they seeded on ultra-low attachment plate instead of on Matrigel (Figure 4.31.C).

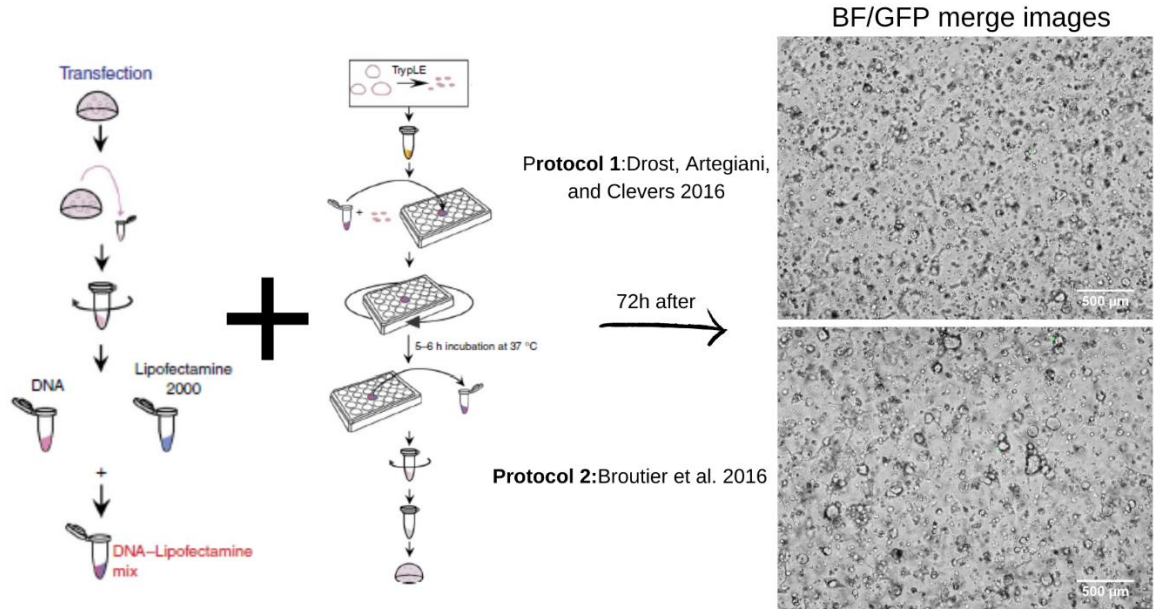
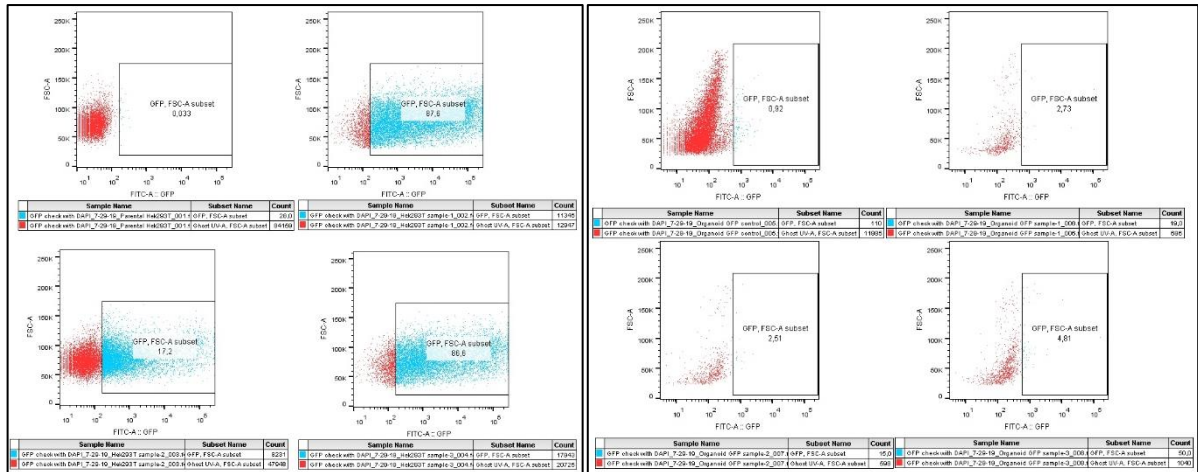
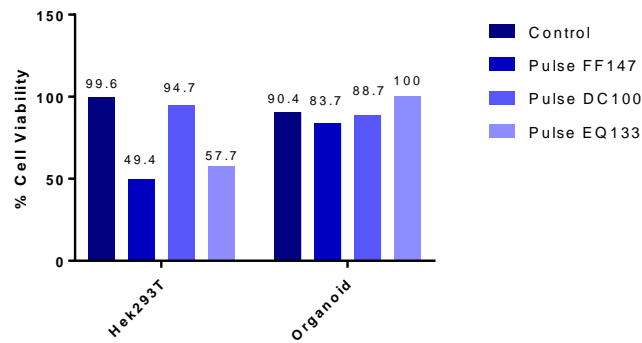


Figure 4.30: Transfection method of hepatic organoids with Lipofectamine 2000 and its results.

A.



B.



C.

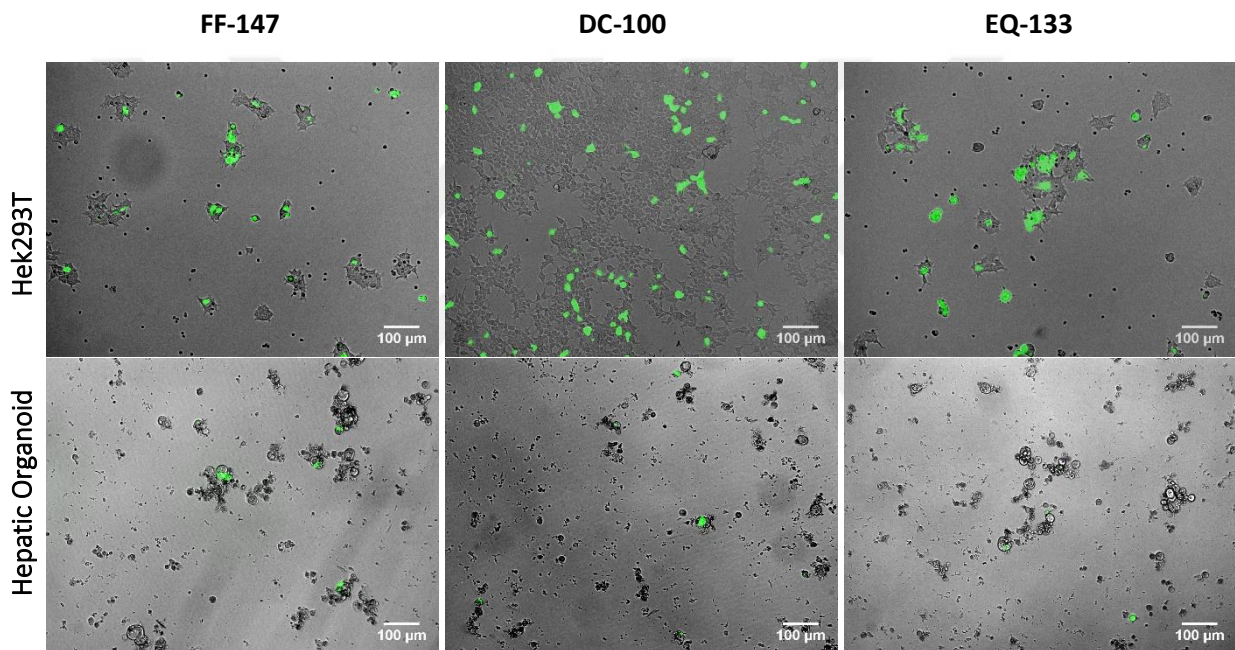


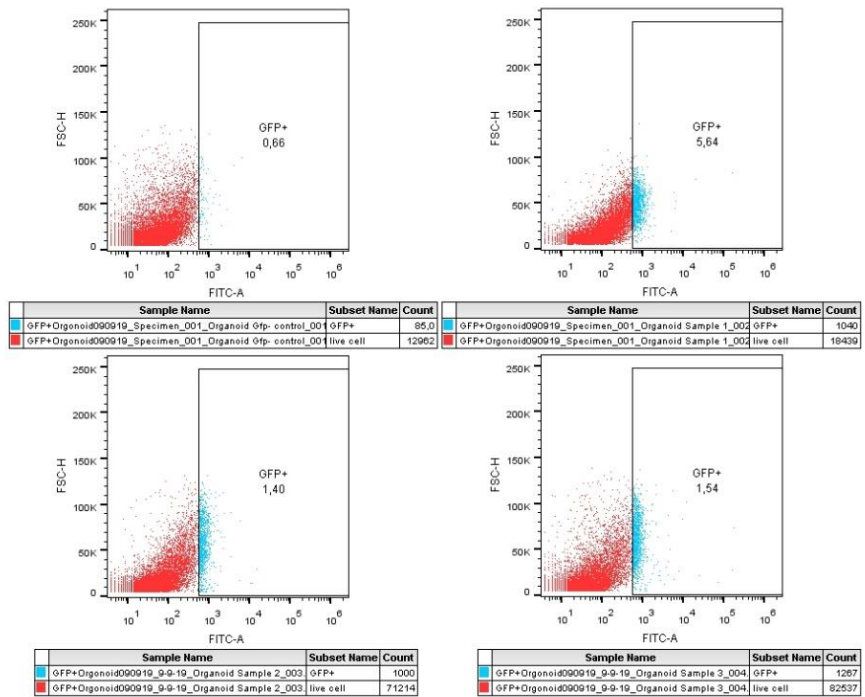
Figure 4.31: Transfection of Hepatic Organoids and HEK293T cells with Nucleofector System.

A. Flow analysis of cells 72h after transfection. (Sample 1;FF-147, Sample 2;DC-100, Sample 3;EQ-133) B. Cell viability percentage according to flow analysis. C. Fluorescence microscopy images in 2D suspension culture 72h after transfection.

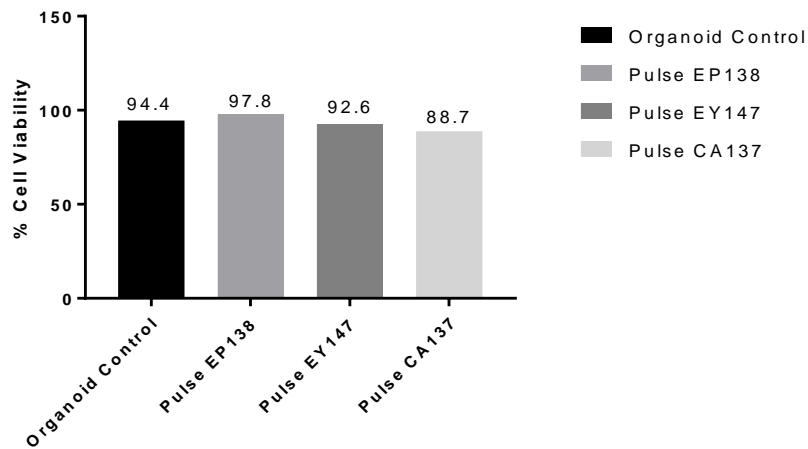
These three pulses showed different transfection efficiencies on both HEK293T cell and hepatic organoid. While the transfection efficiency was 17-87 % in Hek233T, it was 2-4 % in hepatic organoids (Figure 4.31.A). The viability of the cells also was different in each group and the harsh pulse was FF-147 in both groups (Figure 4.31.B). Because of the low transfection efficiency in organoids with the nucleofector system, we continued to search for a suitable pulse. For this purpose, 3 more pulses that were EP-138, EY-147, and CA-137 were tried (S kit, 1×10^5 organoids/pulse). Post transfection, cells were seeded in Matrigel for better cell

recovery. In the flow analysis after 72h, the highest amount of GFP cells were observed with 5.6% in the group transfected with EP-138, while there were 1-1.5% GFP+ cells in the other groups (Figure 4.32.A). Cell viability varies between 88-97% between groups (Figure 4.32.B). Although the morphology of the cells was better than the previous experiment, a small number of GFP + cells were observed (Figure 4.32.C).

A.



B.



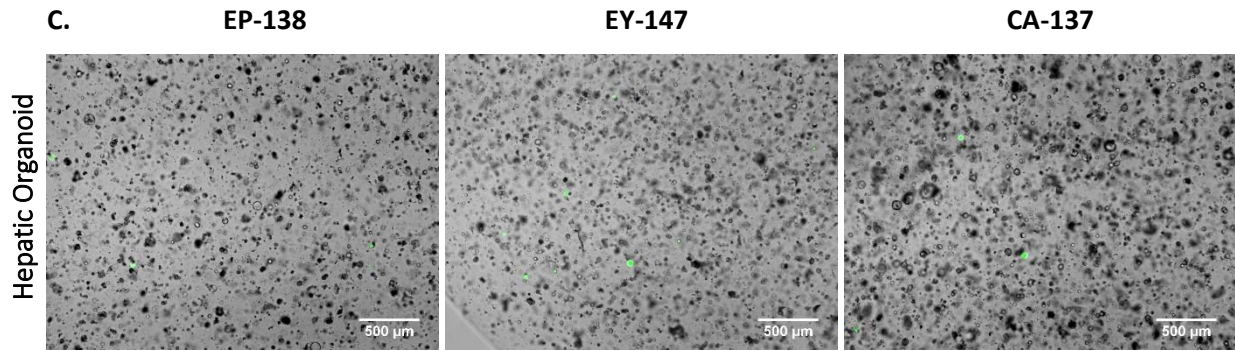
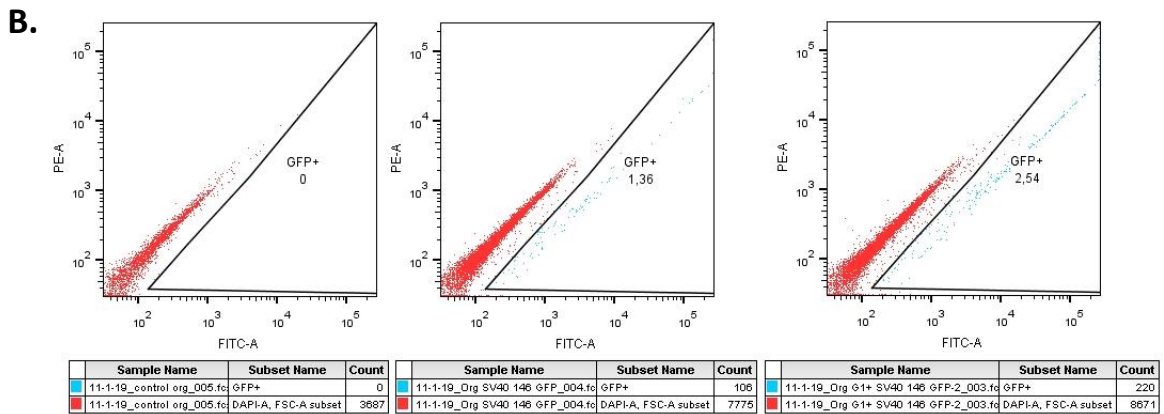
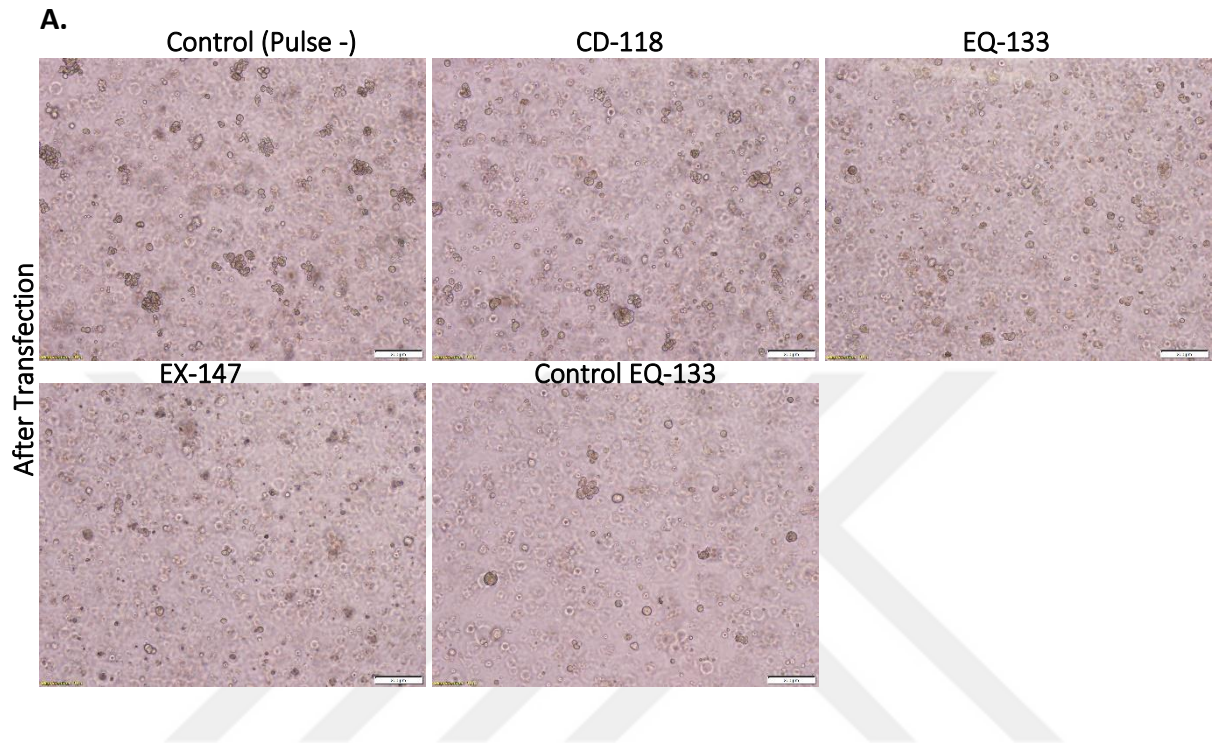


Figure 4.32: Transfection of Hepatic Organoids with Nucleofector System.

A. Flow analysis of cells 72h after transfection. (Sample 1;EP-138, Sample 2;EY-147, Sample 3;CA-137) B. Cell viability percentage according to flow analysis. C. Fluorescence microscopy images in 3D culture 72h after transfection.

Next, previously tested three pulses with higher efficiency (approx. 6-8%), (Figure 4.34.D) were used for transfection set up of the first step of hTERT modification. In this study, we increased the cell number that is transfected (L kit, 5×10^5 organoids/pulse). According to experimental design, the experimental group which includes DT GFP 146 and G1 plasmid were transfected with three pulses that were CD-118, EX-147, and EQ-133. The control group which includes only DT GFP 146 was transfected with pulse EQ-133. Post transfection cells were seeded in Matrigel and they had a healthy phenotype (Figure 4.32.A). On day 7 after transfection, FACS was carried out to enrich for the GFP + cells by collecting all samples in the same tube. In the flow analysis, there were 1.3% GFP + population in the control and 2.5 % GFP + population in the experiment group (Figure 4.33.B). Before the sorting of the cells, the image of each sample was taken on the fluorescence microscope. Pulses EQ-133 and FF-147 had a more severe effect on cell viability. Pulse CD-118 had better morphology and cell number than other pulses observed (Figure 4.33.C). On days 14 and 21, there were FACS to generate single-cell clones, but we did not carry out because of the insufficient cell number (Figure 4.33.D). On days 14 and 21, there were FACS to generate single-cell clones, but we could not carry out because of the insufficient cell number. Thus, on day 19, only the experiment group which has GFP+ organoids were dissociated into a single cell. Each Matrigel dot was seeded to contain less cell to pull GFP+ organoid which came from a single cell (Figure 4.33.E). We continued the observation of the organoids, but GFP signal lost day by day. After organoids grow, they gave false positive GFP signals because of their 3D structure in Matrigel. We could

not follow GFP signal, because GFP+ cell enrichment could not continue after day 7 due to the low cell number.



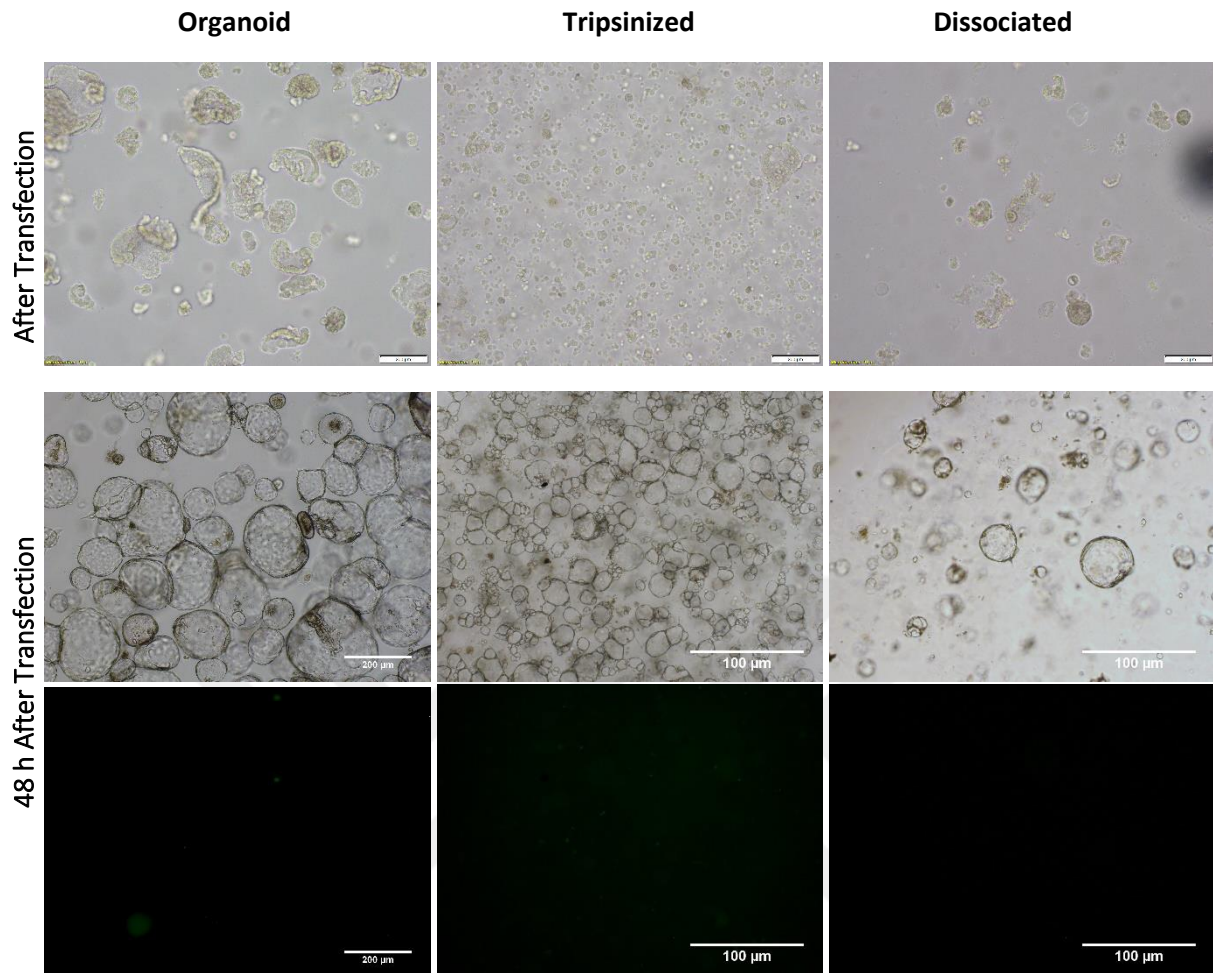


Figure 4.34: BF and fluorescence microscopy image after transfection.

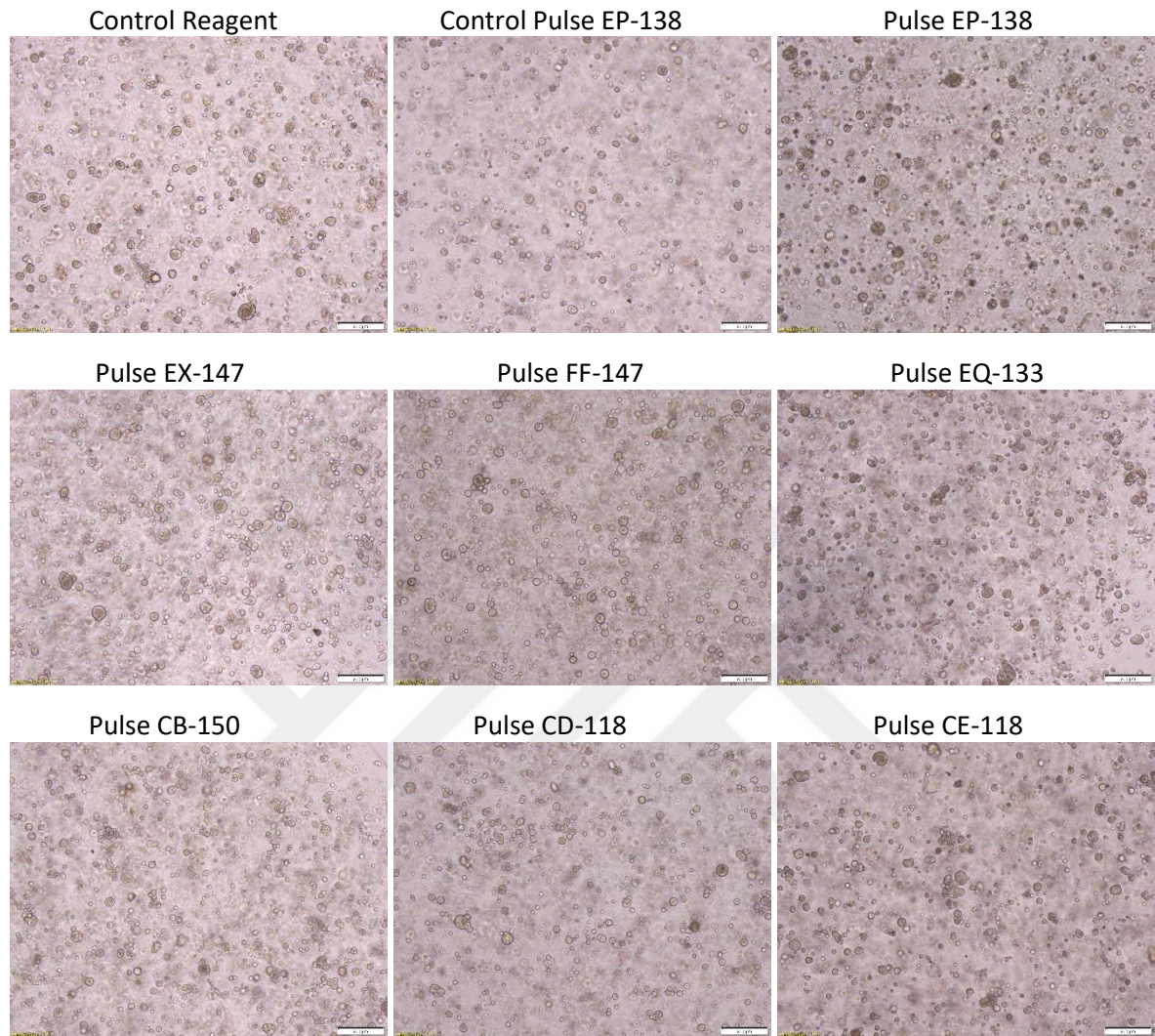
In addition, the most effective pulse was utilized, CD-118, for testing the effect of the pulse which was given two times, and the effect of the single-cell dissociation. For this purpose, organoids were used directly after removing Matrigel, subsequently, organoids were trypsinized by TrypLE and dissociated via pipetting. Nucleofection with CD-118 to two times was applied to these three groups. 48h after transfection, we could not observe the GFP signal under the fluorescence microscope. It was shown that there was not a better effect of the pulse which applied two times (Figure 3.34).

4.6. Transfection of Hepatic Organoids for the Knock-Out of TP53

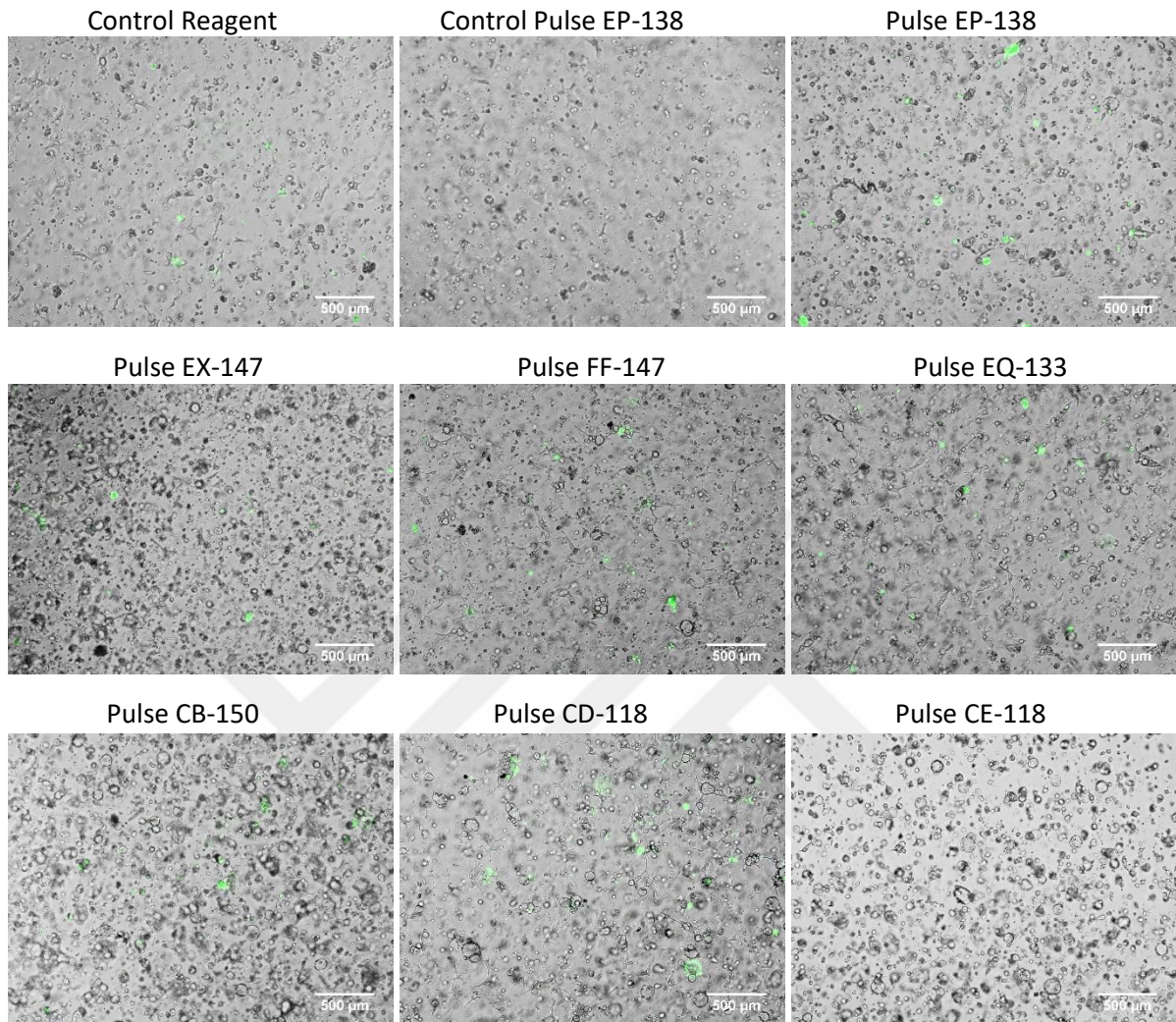
In order to show the impact of CRISPR-Cas9 system on hepatic organoid and growing efficiency of organoids taken from single-cell sorting, we used TP53-pX458 plasmid which activity was shown by Senturk lab previously (pX458 addgene cat no; 48138, TP53 gRNA sequence; 5'- CCATTGTTCAATATCGTCCG-3'). This plasmid provides tracing of the cells by GFP signal after transfection and obtaining isogenic clones. This system creates DS break in the target region on the genome and triggers NHEJ repair mechanism in the cell.

Firstly, seven different pulses were chosen to show transfection efficiency. These pulses were EP-138, EX-147, FF-147, EQ-133, CB-150, CD-118 and CE-118. There was a control group to show the effect of the transfection reagent, so this group did not take nucleofection. Besides, there was another control group to show the effect of transfection reagent and the effect of the pulse (EP-138), so this group did not include TP53- pX458 plasmid. For the knock out of the TP53, TP53-pX458 plasmid was transfected (S kit, 1×10^5 organoids/pulse) with seven pulses. After transfection, cells in each group were healthy morphology (Figure 4.35.A). On 72h post-transfection, transfected cells which can be followed by GFP on the pX458 were sorted as a single cell on the plate based on the GFP signal. Under fluorescence microscopy, few numbers of GFP cells were observed (Figure 4.35.B). Before the single-cell sorting, the efficiency of each pulse was analyzed. Results show that the success of transfection was a range between 2% and 8%. (Figure 4.35.D) Cell viability of the cells from different pulses differ from each other, and the least viable one was the reagent control group between all samples (Figure 4.35.C). Two days after single-cell sorting on Matrigel-coated 96 well plate, GFP+ cells were observed on the plate, and their growth was followed (Figure 4.35.E). Single-cell sorting efficiency was low there were approximately 80 cells in two 96 well plates. There were approximately 20 cells made organoid structure, three of them continued to grow and reached a size that can be passaged. For the higher efficiency, after single-cell sorting, we used a mix of the fresh and condition medium with the rate 1:1.

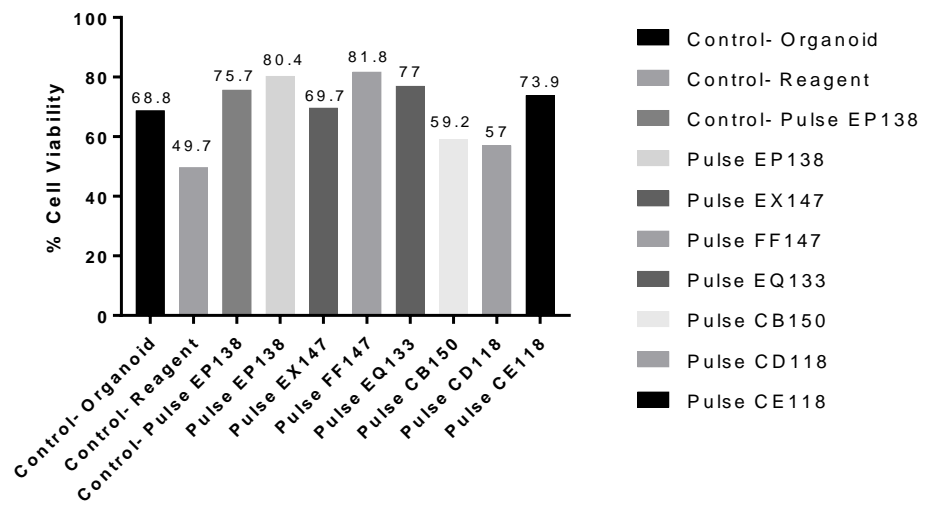
A.



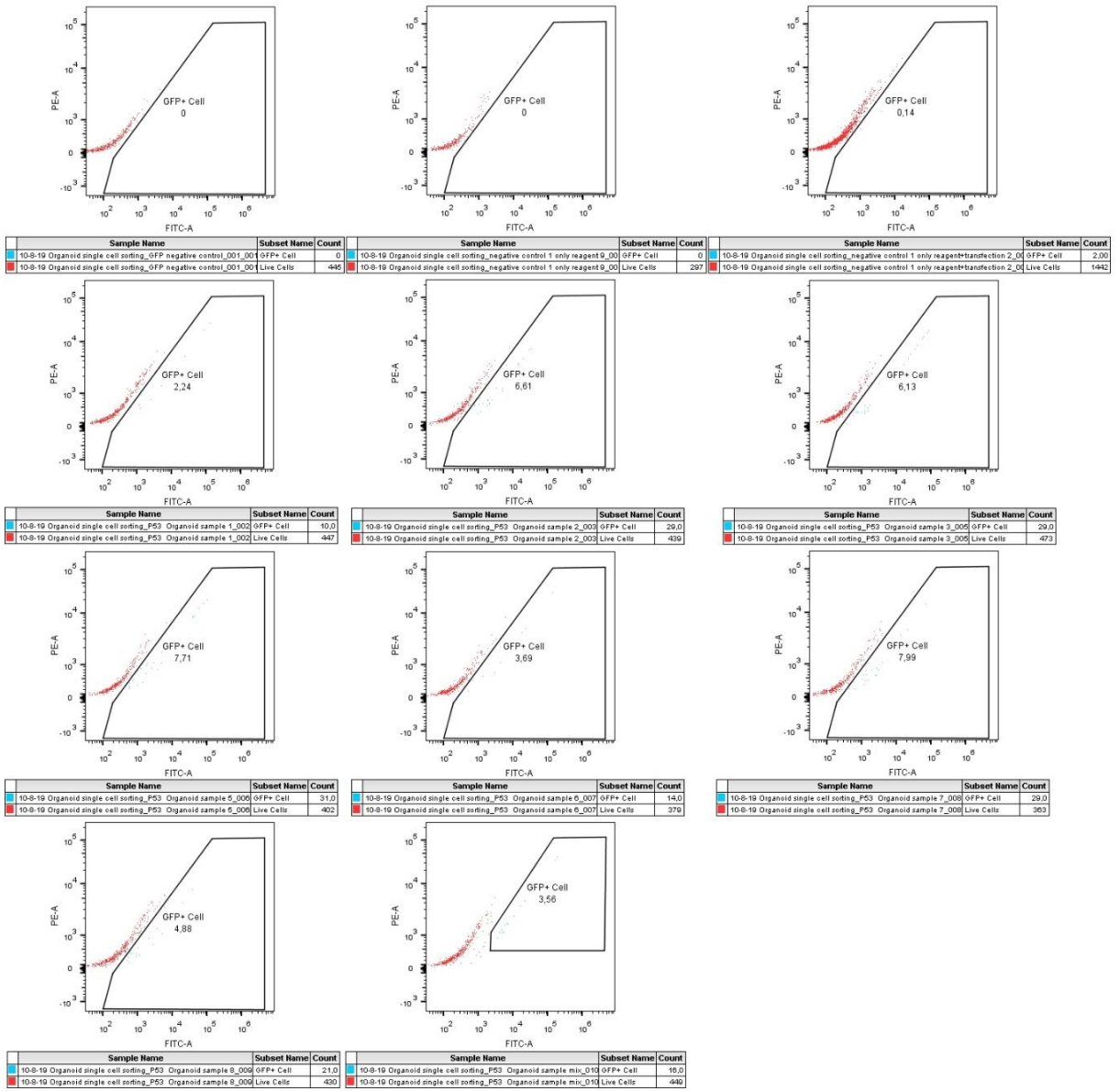
B.



C.



D.



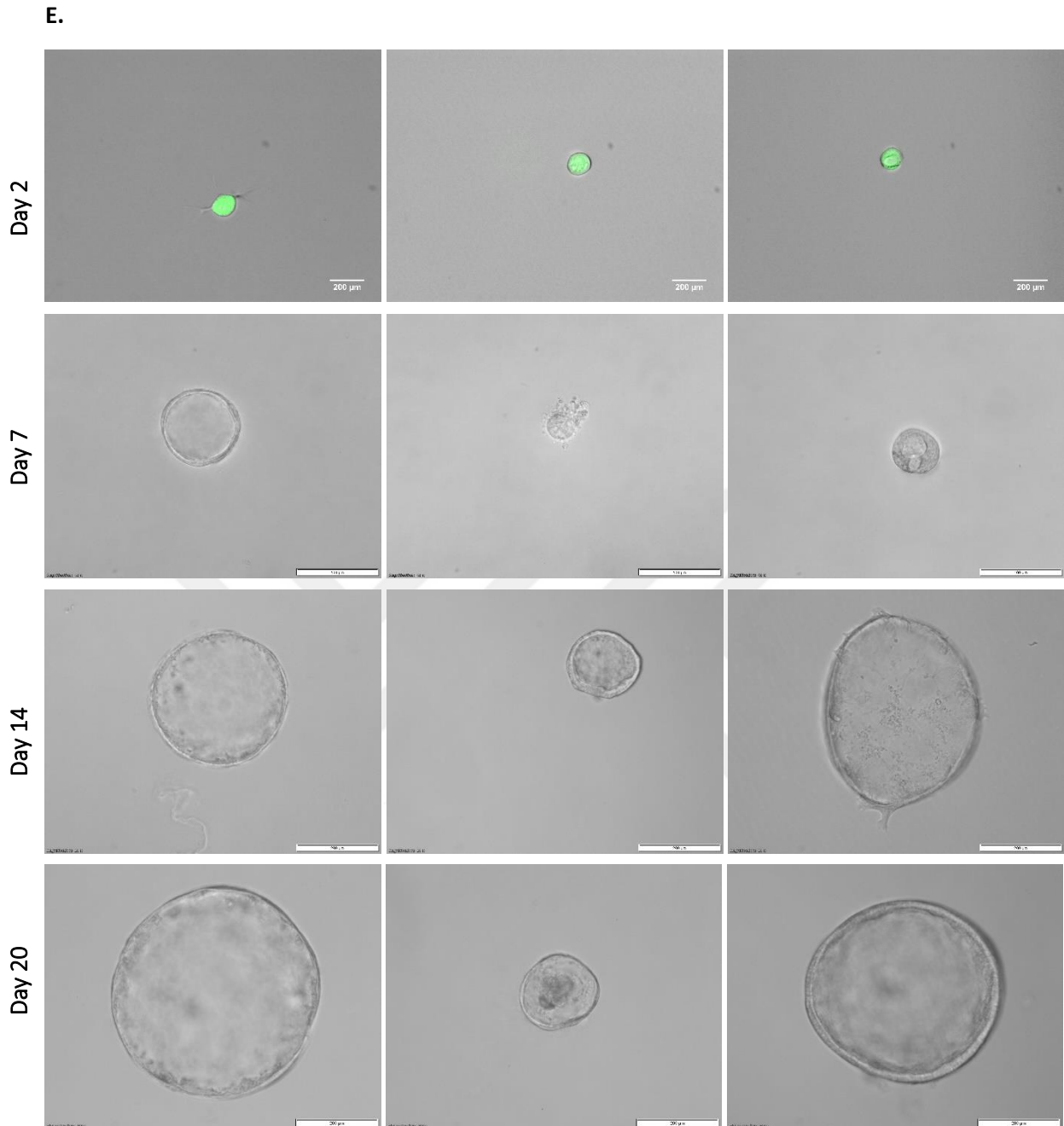


Figure 4.35: Transfection of Hepatic Organoids with Nucleofector System for the TP53 knock-out

A. BF images of organoids after nucleofection. (Control Reagent; only reagent & no pulse, Control Pulse EP-138; reagent & pulse & no plasmid, Other pulses; pulse & TP53 pX458 plasmid) B. Fluorescence microscopy image 72h after transfection. C. Cell viability percentage according to flow analysis. D. FACS on 72h post-transfection (sample 1; EP-138, sample 2; EX-147, sample 3; FF-147, sample 5; EQ-133, sample 6; CB-150, sample 7; CD-118 sample 8; CE-118, sample mix; cell mixture for GFP+ single cell sorting) E. Fluorescence microscopy image 48h after single cell sorting and BF images on day 7,14 and 20.

Between the three TP53 clones, only one of them reaches a usable number of organoids. This clone G5-2 P53 has a different morphology than wild type (WT) hepatic organoid by showing smaller and deformed structures (Figure 4.36). There were shown that tumor organoids exhibit a range of patient-specific morphologies and different cellular architectures that recapitulate the histological features of the patient's tissue and tumor subtype in many reports. The lack of a morphological phenotype does not necessarily indicate that the cells are normal, but the presence of a morphological phenotype might indicate cancerous cells (Wallaschek et al. 2019).

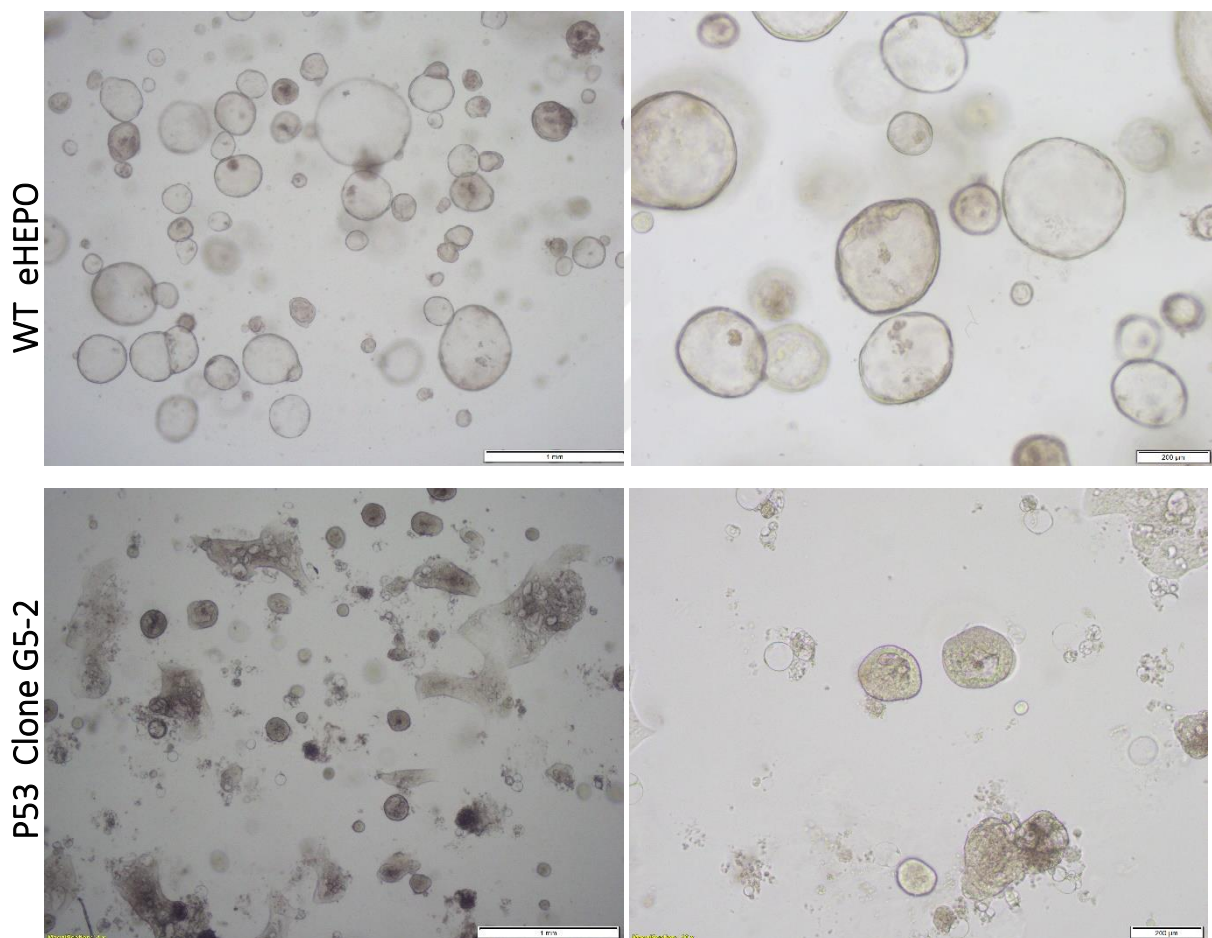


Figure 4.36: BF images of WT Hepatic Organoid and P53 Clone G5-2

BF images show that P53 Clone G5-2 have a different morphology than WT hepatic organoids.

Different types of cancers exhibit mutations in the p53 pathway and can, therefore, be selected with the application of the small molecule Nutlin-3, which stabilizes TP53 by disrupting the binding of TP53 to its negative regulator E3 ubiquitin ligase, MDM2 (Matano et al. 2015; Bartfeld et al. 2015). Thus, tumor organoids that have alterations in the p53 pathway can stay alive under selective pressure from the application of Nutlin-3, while normal organoids die. We showed under increasing Nutlin-3 conditions, while WT hepatic organoid growing affected, possibly p53 knockout clone continued to grow. (Figure 4.37).

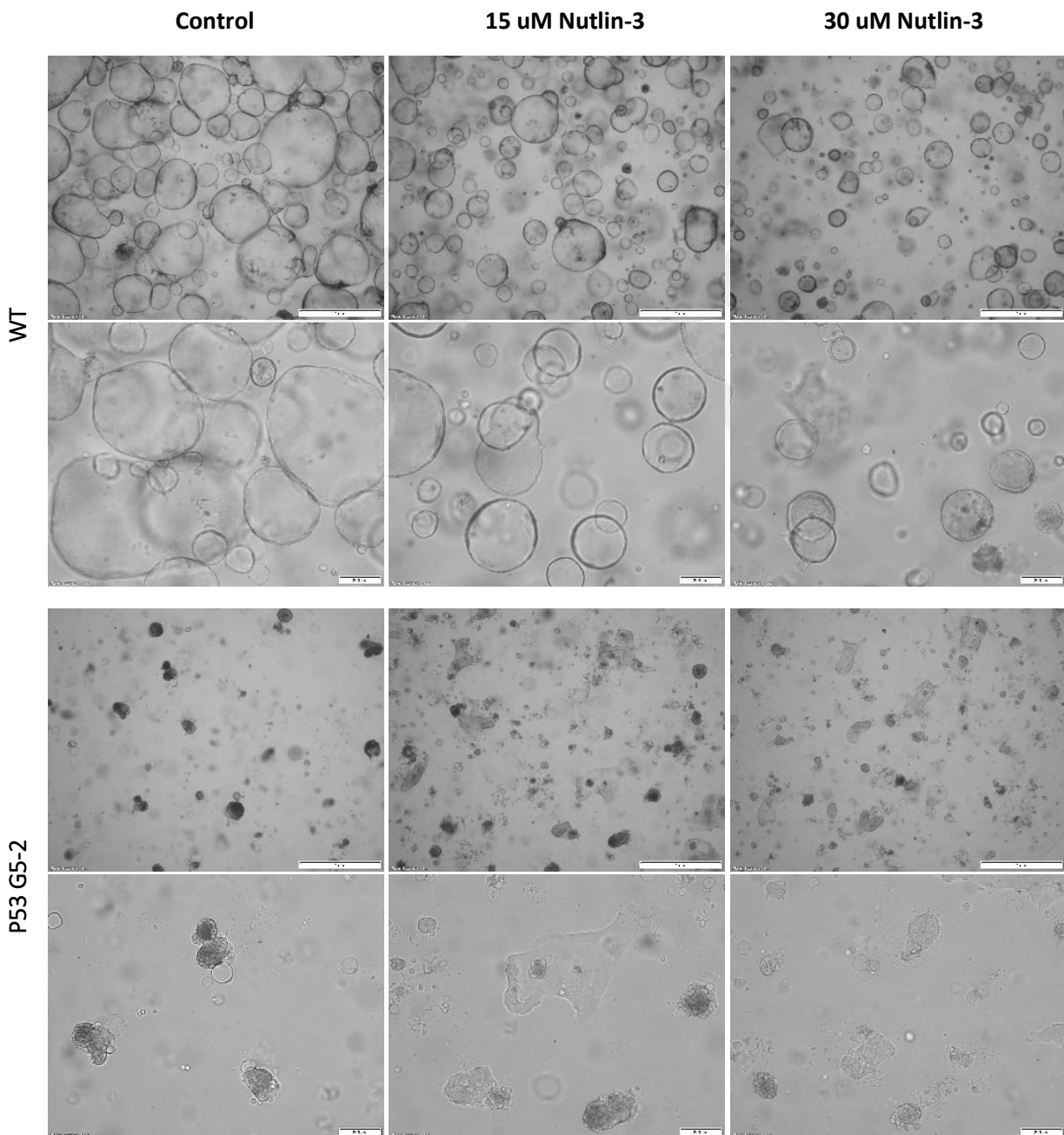


Figure 4.37: Brightfield images of wild-type and TP53- mutant organoid after 7 days of Nutlin-3 selection.

5. DISCUSSION

In HCC, the most frequently seen mutation comprises of the single-nucleotide alterations on TERT promoter mutations with more than 60% of the cases (Lee 2015). Among these alterations on hTERT promoter, the substitutions on C-124T and C-146T are the most abundant ones and it has been identified that these mutations create new binding sites for the ETS transcription factors which increase promoter activity and expression of TERT. (Nault and Zucman-Rossi 2016). It has been also reported that TERT promoter mutations are associated with higher production of TERT protein, higher telomerase enzyme activity, and longer telomeres in urothelial cancer (UC), and associated with poor patient survival (Borah et al. 2015). Furthermore, another study showed that the telomere length is shorter in the high-grade HCCs within the presence of a TERT promoter mutation (Lee et al. 2017). However, there is very little information about the molecular mechanisms for explaining the hTERT mutation related to hepatocarcinogenesis. Thus modeling of TERT promoter mutations becomes crucial in the liver to study the mechanism of TERT transcription and identification of the new molecules and or signaling partners that included in the promoter activity during the hepatocarcinogenesis process.

Organoids are the most powerful cell culture tool to study human biology in health and disease until now (Tuveson D. and Clevers H. 2019; Lancaster M and Huch M. 2019). They are defined as the structures grown in matrix resembling organs in terms of architecture and function. Insights on the recently established protocols liver-specific organoids can be obtained from either pluripotent stem cells or liver-specific stem/progenitor cells inappropriate conditions with 3D matrix and signaling factors. In the different issues, organoids derived from normal tissue can be used to model cancer by sequentially introducing tumor-related or driver gene mutations. The advantage of the model is to be able to understand the effect of mutations in the isogenic (identical genetic) background. Different laboratories have independently established mutant organoids by introducing mutations into normal colon organoids for at least four of the most commonly altered genes in colorectal carcinoma, namely KRAS, APC, TP53, SMAD4 and PIK3CA (Artegiani et al. 2019; Huang et al. 2015; Matano et al. 2015). When these mutant organoids were transplanted into the kidney capsule of mice, adenocarcinomas developed as characteristics of colon cancer progression. Recently, organoids and CRISPR/Cas9 systems have also been used together to study the mechanism of pancreatic

cancer progression (Seino et al. 2018). To model hepatocellular carcinoma progression based on creating the most frequent mutations has not been used yet.

The overall goal of the project is to create a model for HCC via genome editing strategy in which introducing hTERT mutations and knocking out of p53, NF1 and APC genes were done on normal hepatic organoids. In this study, we first specifically focused to create hTERT promoter mutations on hepatic organoids. This model can be used to understand the state of the activated TERT gene and the steps involved in telomerase reactivation in HCC. In the strategy of obtaining hepatic organoids that included TERT promoter mutations, the CRISPR-Cas9 system was used according to reference article which found TERT to be one of the loci with a low targeting efficiency and develop a strategy called "pop in and pop out" (Xi et al. 2015). This strategy has advantages in the genome editing of hTERT. hTERT is not a very actively transcribed gene and the chromatin environment might prevent the accession of the Cas9–sgRNA complex. However, the tracing of the edited clones with GFP is to increase the efficiency of editing. Another advantage is the addition of the single base pair substitution that targeted by gRNA in the first step of editing. Due to this substitution gRNA cannot recognize the edited genome and this also increases the efficiency.

Firstly, we used HEK293T cells to confirm the working of the system. According to Sanger sequencing results, we found that in all groups that are C-146T, C-124T and both C-146T & C-124T have only C-146T mutation come from first step editing. We produced C-146T mutation with unwanted deletions in the two HEK293T clones. Insertion of the eGFP cassette in the first step was performed successfully, but in the second step, cells could be repaired through NHEJ instead of HDR system in the sequenced clones. Also, Xi et al. showed out of eight clones six of them have unwanted deletions on the promoter besides specific hTERT mutation introduced. Moreover, they showed that out of 200 clones only three successfully edited to WT TERT promoter sequence at ScaBER cells which have originally C-124T mutation (Xi et al. 2015). Therefore, the limitation of the system can be screening a high number of edited clones to find the correct clone.

For the first step transfection of hepatic organoids, different transfection methods were used. Previously published protocol for transfection of mouse and liver organoids with lipofectamine 2000 was failed to transfect iPSC derived hepatic organoids (Broutier et al. 2016). There are some transfection methods such as chemical (reagents/lipofection), physical

(electroporation/nucleofection) or viral transfection. Two different methods that are chemical-based and nucleofection system were used to transfect hepatic organoids. While the chemical-based transfection did not successful, there were better results with nucleofection that enables the entrance of gRNA/Cas9 directly to the nucleus. However, there are limitations of the system that the parameters of each program are not identified and cannot be individually controlled by the user. According to results, transfection efficiency with nucleofection was not enough for the GFP enrichment in the first step of TERT editing. In conclusion, there is a need for more optimization of nucleofection to have TERT mutation in the hepatic organoids. Besides, we need to start the transfection with a higher amount of organoids.

In the literature, the difficulties of transfection for the 3D cultured cells or organoids are well defined and researchers developed novel systems to enhance transfection such as microcarriers (Laperrousaz et al. 2018), microinjection with electroporation. Recently, a study showed that human liver organoids can be transfected with electroporation (tweezer electrodes) after micro-injection of the CRISPR/Cas9 plasmids into organoids. Nevertheless, transfection efficiency was shown by 10% in the organoids (Artegiani et al. 2019). Because of the organoid's dense and compact structures that make diffusion, penetration and cellular accumulation of genetic material difficult, it is hard to transfect them via traditional techniques. There is a lack of knowledge about the transfection of organoids/ hepatic organoids in the literature. Thus, transfection on already formed organoids remains challenging (Laperrousaz et al. 2018).

In order to control that the CRISPR system works in hepatic organoids and isogenic organoids clones can be obtained from single cells, we transfected organoids by nucleofector system to knockout TP53 (P53-pX458). Results showed that the single-cell sorting of the GFP+ organoids can be performed, and isogenic organoids can grow. One of the produced TP53 knockout clones showed cancerous organoid morphology and grew under Nutlin-3 condition.

As a summary, we showed that two steps CRISPR- Cas9 editing strategy is relevant to create TERT promoter mutations on the HEK293T with low efficiency. However, there are several limitations to use this system for the transfection of 3D grown hepatic organoids. Firstly, transfection efficiency is not enough for three rounds of enrichment of GFP+ cells in edited organoids. Secondly, single-cell sorting efficiency for organoids is very low with this transfection rate. Besides, the obtained clone number will be not enough for the screening of the mutations. Thirdly, re-growing rate of the organoids from a single cell takes time. Lastly,

the organoid culture and transfection processes are very expensive. When this system can be applied with higher transfection efficiency in hepatic organoids, and with the screening of high numbers of clone, the organoid model that has TERT promoter mutation can be obtained.



6. CONCLUSION AND FUTURE ASPECTS

This study based on introducing hTERT promoter mutations which are alterations in the hepatocarcinogenesis, as well as C-124T and C-146T mutations. All of them have a role in the progression of hepatocellular carcinoma. According to the previous studies, the mechanism of TERT promoter mutations that collaborates with carcinogenesis is not well-understood yet. Recently developed 3D organoid culture technologies have enabled the production of micro-scaled and simplified, functional models of various organs including the liver. Thus, a hepatic organoid (eHEPO) culture system was aiming our target to be generated utilizing human pluripotent stem cell (iPSC). Introducing hTERT promoter mutations into hepatic organoids by CRISPR-Cas9 was the main goal.

The two-step strategy for CRISPR/Cas9 system called “pop in and pop out” has several limitations to make genome editing in 3D grown iPSC derived hepatic organoids such as a low number of single or enriched cells after transfection. To drawback such technical restrictions we will increase the number of transfected cells and allow long period the cells to re-grow organoid structures in culture. Alternatively, genome editing can be done at the beginning of organoid generation steps specifically at iPSC.

7. REFERENCES

- Adli, M. 2018. 'The CRISPR tool kit for genome editing and beyond', *Nat Commun*, 9: 1911.
- Akbari, S., G. G. Sevinc, N. Ersoy, O. Basak, K. Kaplan, K. Sevinc, E. Ozel, B. Sengun, E. Enustun, B. Ozcimen, A. Bagriyanik, N. Arslan, T. T. Onder, and E. Erdal. 2019. 'Robust, Long-Term Culture of Endoderm-Derived Hepatic Organoids for Disease Modeling', *Stem Cell Reports*, 13: 627-41.
- Akbari, Soheil, Nur Arslan, Serif Senturk, and Esra Erdal. 2019. 'Next-Generation Liver Medicine Using Organoid Models', *Frontiers in Cell and Developmental Biology*, 7.
- Artegiani, B., L. van Voorthuijsen, R. G. H. Lindeboom, D. Seinstra, I. Heo, P. Tapia, C. Lopez-Iglesias, D. Postrach, T. Dayton, R. Oka, H. Hu, R. van Boxtel, J. H. van Es, J. Offerhaus, P. J. Peters, J. van Rheenen, M. Vermeulen, and H. Clevers. 2019. 'Probing the Tumor Suppressor Function of BAP1 in CRISPR-Engineered Human Liver Organoids', *Cell Stem Cell*, 24: 927-43 e6.
- Barker, N., J. H. van Es, J. Kuipers, P. Kujala, M. van den Born, M. Cozijnsen, A. Haegebarth, J. Korving, H. Begthel, P. J. Peters, and H. Clevers. 2007. 'Identification of stem cells in small intestine and colon by marker gene *Lgr5*', *Nature*, 449: 1003-7.
- Bartfeld, S., T. Bayram, M. van de Wetering, M. Huch, H. Begthel, P. Kujala, R. Vries, P. J. Peters, and H. Clevers. 2015. 'In vitro expansion of human gastric epithelial stem cells and their responses to bacterial infection', *Gastroenterology*, 148: 126-36 e6.
- Borah, S., L. Xi, A. J. Zaug, N. M. Powell, G. M. Dancik, S. B. Cohen, J. C. Costello, D. Theodorescu, and T. R. Cech. 2015. 'Cancer. TERT promoter mutations and telomerase reactivation in urothelial cancer', *Science*, 347: 1006-10.
- Broutier, L., A. Andersson-Rolf, C. J. Hindley, S. F. Boj, H. Clevers, B. K. Koo, and M. Huch. 2016. 'Culture and establishment of self-renewing human and mouse adult liver and pancreas 3D organoids and their genetic manipulation', *Nat Protoc*, 11: 1724-43.
- Buzzelli, Jon N., Djamilia Ouaret, Graham Brown, Philip D. Allen, and Ruth J. Muschel. 2018. 'Colorectal cancer liver metastases organoids retain characteristics of original tumor and acquire chemotherapy resistance', *Stem Cell Research*, 27: 109-20.
- Calvisi, D. F., C. Wang, C. Ho, S. Ladu, S. A. Lee, S. Mattu, G. Destefanis, S. Delogu, A. Zimmermann, J. Ericsson, S. Brozzetti, T. Staniscia, X. Chen, F. Dombrowski, and M. Evert. 2011. 'Increased lipogenesis, induced by AKT-mTORC1-RPS6 signaling, promotes development of human hepatocellular carcinoma', *Gastroenterology*, 140: 1071-83.
- Castorena-Torres, Fabiola, Katia Peñuelas-Urquides, and Mario Berúmdez de León. 2016. 'Site-Directed Mutagenesis by Polymerase Chain Reaction.' in, *Polymerase Chain Reaction for Biomedical Applications*.
- Clevers, H. 2016. 'Modeling Development and Disease with Organoids', *Cell*, 165: 1586-97.
- Desai, A., S. Sandhu, J. P. Lai, and D. S. Sandhu. 2019. 'Hepatocellular carcinoma in non-cirrhotic liver: A comprehensive review', *World J Hepatol*, 11: 1-18.
- Dhanasekaran, R., S. Bandoh, and L. R. Roberts. 2016. 'Molecular pathogenesis of hepatocellular carcinoma and impact of therapeutic advances', *F1000Res*, 5.
- Ding, X. X., Q. G. Zhu, S. M. Zhang, L. Guan, T. Li, L. Zhang, S. Y. Wang, W. L. Ren, X. M. Chen, J. Zhao, S. Lin, Z. Z. Liu, Y. X. Bai, B. He, and H. Q. Zhang. 2017. 'Precision medicine for hepatocellular carcinoma: driver mutations and targeted therapy', *Oncotarget*, 8: 55715-30.

- Drost, J., B. Artegiani, and H. Clevers. 2016. 'The Generation of Organoids for Studying Wnt Signaling', *Methods Mol Biol*, 1481: 141-59.
- Farazi, P. A., and R. A. DePinho. 2006. 'Hepatocellular carcinoma pathogenesis: from genes to environment', *Nat Rev Cancer*, 6: 674-87.
- Gaj, T., C. A. Gersbach, and C. F. Barbas, 3rd. 2013. 'ZFN, TALEN, and CRISPR/Cas-based methods for genome engineering', *Trends Biotechnol*, 31: 397-405.
- Gaj, T., S. J. Sirk, S. L. Shui, and J. Liu. 2016. 'Genome-Editing Technologies: Principles and Applications', *Cold Spring Harb Perspect Biol*, 8.
- Gao, Dong, Ian Vela, Andrea Sboner, Phillip J Iaquinta, Wouter R Karthaus, Anuradha Gopalan, Catherine Dowling, Jackline N Wanjala, Eva A Undvall, Vivek K Arora, John Wongvipat, Myriam Kossai, Sinan Ramazanoglu, Luendreo P Barboza, Wei Di, Zhen Cao, Qi Fan Zhang, Inna Sirota, Leili Ran, Theresa Y MacDonald, Himisha Beltran, Juan-Miguel Mosquera, Karim A Touijer, Peter T Scardino, Vincent P Laudone, Kristen R Curtis, Dana E Rathkopf, Michael J Morris, Daniel C Danila, Susan F Slovin, Stephen B Solomon, James A Eastham, Ping Chi, Brett Carver, Mark A Rubin, Howard I Scher, Hans Clevers, Charles L Sawyers, and Yu Chen. 2014. 'Organoid Cultures Derived from Patients with Advanced Prostate Cancer', *Cell*, 159: 176-87.
- Guan, Y., D. Xu, P. M. Garfin, U. Ehmer, M. Hurwitz, G. Enns, S. Michie, M. Wu, M. Zheng, T. Nishimura, J. Sage, and G. Peltz. 2017. 'Human hepatic organoids for the analysis of human genetic diseases', *JCI Insight*, 2.
- Heidenreich, B., P. S. Rachakonda, K. Hemminki, and R. Kumar. 2014. 'TERT promoter mutations in cancer development', *Curr Opin Genet Dev*, 24: 30-7.
- Huang, L., A. Holtzinger, I. Jagan, M. BeGora, I. Lohse, N. Ngai, C. Nostro, R. Wang, L. B. Muthuswamy, H. C. Crawford, C. Arrowsmith, S. E. Kalloger, D. J. Renouf, A. A. Connor, S. Cleary, D. F. Schaeffer, M. Roehrl, M. S. Tsao, S. Gallinger, G. Keller, and S. K. Muthuswamy. 2015. 'Ductal pancreatic cancer modeling and drug screening using human pluripotent stem cell- and patient-derived tumor organoids', *Nat Med*, 21: 1364-71.
- Huch, M., C. Dorrell, S. F. Boj, J. H. van Es, V. S. Li, M. van de Wetering, T. Sato, K. Hamer, N. Sasaki, M. J. Finegold, A. Haft, R. G. Vries, M. Grompe, and H. Clevers. 2013. 'In vitro expansion of single Lgr5+ liver stem cells induced by Wnt-driven regeneration', *Nature*, 494: 247-50.
- Huch, M., H. Gehart, R. van Boxtel, K. Hamer, F. Blokzijl, M. M. Verstegen, E. Ellis, M. van Wenum, S. A. Fuchs, J. de Ligt, M. van de Wetering, N. Sasaki, S. J. Boers, H. Kemperman, J. de Jonge, J. N. Ijzermans, E. E. Nieuwenhuis, R. Hoekstra, S. Strom, R. R. Vries, L. J. van der Laan, E. Cuppen, and H. Clevers. 2015. 'Long-term culture of genome-stable bipotent stem cells from adult human liver', *Cell*, 160: 299-312.
- Jafri, M. A., S. A. Ansari, M. H. Alqahtani, and J. W. Shay. 2016. 'Roles of telomeres and telomerase in cancer, and advances in telomerase-targeted therapies', *Genome Med*, 8: 69.
- Kratochvil, Michael J., Alexis J. Seymour, Thomas L. Li, Sergiu P. Paşca, Calvin J. Kuo, and Sarah C. Heilshorn. 2019. 'Engineered materials for organoid systems', *Nature Reviews Materials*, 4: 606-22.
- Lancaster, M. A., and M. Huch. 2019. 'Disease modelling in human organoids', *Dis Model Mech*, 12.
- Lancaster, M. A., and J. A. Knoblich. 2014. 'Organogenesis in a dish: modeling development and disease using organoid technologies', *Science*, 345: 1247125.

- Laperrousaz, B., S. Porte, S. Gerbaud, V. Harma, F. Kermarrec, V. Hourtane, F. Bottausci, X. Gidrol, and N. Picollet-D'hahan. 2018. 'Direct transfection of clonal organoids in Matrigel microbeads: a promising approach toward organoid-based genetic screens', *Nucleic Acids Res*, 46: e70.
- Lee, H. W., T. I. Park, S. Y. Jang, S. Y. Park, W. J. Park, S. J. Jung, and J. H. Lee. 2017. 'Clinicopathological characteristics of TERT promoter mutation and telomere length in hepatocellular carcinoma', *Medicine (Baltimore)*, 96: e5766.
- Lee, J. S. 2015. 'The mutational landscape of hepatocellular carcinoma', *Clin Mol Hepatol*, 21: 220-9.
- Matano, M., S. Date, M. Shimokawa, A. Takano, M. Fujii, Y. Ohta, T. Watanabe, T. Kanai, and T. Sato. 2015. 'Modeling colorectal cancer using CRISPR-Cas9-mediated engineering of human intestinal organoids', *Nat Med*, 21: 256-62.
- Mody, K., and G. K. Abou-Alfa. 2019. 'Systemic Therapy for Advanced Hepatocellular Carcinoma in an Evolving Landscape', *Curr Treat Options Oncol*, 20: 3.
- Nault, J. C., M. Mallet, C. Pilati, J. Calderaro, P. Bioulac-Sage, C. Laurent, A. Laurent, D. Cherqui, C. Balabaud, and J. Zucman-Rossi. 2013. 'High frequency of telomerase reverse-transcriptase promoter somatic mutations in hepatocellular carcinoma and preneoplastic lesions', *Nat Commun*, 4: 2218.
- Nault, J. C., and J. Zucman-Rossi. 2016. 'TERT promoter mutations in primary liver tumors', *Clin Res Hepatol Gastroenterol*, 40: 9-14.
- Ogawa, J., G. M. Pao, M. N. Shokhirev, and I. M. Verma. 2018. 'Glioblastoma Model Using Human Cerebral Organoids', *Cell Rep*, 23: 1220-29.
- Pezzuto, F., L. Buonaguro, F. M. Buonaguro, and M. L. Tornesello. 2017. 'Frequency and geographic distribution of TERT promoter mutations in primary hepatocellular carcinoma', *Infect Agent Cancer*, 12: 27.
- Ran, F. A., P. D. Hsu, J. Wright, V. Agarwala, D. A. Scott, and F. Zhang. 2013. 'Genome engineering using the CRISPR-Cas9 system', *Nat Protoc*, 8: 2281-308.
- Sander, J. D., and J. K. Joung. 2014. 'CRISPR-Cas systems for editing, regulating and targeting genomes', *Nat Biotechnol*, 32: 347-55.
- Seino, T., S. Kawasaki, M. Shimokawa, H. Tamagawa, K. Toshimitsu, M. Fujii, Y. Ohta, M. Matano, K. Nanki, K. Kawasaki, S. Takahashi, S. Sugimoto, E. Iwasaki, J. Takagi, T. Itoi, M. Kitago, Y. Kitagawa, T. Kanai, and T. Sato. 2018. 'Human Pancreatic Tumor Organoids Reveal Loss of Stem Cell Niche Factor Dependence during Disease Progression', *Cell Stem Cell*, 22: 454-67 e6.
- Song, C. Q., Y. Li, H. Mou, J. Moore, A. Park, Y. Pomyen, S. Hough, Z. Kennedy, A. Fischer, H. Yin, D. G. Anderson, D. Conte, Jr., L. Zender, X. W. Wang, S. Thorgeirsson, Z. Weng, and W. Xue. 2017. 'Genome-Wide CRISPR Screen Identifies Regulators of Mitogen-Activated Protein Kinase as Suppressors of Liver Tumors in Mice', *Gastroenterology*, 152: 1161-73 e1.
- Stern, J. L., D. Theodorescu, B. Vogelstein, N. Papadopoulos, and T. R. Cech. 2015. 'Mutation of the TERT promoter, switch to active chromatin, and monoallelic TERT expression in multiple cancers', *Genes Dev*, 29: 2219-24.
- Sung, Y. H., M. Ali, and H. W. Lee. 2014. 'Extracting extra-telomeric phenotypes from telomerase mouse models', *Yonsei Med J*, 55: 1-8.
- Takebe, T., K. Sekine, M. Enomura, H. Koike, M. Kimura, T. Ogaeri, R. R. Zhang, Y. Ueno, Y. W. Zheng, N. Koike, S. Aoyama, Y. Adachi, and H. Taniguchi. 2013. 'Vascularized and functional human liver from an iPSC-derived organ bud transplant', *Nature*, 499: 481-4.

- Tang, A., O. Hallouch, V. Chernyak, A. Kamaya, and C. B. Sirlin. 2018. 'Epidemiology of hepatocellular carcinoma: target population for surveillance and diagnosis', *Abdom Radiol (NY)*, 43: 13-25.
- Thurtle-Schmidt, D. M., and T. W. Lo. 2018. 'Molecular biology at the cutting edge: A review on CRISPR/CAS9 gene editing for undergraduates', *Biochem Mol Biol Educ*, 46: 195-205.
- Tiriac, Hervé, Pascal Belleau, Dannielle D. Engle, Dennis Plenker, Astrid Deschênes, Tim D. D. Somerville, Fieke E. M. Froeling, Richard A. Burkhart, Robert E. Denroche, Gun-Ho Jang, Koji Miyabayashi, C. Megan Young, Hardik Patel, Michelle Ma, Joseph F. LaComb, Randze Lerie D. Palmaira, Ammar A. Javed, Jasmine C. Huynh, Molly Johnson, Kanika Arora, Nicolas Robine, Minita Shah, Rashesh Sanghvi, Austin B. Goetz, Cinthya Y. Lowder, Laura Martello, Else Driehuis, Nicolas LeComte, Gokce Askan, Christine A. Iacobuzio-Donahue, Hans Clevers, Laura D. Wood, Ralph H. Hruban, Elizabeth Thompson, Andrew J. Aguirre, Brian M. Wolpin, Aaron Sasson, Joseph Kim, Maoxin Wu, Juan Carlos Bucobo, Peter Allen, Divyesh V. Sejpal, William Nealon, James D. Sullivan, Jordan M. Winter, Phyllis A. Gimotty, Jean L. Grem, Dominick J. DiMaio, Jonathan M. Buscaglia, Paul M. Grandgenett, Jonathan R. Brody, Michael A. Hollingsworth, Grainne M. O'Kane, Faiyaz Notta, Edward Kim, James M. Crawford, Craig Devoe, Allyson Ocean, Christopher L. Wolfgang, Kenneth H. Yu, Ellen Li, Christopher R. Vakoc, Benjamin Hubert, Sandra E. Fischer, Julie M. Wilson, Richard Moffitt, Jennifer Knox, Alexander Krasnitz, Steven Gallinger, and David A. Tuveson. 2018. 'Organoid Profiling Identifies Common Responders to Chemotherapy in Pancreatic Cancer', *Cancer Discovery*, 8: 1112-29.
- Tuveson, D., and H. Clevers. 2019. 'Cancer modeling meets human organoid technology', *Science*, 364: 952-55.
- Ventura, Andrea, and Lukas E. Dow. 2018. 'Modeling Cancer in the CRISPR Era', *Annual Review of Cancer Biology*, 2: 111-31.
- Villanueva, A. 2019. 'Hepatocellular Carcinoma', *N Engl J Med*, 380: 1450-62.
- Vyas, D., P. M. Baptista, M. Brovold, E. Moran, B. Gaston, C. Booth, M. Samuel, A. Atala, and S. Soker. 2018. 'Self-assembled liver organoids recapitulate hepatobiliary organogenesis in vitro', *Hepatology*, 67: 750-61.
- Wallaschek, N., C. Niklas, M. Pompaiah, A. Wiegner, C. T. Germer, S. Kircher, S. Brandlein, K. Maurus, A. Rosenwald, H. H. N. Yan, S. Y. Leung, and S. Bartfeld. 2019. 'Establishing Pure Cancer Organoid Cultures: Identification, Selection and Verification of Cancer Phenotypes and Genotypes', *J Mol Biol*, 431: 2884-93.
- Wang, H., M. La Russa, and L. S. Qi. 2016. 'CRISPR/Cas9 in Genome Editing and Beyond', *Annu Rev Biochem*, 85: 227-64.
- Xi, L., J. C. Schmidt, A. J. Zaug, D. R. Ascarrunz, and T. R. Cech. 2015. 'A novel two-step genome editing strategy with CRISPR-Cas9 provides new insights into telomerase action and TERT gene expression', *Genome Biol*, 16: 231.
- Zender, L., A. Villanueva, V. Tovar, D. Sia, D. Y. Chiang, and J. M. Llovet. 2010. 'Cancer gene discovery in hepatocellular carcinoma', *J Hepatol*, 52: 921-9.
- Zhan, T., N. Rindtorff, J. Betge, M. P. Ebert, and M. Boutros. 2018. 'CRISPR/Cas9 for cancer research and therapy', *Semin Cancer Biol*.
- Zhang, R. R., M. Koido, T. Tadokoro, R. Ouchi, T. Matsuno, Y. Ueno, K. Sekine, T. Takebe, and H. Taniguchi. 2018. 'Human iPSC-Derived Posterior Gut Progenitors Are Expandable and Capable of Forming Gut and Liver Organoids', *Stem Cell Reports*, 10: 780-93.

Zucman-Rossi, J., A. Villanueva, J. C. Nault, and J. M. Llovet. 2015. 'Genetic Landscape and Biomarkers of Hepatocellular Carcinoma', *Gastroenterology*, 149: 1226-39 e4.



8. CURRICULUM VITAE (CV)

Canan ÇELİKER

Year of Birth	1993
Adress	İzmir Uluslararası Biyotıp ve Genom Enstitüsü (iBG-izmir) Dokuz Eylül Üniversitesi Sağlık Yerleşkesi, Balçova 35340 İzmir
Mobile	+90 545 969 85 41
E-mail	clkrcnn@gmail.com

EDUCATION

Country Code	Unviersity	Faculty/Institute	Field	Degree	Year
TR	Dokuz Eylül University	İzmir Biomedine and Genome Institute	Moleculer Biology and Genetics	MSc	2017-2019
TR	Yıldız Technical University	Faculty of Science and Letter	Moleculer Biology and Genetics	BS	2014-2016
TR	İstanbul Arel University	Faculty of Science and Letter	Moleculer Biology and Genetics	BS	2011-2014

RESEARCH FIELDS

Molecular Biology and Genetics, Hepatocellular Carcinoma
--

ACADEMIC EXPERIENCES

Intern Student: 22/07/2013–02/08/2013 Istanbul University, Capa Faculty of Medicine, Medical Biology Laboratory, Istanbul (Turkey)
Volunteer Instructor: 02/09/2013–22/09/2013 Ege University Faculty of Pharmacy, Tubitak 4004 Nature Education and Science Schools "MOBILYO" Project
Intern Student: 07/07/2014–18/07/2014 Istanbul Technical University, Laboratory of Molecular Immunology, Istanbul (Turkey)
Intern Student: 20/07/2015–28/08/2015 Izmir Institute of Technology, The Doğanlar/Frary Laboratory for Plant Moleculer Genetics and Breeding, Izmir (Turkey)
Intern Student: 19/09/2016–14/02/2017 Dokuz Eylul University, International Biomedicine and Genome Institute, Stem Cells, Regeneration & Homeostasis Laboratory